IOWA STATE UNIVERSITY
Digital Repository

Graduate Theses and Dissertations

Iowa State University Capstones, Theses and Dissertations

2009

A method to reduce smearing in the milling of metal foams

Christopher Vaira Hunt
Iowa State University

Follow this and additional works at: https://lib.dr.iastate.edu/etd

 Part of the Industrial Engineering Commons

Recommended Citation
Hunt, Christopher Vaira, "A method to reduce smearing in the milling of metal foams" (2009). *Graduate Theses and Dissertations*. 10614.
https://lib.dr.iastate.edu/etd/10614

This Thesis is brought to you for free and open access by the Iowa State University Capstones, Theses and Dissertations at Iowa State University Digital Repository. It has been accepted for inclusion in Graduate Theses and Dissertations by an authorized administrator of Iowa State University Digital Repository. For more information, please contact digirep@iastate.edu.

www.manaraa.com

A method to reduce smearing in the milling of metal foams

by

Christopher Vaira Hunt

A thesis submitted to the graduate faculty

in partial fulfillment of the requirements for the degree of

MASTER OF SCIENCE

Major: Industrial Engineering

Program of Study Committee:
Matthew C. Frank, Major Professor
Frank E. Peters
L. Scott Chumbley

Iowa State University

Ames, Iowa

2009

Copyright © Christopher Vaira Hunt, 2009. All rights reserved.

www.manaraa.com

TABLE OF CONTENTS

LIST OF FIGURES……iv

LIST OF TABLES……...vi

ABSTRACT……...vii

CHAPTER 1. INTRODUCTION……1

CHAPTER 2. LITERATURE REVIEW……8

CHAPTER 3. PROBLEM FRAMEWORK AND SOLUTION APPROACH……16

CHAPTER 4. SURFACE POROSITY ANALYSIS……27

4.1 2^3 full factorial design of experiments……29

4.1.1 2^3 full factorial machining experiment methodology……...29

4.2 Infiltration process methodology……31

4.3 Machine setup and cutting methodology……31

4.4 Machined surface data collection and analysis……34

4.4.1 Reticle analysis methodology……...35

4.5 Comprehensive tool wear analysis methodology……37

4.6 2^3 full factorial machining experiment results……38

4.7 Analysis of Variance methodology……43

4.7.1 ANOVA results – Tool A……44

4.7.2 ANOVA results – Tool B……51

4.8 2^3 full factorial machining experiment results – Comparison of Tool A and Tool B……...……54

4.9 Comprehensive tool wear analysis results……...59

4.9.1 Comprehensive tool wear analysis – tool wear condition results…….62

www.manaraa.com

4.9.2 Comprehensive tool wear analysis – machining environment temperature results……64

CHAPTER 5. IMPLEMENTATION……66

CHAPTER 6. CONCLUSION AND FUTURE WORK……...72

REFERENCES……...……76

APPENDIX 1. 2^3 Full Factorial Experimental Results……..…81

APPENDIX 2. Average 23 Full Factorial Surface Porosity Results Per Factor……...……83

APPENDIX 3. 2^3 Full Factorial ANOVA All Factor Analysis - Tool A…….…….84

APPENDIX 4. 2^3 Full Factorial ANOVA Normal Plot of Effects - Tool A…….86

APPENDIX 5. 2^3 Full Factorial ANOVA Half-Normal Plot of Effects - Tool A…….87

APPENDIX 6. 2^3 Full Factorial ANOVA Effects Charts - Tool A……...88

APPENDIX 7. 2^3 Full Factorial ANOVA Two-Factor Plots - Tool A……..90

APPENDIX 8. 2^3 Full Factorial ANOVA All Factors Residuals Information - Tool A…...91

APPENDIX 9. 2^3 Full Factorial ANOVA All Factor Analysis (Infiltrant Hardness and Temperature Only) - Tool A……92

APPENDIX 10. 2^3 Full Factorial ANOVA All Factor Analysis - Tool B…….……93

APPENDIX 11. 2^3 Full Factorial ANOVA Normal Plot of Effects - Tool B……...95

APPENDIX 12. 2^3 Full Factorial ANOVA Half-Normal Plot of Effects - Tool B……..96

APPENDIX 13. 2^3 Full Factorial ANOVA Effects Charts - Tool B……97

APPENDIX 14. 2^3 Full Factorial ANOVA Two-Factor Plots - Tool B……99

APPENDIX 15. 2^3 Full Factorial ANOVA All Factors Residuals Information - Tool B...100

APPENDIX 16. Surface Porosity Analysis - Varying Feed Rate……...101

APPENDIX 17. Surface Porosity Analysis - Varying Infiltrant Hardness…….102

APPENDIX 18. Surface Porosity Analysis - Varying Temperature……...……103

ACKNOWLEDGEMENTS……..104

www.manaraa.com

LIST OF FIGURES

Figure 1.1 – Porosity comparison of cancellous bone to Trabecular Metal™

Figure 1.2 – Trabecular Metal™ before and after machining

Figure 2.1 – Metal foam application type and their respective cellular structure

Figure 3.1 – Resultant smeared surface after machining

Figure 3.1 – Resultant smeared surface after traditional machining

Figure 3.2 – The bending of a pore wall approximated by the bending of a cantilevered beam

Figure 3.3 – Infiltration and machining process sequence: foam is infiltrated, infiltrated foam is cut, and infltrant is removed from foam resulting in porous surface

Figure 3.4 – CNC-RP rapid machining (a) set up and (b) processing steps for machining a toy jack

Figure 4.1 – The effect of surface smearing when using the infiltrant method

Figure 4.2 – Machining setup showing tool movement along the y-axis

Figure 4.3 – Tool cutting position for an example cut

Figure 4.4 – Microscopic image of fresh TM taken at 40x magnification

Figure 4.5 – Locations of microscopic images on the cut surface (magnification of 25x)

Figure 4.6 – Unprocessed TM with reticle grid imposed atop microscopic image

Figure 4.7 – Fitted main effects chart for Tool A

Figure 4.8 – Two-factor plot for factor combination of infiltrant hardness and temperature

Figure 4.9 – Fitted main effects chart for Tool B

Figure 4.10 – Resulting surface porosity when varying feed rate with Tool A

Figure 4.11 – Resulting surface porosity when varying feed rate with Tool B

Figure 4.12 – Resulting surface porosity comparison using Tool A and Tool B

www.manaraa.com

Figure 4.13 – Resulting surface porosity when varying infiltrant hardness with Tool A

Figure 4.14 – Resulting surface porosity when varying infiltrant hardness with Tool B

Figure 4.15 – 2^3 full factorial surface porosity results throughout life of tool

Figure 4.16 – Resulting surface porosity across tool life of Tool A and Tool B

Figure 4.17 – Tool wear after machining for zero minutes, 1.83 minutes, and 5.32 minutes

Figure 4.18 – Worn tool surface porosity analysis cooling with liquid nitrogen

Figure 4.19 – Surface porosity results at different machining temperatures using Tool B

Figure 5.1 – Bone fracture fragment data processing sequence: CT data, CAD file, CAD file with support structures, and machining of bone fragment geometry

Figure 5.2 – Bone fracture fragment prototypes: aluminum, ceramic, and Delrin™ plastic

Figure 5.3 – CAD file with sacrificial support and finished TM bone fracture fragment

www.manaraa.com

LIST OF TABLES

Table 4.1 – Investigated machining parameters

Table 4.2 – 2^3 full factorial experimental conditions

Table 4.3 – 2^3 full factorial machining experiment results with Tool A

Table 4.4 – 2^3 full factorial machining experiment results with Tool B

Table 4.5 – *t*-test results

Table 4.6 – All factor analysis results for machining experiment when using Tool A

Table 4.7 – *p*-values calculated for all factors and combinations using Tool A

Table 4.8 – Contribution to sum of squares using Tool A

Table 4.9 – Resulting average surface porosity comparison at low and high parameter settings for Tool A

Table 4.10 – All factor analysis results for machining experiment when using Tool B

Table 4.11 – *P*-values calculated for all factors and combinations using Tool B

Table 4.12 – Resulting average surface porosity comparison at low and high parameter settings for Tool B

Table 5.1 – Surface porosity analysis of TM bone fracture fragment

www.manaraa.com

ABSTRACT

This research involves the investigation of process parameters for a new rapid machining process designed for metal foams. Metal foams are structures that contain a network of interconnected pores throughout the structure and surrounding surfaces. Traditional machining methods break down the pore walls of metal foams, creating a smeared surface finish with little to no surface porosity. The described research tasks include defining the significant process parameters for machining complex geometries of a metal foam, Trabecular Metal™, commonly used in medical applications. It was found that feed rate significantly reduces the effect of surface smear, especially at faster rates. Machining with harder infiltrant materials and in a cryogenic environment will also better maintain surface porosity during machining. The impact of this research will allow for the creation of complex porous parts with a variety of applications including custom artificial bone implants.

www.manaraa.com

CHAPTER 1. INTRODUCTION

Metal foams (also known as metallic foams, porous metals, cellular metals, or metal sponges) are a class of materials with low densities and novel physical, thermal, electrical, and acoustic properties (Ashby *et al*., 2000). They can be composed of many different materials including aluminum, nickel, magnesium, lead, zinc, bronze, titanium, copper, steel, and even gold (Ashby *et al*., 2000; Gagliardi *et al*., 2008). Metal foams are classified into two different cellular structures, open or closed. Within an open-cell structure, the pores of the foam are interconnected throughout and comprise the external surface. All of the pores of a closed-cell structure are enclosed within the material. This research focuses only on metal foams with an open-cell structure.

Metal foams have a wide array of applications. These include filters for separating solids from liquids and gases, fluid flow metering and pressure control, storage reservoirs for liquids, flame and spark arrestors for safe handling of flammable gases, sound dampening, and attenuation, among many others (*Porous Metal Design Guidebook*, 2007). An important characteristic of metal foams also allows them to be an excellent candidate for use in orthopaedic implants. Due to the open-cell structure of such foams, when implanted into the body the interconnected porous network allows for the flow of blood through the implant, which enables bone growth into the foam. This bone growth secures the implant attachment with the host bone through osseointegration.

This research focuses on the machining of a specific biocompatible metal foam used in orthopaedic implants, however the machining methodology presented here is not limited to such materials or applications. This process can be applied to any number of open-cell

www.manaraa.com

porous materials; however the process parameters will have to be modified to apply to the particular material of choice.

Metal foams frequently used in orthopaedic implants come in forms of various alloys of titanium and cobalt, most commonly as Ti-6Al-4V and Co-Cr, respectively (Aponte *et al*., 2003; Soboyejo *et al*., 2007; Harrysson *et al*., 2008). Other biocompatible materials that have been used in implants in the past include porous hydroxyapatite, coral, and natural allograft or autograft bone (Soboyejo *et al*., 2007). Material selection for orthpaedic use depends on the implant type and the material's similarity to the physical and mechanical properties of the host bone.

Trabecular Metal™ (TM) composed of tantalum and manufactured by Zimmer, Inc. (Warsaw, IN), was chosen for use because of its prominence in the orthopaedic implant industry. TM has been used in a large number of orthopaedic implants since its inception in the early 1990's by Ultramet, a research and development firm (Deglurkar *et al*., 2006). The cellular structure of Trabecular Metal™ was designed to imitate the physical and mechanical properties of natural bone and is approximately 70 – 85% void space (Bobyn *et al.*, 1999; Voort *et al*., 2004; Medlin *et al*., 2005; Callaghan *et al.*, 2006; Levine *et al*., 2006; Levine *et al*., 2008). The crystalline microtexture of the tantalum struts that compose TM is conductive to direct bone apposition (Bobyn *et al.*, 1999). Along with biocompatibility, elemental tantalum combines high strength with great corrosion resistance making it an ideal material for orthopaedic use (Black, 1994). These characteristics are justification for the use of tantalum in orthopaedic implants for more than 50 years (Black, 1994).

For the purpose of this research, it is assumed that the surface porosity measurement of unprocessed open-cell foam is equal to its bulk porosity value. This assumption is

www.manaraa.com

validated by the definition of open-cell foams which states, foam is said to be open-celled if the solid of which the foam is made is contained in the cell edges only, so that the cells connect through open faces (Gibson *et al*., 1988). Therefore, the surface of unprocessed TM can be 70 – 85% porous. This is quite high considering other orthpaedic porous metals are only 35 – 50% porous (Bobyn *et al*., 1999; Shimko *et al*., 2005). For example, the porosity of Co-Cr sintered beads is between 30 – 35% and fiber metal has a porosity range of 40 – 50% (Levine *et al.*, 2006).

Due to the high porosity of Trabecular Metal™, TM is uniquely conducive to bone formation, enabling both strong attachment and fast, extensive tissue infiltration (Bobyn *et al.*, 1999). The similarity of the internal strut configuration of Trabecular Metal™ to cancellous bone is illustrated in Figure 1.1. TM has been primarily used in spinal and joint reconstructive implants; these implants are not typically made entirely of open-cell TM; rather, only select areas and implant surfaces that interact with host bone.

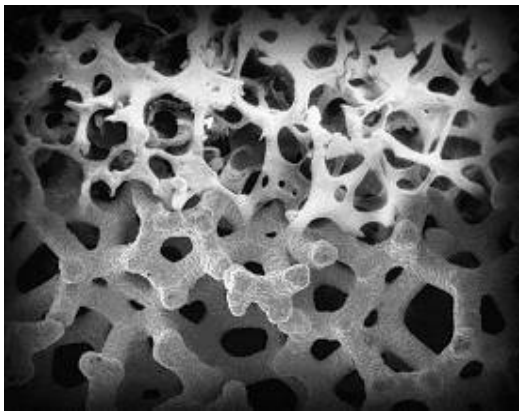

Figure 1.1 – Porosity comparison of cancellous bone (top) to Trabecular Metal™ (bottom) (www.zimmer.com)

www.manaraa.com

Maintaining the porosity of an open- or closed-cell metal foam during processing is vital in preserving the metal's functionality and performance. Due to the cellular structure of metal foams, the surface porosity is often modified during processing due to a smearing effect left by traditional machining methods (Ashby *et al*., 2000; Bram *et al*., 2003; Laptev *et al*., 2004; Chen *et al*., 2005; Deglurkar *et al*., 2006; *Porous Metal Design Guidebook*, 2007; Frank *et al*., 2008). The thin interconnected cell walls offer little internal support against the machining forces created by such processes (Deglurkar *et al*., 2006). The resulting smearing takes place when the cellular walls collapse under these forces and compromise the surface porosity. The degree to which this smearing occurs varies among different materials and the specific machining method and machining parameters. Figure 1.2 shows this smearing effect with a sample of Trabecular Metal™ before and after being cut with an end mill.

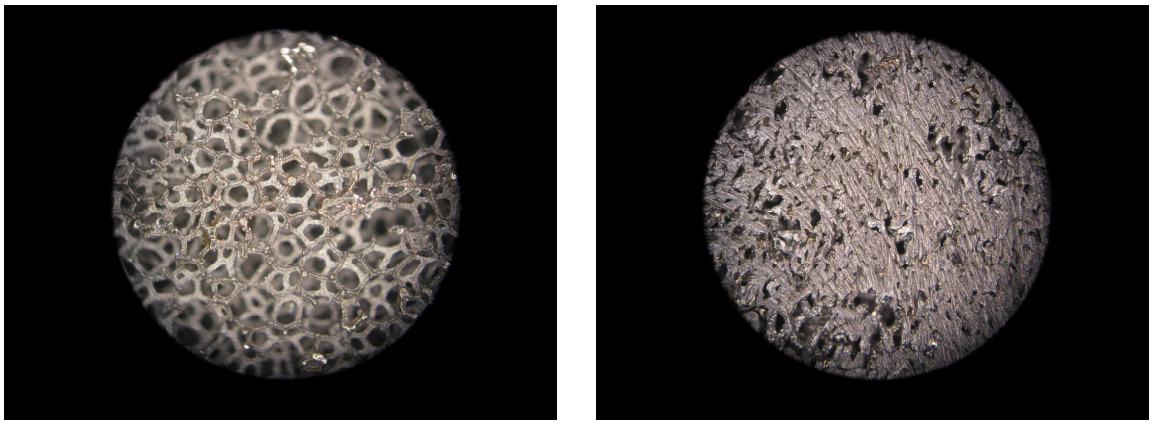

(a) (b)

Figure 1.2 – Trabecular Metal™ (a) before and (b) after machining (magnification 40x)

www.manaraa.com

Currently, electrical discharge machining (EDM) is the preferred method for cutting Trabecular Metal™ (Deglurkar *et al*., 2006). The EDM process removes material by a series of discrete electrical discharges (sparks) produced by a formed electrode tool, these sparks cause localized temperatures high enough to melt or vaporize the metal in the immediate vicinity of the discharge (Groover, 2002). Deglurkar *et al*. (2006) looked at the resulting surface porosity when machining Trabecular Metal™ with a conventional lathe and an electric discharge wire cutting (wire EDM) machine. Wire EDM is a special form of EDM that uses a small diameter wire as the electrode (Groover, 2002). The outcome of their research proved that the wire EDM process caused less smearing upon the TM samples than that left by the lathe. Although good for reducing the effect of smearing, EDM is limited to producing only simple geometric shapes due to the nature of its cutting device.

Because current metal foam machining methods are limited to simple geometries, it is almost impossible to create orthopaedic implants that will consistently fit every patient in need. It could be advantageous for a patient to receive a custom fabricated orthopaedic implant that would better fit into their unique bone structure. An implant that better fits into host bone could create a stronger attachment that could offer more functionality for the patient and reduce the chances of implant loosening (Werner *et al*., 2000). The option for customizable, patient-specific, orthopaedic implants is not commercially feasible at this time but could be of great benefit to any patient requiring such medical attention. With the commercially available orthopaedic implants used today, often orthopaedic surgeons are forced to make necessary implant modifications during surgery, in order to better fit the implant to the patient (Singare *et al.*, 2005). This not only increases the amount of time a patient is in surgery but it may also make the surgery more invasive (Singare *et al.*, 2005).

www.manaraa.com

Orthopaedic surgeons want to minimize the occurrence of both of these situations to promote a quick and successful recovery for the patient.

The work presented in this thesis describes an initial step toward the custom manufacture of patient-specific orthopaedic implants from a variety of biocompatible materials, including Trabecular Metal™. Not only does this work apply to the standard orthopaedic implants manufactured in generic sizes but more importantly those one of a kind, custom bone implants needed to replace bone fracture fragments, bone tumor resections, or other segmental bone defects.

A novel method for machining metal foam is the subject of the research presented in this thesis. This method allows metal foams to be machined using computer numerically controlled (CNC) machining technology without the resultant surface smearing common with current practices. The ability to machine foam in a CNC machining center significantly increases the possibilities of geometric shapes that can be created. This patent-pending process involves infiltrating the stock foam material prior to machining in order to reduce the effect of surface smear left by the cutting process. Upon completion of all necessary machining steps, the infiltrant is removed from the machined part. It is predicted that surface smearing can be reduced by machining with the infiltrant. Utilizing this new process should not only reduce surface smearing but could inhibit machining debris from entering the porous structure during machining.

Through the use of this new infiltration process, CNC machining, and Rapid Prototyping (RP) technology, it may be possible to machine freeform geometric shapes from metal foam while minimizing the effect of surface smearing. The ultimate goal of this research is to determine the optimal machining parameters for milling Trabecular Metal™ in

www.manaraa.com

order to maintain a surface porosity value sufficient for successful osseointegration in orthopaedic surgery. The concept of customizable bone implants begins with the ability to machine custom geometries based on the patient's bone structure. However, the implant must also maintain a sufficient surface porosity to enable osseointegration. The process described here is the first step in making these customizable, patient-specific bone implants become a reality.

The following chapters describe this new machining process in more detail and a set of experiments performed to evaluate the effect of its parameters on surface porosity. Next, the experimental results and an implementation demonstration of the process for a human bone fracture fragment are presented. Finally, conclusions and future research directions are presented in the final chapter.

www.manaraa.com

CHAPTER 2. LITERATURE REVIEW

Metal foams, or cellular solids, are one of the most fascinating and significant engineering materials in existence and this is proven by their expansive list of applications and functionalities. There are many different kinds of cellular solids, some are naturally occurring such as coral, cork, or sea sponge, and others are composed of synthetic materials. Cellular solids are considered any solid that is made up of an interconnected network of solid struts or plates which form the edges and faces of cells (Gibson *et al*., 1988). Foams are known to have many interesting combinations of physical and mechanical properties, such as high stiffness in conjunction with very low specific weight, or high gas permeability combined with high thermal conductivity (Evans *et al*., 1998; Banhart, 2001). One of the most important features of a cellular solid is its relative density, ρ^*/ρ_s; where ρ^* is the density of the cellular material and ρ_s is the density of the solid from which the cell walls are made (Gibson *et al*., 1988). This ratio increases as the cell walls thicken and the pore space shrinks; for example natural cork has a relative density measured at 0.14 and cancellous bone has a relative density of 0.20, if a material's relative density measurement exceeds 0.30, the material is no longer considered a true cellular solid but rather a solid containing isolated pores (Gibson, 1985; Gibson *et al*., 1988). The metal foams subject to this research do not exceed relative densities of 0.30.

Metal foams serve a wide range of functions in many different industries. These include aerospace, automotive, defense, construction, electrical, nautical, biomedical, and the military, among many others (Gibson *et al*., 1988; Ashby *et al*., 2000; Claar *et al*., 2002; Soboyejo *et al*., 2007). A common application for metal foams involves their presence as

www.manaraa.com

cores within sandwich structures; these structures offer high stiffness and low weight while making great aerospace components (Ashby *et al*., 2000; Soboyejo *et al*., 2007). In *Metal Foams: A Design Guide* by Ashby *et al*. 2000, eight case studies are presented describing eight different metal foam applications. One case study explained how aluminum foam structures could be used for automotive body panels; another use involved the installation of a porous metal sound-proofing material along the sides of roads and highways to reduce traffic noise (Ashby *et al*., 2000). Specific metal foam products are manufactured with open- or closed-cell structures and at any type of porosity between (Banhart, 2001). A graph representing different metal foam products and their respective type of cellular structure is shown in Figure 2.1.

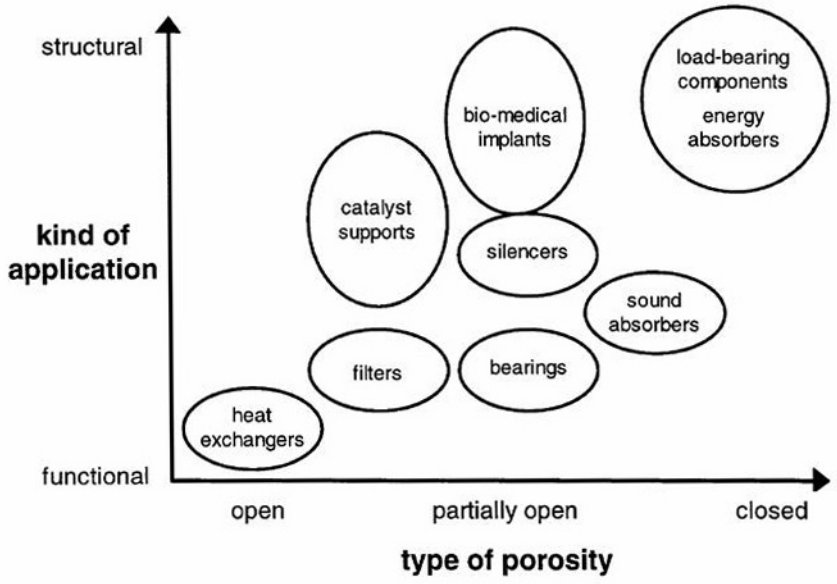

Figure 2.1 – Metal foam application type and their respective cellular structure (Banhart, 2001)

As illustrated in Figure 2.1, depending on the specific application, various degrees of porosity may be required. This range includes the "very open" foam structures capable of

www.manaraa.com

high rate fluid flow used in heat exchangers to those "completely closed" metal foams used in load-bearing structural applications (Banhart, 2001).

In addition to metal foams, many other materials can be foamed, such as polymers, ceramics, glasses, and even composites (Gibson *et al*., 1988). There are many different ways to manufacture foams. These methods vary depending on the material being used, the desired geometry of the cellular structure, or the final function of the metal foam being created. For example, polymer foams are created by introducing gas bubbles into the liquid monomer, allowing the bubbles to grow and stabilize, and then solidifying the sample by cooling (Gibson *et al*., 1988). Glass foams are made in a similar fashion by forcing a blowing agent into molten glass. Porous ceramic is made by infiltrating polymer foam with a slip; when the aggregate is fired, the slip bonds to give an image of the original foam which burns off (Gibson *et al*., 1988).

Metal foams can be manufactured through a variety of processes. These methods include, direct foaming through the creation of gas bubbles within a liquid metal, foaming by gas injection, foaming with blowing agents, solid-gas eutectic solidification, powder compaction, casting around space holders, sintering of metal powders, vapor deposition, and investment casting, among others (Gibson *et al*., 1988; Evans *et al*., 1998; Ashby *et al*., 2000; Banhart, 2001; Deglurkar *et al*., 2006; *Porous Metal Design Guidebook*, 2007). Trabecular Metal™ is manufactured to a controlled structural porosity and metal density through the vapor deposition of tantalum onto a carbon mesh skeleton (Deglurkar *et al*., 2006). The metal is then formed and cut to the desired shape before returning to the vapor deposition reactor to have the final layers of tantalum deposited (Deglurkar *et al*., 2006).

www.manaraa.com

During processing, the carbon skeleton is burned off leaving a purely tantalum, cellular structure.

In *Metal Foams: A Design Guide* by Ashby *et al*., 2000, every aspect of metal foam, from creation and extensive material property examinations, to the cutting, finishing, and joining of such foams is described. Within this text, it has been found that conventional cutting and machining techniques (including band sawing, milling, drilling) cause severe surface distortion or damage to low-density metal foams, such as the porous metals discussed here. Accurate cutting (significantly reducing surface smearing) of metal foam is only possible by EDM, chemical milling, water-jet cutting, or by use of high-speed fly-cutters (Ashby *et al*., 2000). The proposed machining method introduced in this research utilizes a traditional CNC vertical machining center (VMC).

The effect of conventional machining processes on the resulting surface characteristics of Trabecular Metal™ was investigated by Deglurkar *et al.*, 2006. They found that conventional machining, in the form of a lathe, had a dramatic effect on the occlusion of surface pores; the results of their experimentation showed that EDM was the preferred method of cutting TM while reducing surface smearing. To date there has been very little published research focused on the investigation of machining metal foams, especially porous tantalum.

In 2005, Chen *et al.* looked at the combined effects of tool geometry, tool material, work material properties, and machining conditions for the contour turning of porous tungsten. The unique thermal and mechanical properties of this material make it desirable for a wide range of industrial applications, most common being the manufacture of dispenser cathodes (Chen *et al.*, 2005). The objective of this research was to establish a

www.manaraa.com

methodology of predicting smearing and surface defects from measuring cutting edge radii and monitoring cutting forces. Their observations support that tool geometry and cutting edge radius variation are key factors influencing surface smearing (Chen *et al.*, 2005).

Biocompatible porous titanium is often used in orthopaedic applications due to its very low weight, high stiffness, and sufficient material strength (Bram *et al*., 2003). Bram *et al*., 2003, investigated the surface smearing effects of face milling and peripheral grinding titanium foam. These experiments determined optimal titanium foam milling is done with high cutting speeds and low feed per tooth and cutting depths. However, they found that it is quite difficult to machine a surface with an acceptable straightness under these cutting parameters (Bram *et al*., 2003). Silicon carbide grinding wheels were found to outperform corundum grinding wheels when trying to minimize the smearing caused by grinding. Utilizing an up-grinding mode at higher cutting speeds with moderate work piece feeds resulted in comparatively good results (Bram *et al*., 2003).

The following chapters describe am innovative machining process for milling metal foams, specifically porous tantalum in the form of Trabecular Metal™. This material was machined using a Haas, 3-axis CNC vertical machining center. Later on, an implementation demonstration is described that utilizes a manufacturing process planning and execution approach for rapid prototyping and CNC machining, called CNC-RP (Frank, *et al*., 2008). CNC-RP is a rapid machining technology that uses rapid prototyping techniques to manufacture permanent components.

Rapid prototyping is a technology used to create engineering prototypes in the quickest possible lead times based on the computer-aided design (CAD) model of the item at hand (Groover, 2002). This layer-based technology has been around since the late 1980's

www.manaraa.com

and can be divided into two basic categories: (1) material addition processes and (2) material removal processes (Groover, 2002).

Material addition processes involve depositing layers of material upon each other to build the desired shape. These processes utilize a wide variety of materials such as papers, polymers, and some metals. There are many different commercially available examples of RP technologies that make use of material addition such as stereolithography (SLA), 3-dimensional printing (3DP), laminated object manufacturing (LOM), fused deposition modeling (FDM), laser engineered net shaping (LENS), selective laser sintering (SLS), direct metal laser sintering (DMLS), and electron beam melting (EBM).

As opposed to material addition processes, material removal processes involve sequentially removing layers of material from stock to create specific geometric shapes; these processes mainly include milling, turning, and drilling. The use of these processes has been integrated with numerical control in order to expand the complexity of geometric shapes possible. For example, CNC-RP is an example of a material removal machining process. These rapid technologies have served a purpose in a vast number of manufacturing industries and have also been the inspiration for the development of many innovative applications. Traditionally, RP technologies were created for the sole purpose of fabricating prototypes or models, only recently have they been used in the design and manufacture of fully functional products.

RP technology has been the subject of many research endeavors since its inception. More specifically, the use of RP technology and methodologies to machine permanent parts commonly referred to as rapid machining. A novel approach to this concept was introduced with the development of CNC-RP (Frank *et al*., 2002; Frank, 2007; Frank *et al*., 2008). This

www.manaraa.com

research introduced how a 3-axis vertical machining center, with the use of a 4th axis indexer, could be used to RP parts made of a large array of materials with varying material properties. These included materials strong enough to endure post production rigorous performance and failure testing (Frank *et al*., 2002). Having this capability is of great benefit to any manufacturer responsible for the design and development of product.

This concept of rapid prototyping permanent parts has been utilized in the dental and medical implant manufacturing industries for years (Sarment *et al*., 2003; Hieu *et al*., 2005; Singare *et al*., 2005 and 2006; Harrysson *et al*., 2008). Due to the nature of the human body and how its elements are very much unique to the specific individual, it is a constant challenge to fabricate implants that will fit every body type. Due to the layer-based nature of RP technologies, the creation of these unique complex freeform shapes is more feasible.

Two research publications by Singare *et al.* (2005 and 2006) involved the use of CT (computed tomography) and CAD data to create SLA parts. These SLA parts were then used to cast maxillofacial implants from titanium. Maji *et al.*, 2007, used a similar process but instead created a wax model from their SLA interpretation for an investment casting of a craniofacial implant.

There has been little research involving the use of CT data for the manufacture of medical implants via machining of metal. Werner *et al*., 2000, outlined a methodology for the design and manufacture of a custom femur endoprosthesis. Again, in this methodology the CAD data for the specific bone came from a CT scan. From this CT data, a 3D geometric model of the femur was created and used to generate tool paths for a CNC mill. However, the accuracy of the finished product was limited due to their machining process. This part required an elaborate fixing system and only utilized two cutting orientations.

www.manaraa.com

Michele Truscott *et al*., 2007, developed a similar method that involved machining an elbow bone from titanium stock. The machined titanium implant took approximately 104 hours of machining, over eight days (Truscott *et al*., 2007).

The use of the aforementioned CNC-RP technology enables the rapid machining of complex geometries not possible within a traditional 3-axis machining environment. This process allows for the fabrication of organic shapes characteristic of bones and bone fragments. As previously mentioned, bone fragments have already been machined using this rapid machining process from aluminum, ceramic, Delrin® plastic, and Trabecular Metal™. The TM bone fragment will be discussed as a process implementation example in greater detail in Chapter 5.

www.manaraa.com

CHAPTER 3. PROBLEM FRAMEWORK AND SOLUTION APPROACH

Currently, commercially available Trabecular Metal™ is cut into shapes using an electrical discharge machining process. This process is used because it does not smear the material surface (Deglurkar *et al*., 2006). However, this process is limited to the creation of simple shapes, without the ability to fabricate complex, custom geometries. This limitation prevents this process from being used to fabricate the metal foam custom shapes needed to replace bone fracture fragments, bone tumor resections, or other segmental bone defects. This thesis evaluates the possibility of using a new rapid machining approach to create these organic shapes while maintaining the porous characteristics needed for successful osseointegration.

The internal structure of Trabecular Metal™ is composed of a metallic strut configuration similar to that of cancellous bone (Bobyn *et al.*, 1999; Medlin *et al*., 2005). These struts act as cellular walls creating the pores that comprise this metal foam. The cellular structure and bone-like physical and mechanical properties of Trabecular Metal™ make it one of the best material options for use in orthopaedic implants. The porous characteristic of TM allows for a secure implant/bone interface due to its ability to allow adequate blood flow throughout the portion of the implant set within bone. This blood flow enables bone to grow into the Trabecular Metal™, strengthening its bond with the host bone through osseointegration.

Traditional machining techniques lack the ability to maintain adequate surface porosity while cutting metal foam materials. It is proposed that this surface smearing, or pore occlusion, occurs during machining because the cellular walls (composed of metallic

www.manaraa.com

struts in the case of TM) are not strong enough to withstand the machining forces created by the tool. When the rotating tool moves across the cellular surface, the struts collapse, or bend over, closing the open voids. This smearing effect is shown as the tool cuts the porous material in Figure 3.1.

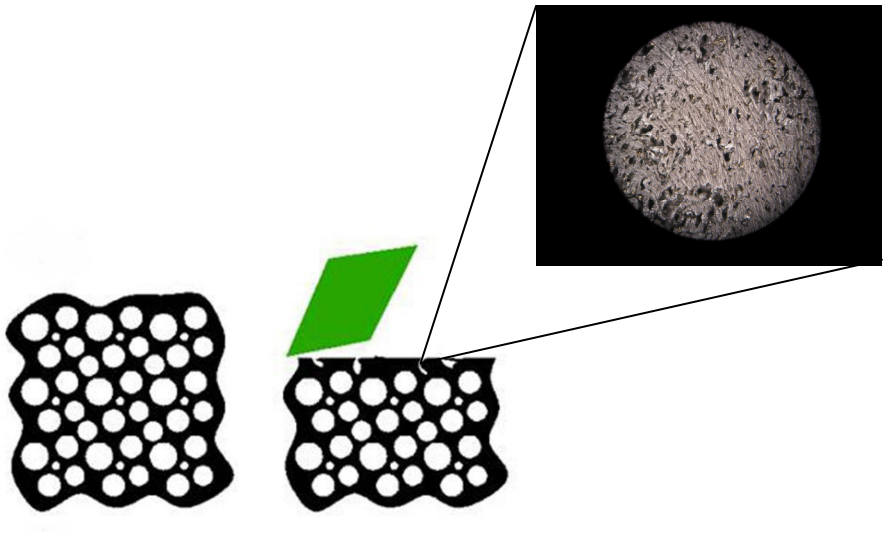

Figure 3.1 – Resultant smeared surface after traditional machining (microscopic image taken at 40x) (Frank, 2008)

At a microscopic level, this phenomenon looks much like a cantilevered beam experiencing a load upon its unsupported end. In Figure 3.2, the machining force created by the tool is represented by the load, P and travels in the same direction as the tool path. In order to maintain equilibrium, there is a resultant shear force and moment about the cantilevered end; these are represented by V_R and M_R, respectively (Patnaik, 2004; Huston, 2008). When the machining force is greater than the opposing shear force and moment, the strut (or beam) begins to bend; this bending motion creates a stress upon the struts of

www.manaraa.com

tantalum material. When this stress exceeds the material yield strength, plastic deformation occurs and results in permanent pore occlusion.

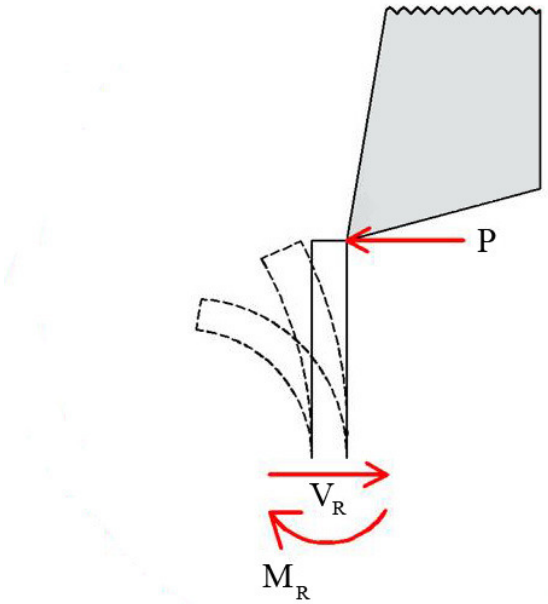

Figure 3.2 – The bending of a pore wall approximated by the bending of a cantilevered beam

Owing to the temperature of the machining environment while being cut, the struts experience ductile fracture when they fail. This is due the body centered cubic crystal structure of pure tantalum (Callister, 1994). Different cooling agents used in this research are discussed later on in this chapter; one includes liquid nitrogen capable of reaching temperatures as low as -196°C. It was initially thought that while machining with the use of this coolant, the pure tantalum material would reach its ductile brittle transition temperature of -195°C causing the struts to experience brittle fracture when cut (Schwartz, 1995). However it was determined that the tantalum would never reach its transition temperature

www.manaraa.com

point due to conduction. Within the machine, the 0.5 inch diameter sample was held in a steel collet with a combined mass of approximately 0.91 kg. Due to this massive machining fixture, the small amount of tantalum being cut does not reach its transition temperature of -195°C. The cooling process is discussed in more detail later on.

In order to machine metal foam without pore occlusion something must be done to inhibit the cellular struts from bending. The new machining process described here suggests that providing a form of resistance to oppose the cutting forces could reduce smearing. This resistance is provided by introducing an infiltrant material within the cellular structure of the metal foam. This material fills the void space (pores) and acts as a structural member, stiffening the framework of the metal foam while still being cut by the tool. When the tool cuts through the infiltrated foam, the cellular struts are braced by the infiltrant opposing the cutting forces and they remain or return to their upright position after being cut. The infiltrant also inhibits any kind of cutting debris, coolant, oils, or other contaminants to enter the cellular structure of the foam during machining. After the cut has been made, the infiltrant material is then removed. The use of this infiltrant during machining and its resulting surface porosity is illustrated in Figure 3.3.

www.manaraa.com

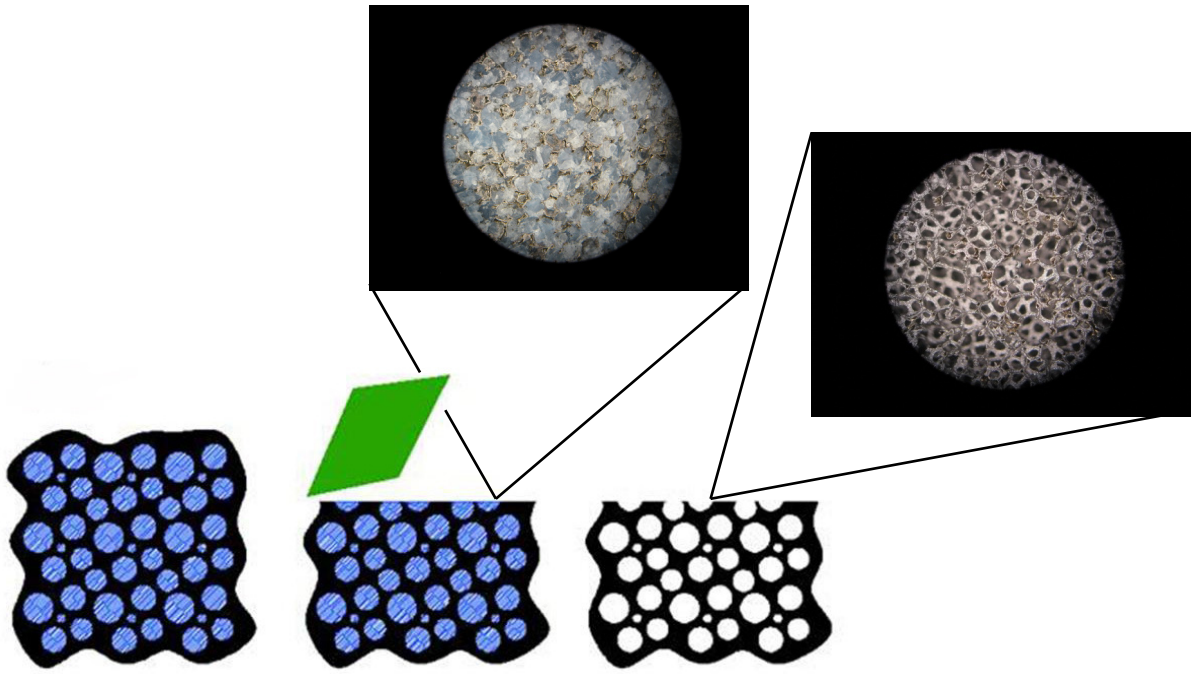

Figure 3.3 – Infiltration and machining process sequence: (a) foam is infiltrated, (b) infiltrated foam is cut, (c) infltrant is removed from foam resulting in porous surface (microscopic image taken at 40x) (Frank, 2008)

This infiltration process has been previously described in a patent application (Frank, 2008). Preliminary experimentation of this process has not yet determined optimal machining parameters to reduce surface smearing, which will be addressed in this thesis. This infiltration method is applicable to many machining processes and porous materials but the research presented here focuses only on its use milling Trabecular Metal™ in a CNC vertical machining center.

The infiltrant material investigated in this thesis is limited to machinable wax, although the process has been previously tested with both paraffin and machinable epoxy. The infiltration process entails submerging the stock material into molten wax and then

www.manaraa.com

placing it in a vacuum environment. This ensures that there are no voids in the molten wax and that the stock material is completely infiltrated. Once the wax has hardened, any excess wax is removed before the infiltrated stock material is ready to be machined.

The purpose of using this infiltration method is that it enables the use of CNC machining technologies to fabricate freeform geometric shapes in metal foam without causing significant surface smearing. Applying this method to rapid CNC machining technology allows for the creation of such shapes that could be used to replace segmental bone defects that are caused by traumatic fracture or bone loss due to tumor resection. The implementation section describes the use of this infiltration process to machine a bone fracture fragment from two biocompatible foam materials. The bone fragments were cut using a Subtractive Rapid Prototyping (SRP) approach to the manufacturing process planning and execution called CNC-RP (Frank *et al*., 2008). Rapid prototyping using CNC machining, or CNC-RP, is a fully functional SRP system that can automatically generate process parameters including all numerical control (NC) code for creating a part, directly from a CAD file (Frank *et al*., 2004 and 2008).

The CNC-RP process used in this research begins after the foam has been infiltrated, with the analysis of a part's CAD data. The results of this analysis automatically determine all aspects of process planning for rapid machining the part, including tool path planning, tool geometry selection, machining setup orientations, and all necessary support fixturing geometry (Frank *et al*., 2004). The actual machining of the part is a layer-based, material removal process that creates geometries with an end mill from calculated cutting orientations about the axis of material bar stock. This bar stock is fixed in a 4th axis indexer and tailstock within the VMC which rotates the bar of material to the specific cutting

www.manaraa.com

orientations required to machine all necessary geometry. CNC-RP calculates the minimum number of machining orientations to create all necessary geometry, including any sacrificial support structures (Frank *et al*., 2004). For example, a toy jack was machined using CNC-RP and it was determined that all surfaces could be machined from four cutting orientations. This meant that the machining process started with the bar stock set at the first orientation while an end mill cut material. When all of the necessary material had been removed from that angle, the bar stock rotated to its next orientation where machining presumed. This cycle was repeated three more times until all necessary material was removed to create the part. This rapid machining process example is illustrated in Figure 3.4 with the setup and processing steps taken to machine a toy jack.

www.manaraa.com

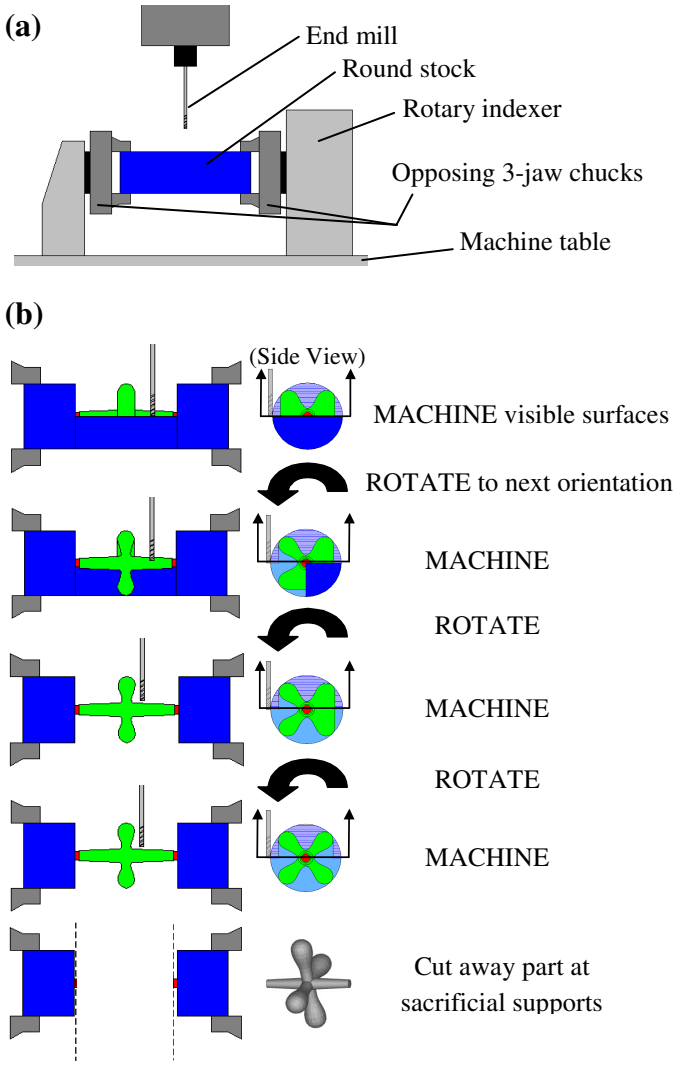

Figure 3.4 – CNC-RP rapid machining (a) set up and (b) processing steps for machining a toy jack (Frank *et al.*, 2008)

The use of CNC-RP technology is an essential tool in achieving the ability to machine custom orthopaedic implants from metal foam. This rapid machining technology was used to machine all of the bone fragments discussed in the implementation section.

While the material is being cut, the physical properties of the infiltrant can be affected by the heat created from machining. This heat softens the wax and weakens its

www.manaraa.com

resistance to the cutting forces. To counter this problem, a cooling agent is introduced to maintain the infiltrant material hardness during machining. This agent is applied to the stock material for an amount of time before cutting begins and then continues to cool until the machining process is complete. The cooling agents used in this research are a commercially available freezing spray, Cyto-Freeze™, and liquid nitrogen applied using a portable spraying unit.

After machining geometry from all necessary cutting orientations, the part is removed from the indexer and then heated so that the remaining infiltrant can be removed through melting and wicking. When most of the wax has exited the part, the residual traces can be removed with steam (at 35.0 psia or higher). When the part is rid of all residual infiltrant, the part is dried and then ready for use barring any other necessary post processing sterilization steps.

Much like traditional CNC milling, machining at specific feed rates and spindle speeds will affect the resulting surface finish. In this case, it is not so much important to maintain a certain aesthetic quality but rather to maintain the functionality of the cellular structure. The feeds, speeds, and machining temperatures evaluated in this research were chosen to maintain the solid state of the infiltrant during machining in order to eliminate cell wall collapse. At this time there is little to no published research that suggests such optimal machining parameters to maintain these conditions for metal foams, thus this is a main objective of this research endeavor.

For the purpose of the experiments described in this thesis, two types of machinable wax were chosen due to their prevalent use in industry. The two waxes are commercially available through McMaster-Carr and carry a hardness rating of Shore 50D and 52D

www.manaraa.com

(www.mcmaster.com). The two waxes used for the infiltration process will be referred to as "hard" and "very hard," with hardness ratings of 50D and 52D, respectively. The hard wax begins to soften around 105°C (222°F) while the very hard wax will begin to melt at approximately 117°C (244°F). Preliminary machining experiments involved using Paraplast™ tissue embedding medium. This paraffin wax offered a significantly lower softening temperature and hardness rating.

Three machining temperatures were investigated while milling Trabecular Metal™, these included 21°C (room temperature, 69°F), -51°C (-59°F), and -196°C (-320°F). Technically, the trials ran at -196°C are considered to be in a cryogenic machining environment. The two colder temperatures were reached using Cyto-Freeze™ spray (-51°C) and liquid nitrogen (-196°C) applied with a Brymill CRY-AC® cryosurgical device. Each sample was sprayed incessantly for 30 seconds prior to starting the milling machine. After 30 seconds, the machine was started and the sample was continuously sprayed while the tool approached and cut through the material.

It is predicted that the use of this infiltration process will reduce the effect of surface smearing while machining Trabecular Metal™. The following chapter provides a detailed description of the experimental design and testing results conducted for this thesis. Through these experiments, the following hypotheses were tested:

www.manaraa.com

1. The use of the infiltrant method while machining Trabecular Metal™ will result in reduced surface smearing
2. Feed rate has a significant effect on the amount of surface smearing that occurs during machining
3. Tool wear will increase the effect of surface smearing
4. Using a cooling agent to maintain infiltrant hardness during machining will result in reduced smearing effect

The results of this hypothesis testing will provide insight as to how machining parameters affect the surface smearing of Trabecular Metal™ during milling. This insight will help define optimal parameter settings to reduce smearing when machining metal foams in the future.

www.manaraa.com

CHAPTER 4. SURFACE POROSITY ANALYSIS

In order to compare the surface porosity before and after machining, a method of measurement was developed. This method quantified the degree to which surface smearing took place as a result of machining. A statistically sound quantity of samples was taken in order to ensure an accurate representation of the effect various combinations of machining parameters had on the resulting surface porosity. A series of cutting experiments was conducted examining the combination of different infiltrant hardness ratings, machining temperatures, and feed rates. The different machining parameters investigated are listed in Table 4.1.

Table 4.1 – Investigated machining parameters

	Infiltrant Hardness	**Temperature (°C)**	**Feed Rate (IPM)**
Low	Hard	-196	10
High	Very Hard	-51	40

Over the course of this research, a number of different machining experiments were conducted, resulting in over 200 data points averaged from approximately 600 individual surface porosity measurements. These tests exposed many characteristics of the machining parameters and their effect on surface smearing. As these characteristics were revealed, their results were used to design subsequent tests until there was sufficient data to support an experimental design. These preliminary experiments determined the first hypothesis true in that use of the infiltrant method while machining Trabecular Metal™ did result in reduced surface smearing. The machining example illustrated in Figure 4.1 shows that there is an increase in pore occlusion when machining TM without infiltrant over time.

www.manaraa.com

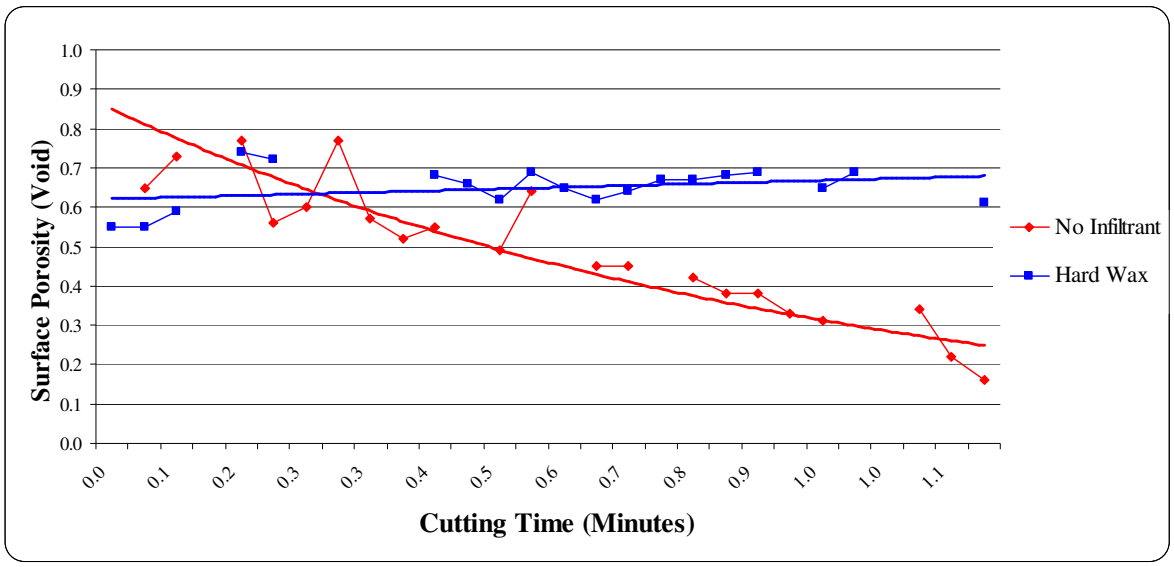

Figure 4.1 – The effect of surface smearing when using the infiltrant method

It is also seen in this machining experiment that when using the infiltrant method, the surface porosity maintained an average value of approximately 65%. Unprocessed TM carries a nominal surface porosity measurement between 70 – 85% (Bobyn *et al.*, 1999; Callaghan *et al.*, 2006; Levine *et al.*, 2006; Levine *et al.*, 2008; Medlin *et al.*, 2005; Voort *et al.*, 2004). In this example, the infiltrant method allowed machining to occur without significant pore occlusion; the surface porosity of the Trabecular Metal™ decreased about 10 – 15% over one minute of machining. After many different experiments, investigating various combinations of machining parameters, a design of experiments was developed to make certain accurate data was collected to permit objective analysis.

www.manaraa.com

4.1 2^3 full factorial design of experiments

A 2^3 full factorial design of experiments was utilized in order to ensure the statistical accuracy of the results. This design of experiments considered three different machining parameters, or factors, (infiltrant hardness, temperature, and feed rate) at two different levels (low and high), as shown in Table 4.1. The benefit of using a 2^3 full factorial design is that it allows for several factors to be evaluated in a feasible number of experiments (Vardeman *et al*., 1999). These factor values were chosen after a significant amount of evaluation through preliminary machining experiments; many preconceived ideas of how these parameters would affect surface smearing were amended after analyzing the results of these preceding tests. Successive experiments were then designed based on the knowledge gained to make certain only the most relevant machining parameters and their settings were investigated.

4.1.1 2^3 full factorial machining experiment methodology

A 2^3 full factorial design of experiment generated the specific machining trials to perform as well as their order. Multiple combinations of parameters were tested in each trial of the experiment. The trials shown in Table 4.2 were first randomized to ensure the elimination of any non-experimental variables or ambient conditions impacting the response (Vardeman *et al*., 1999). It was determined that upper and lower control limits for all collected data would be calculated at two standard deviations above and below the grand mean of a data set (Warner, 2007). Any recorded values outside of this range would be considered outliers and eliminated from further statistical analysis. It is generally suggested to calculate control limits at three standard deviations away from the mean; however for the

www.manaraa.com

purpose of this research it was decided that two standard deviations would induce a greater control on the process and reduce variability (Ratliff, 2003).

Table 4.2 – 2^3 full factorial experimental conditions

Trial	Infiltrant Hardness	Temperature (°C)	Feed Rate (IPM)
1	Hard	-196	10
2	Very Hard	-196	10
3	Hard	-51	10
4	Very Hard	-51	10
5	Hard	-196	40
6	Very Hard	-196	40
7	Hard	-51	40
8	Very Hard	-51	40

Each of these factors were fitted with their low and high values and arranged in a manner that considered all possible combinations. All trials were run at a spindle speed of 1000 rotations per minute (RPM), a value determined as a result of preliminary analysis. Two replications of this experiment were run for a total of 16 machining trials and then the results were analyzed in an Analysis of Variance (ANOVA) study. This ANOVA study will be discussed in greater detail later on in this chapter.

www.manaraa.com

4.2 Infiltration process methodology

The 2^3 full factorial machining experiment started with infiltrating two lengths of 0.5 inch diameter bar stock of Trabecular Metal™. One length of TM was infiltrated with hard wax and the other with very hard wax; despite differences in infiltrant material hardness, both samples endured the same infiltration process steps.

The infiltration process began with melting the wax in a metal container upon a hot plate. A sample of TM was then placed in this container of wax so that one end (an approximate 0.75 inch long section) was submerged in molten wax. The container and sample were then removed from the hot plate and placed in a vacuum at 25 in. Hg. for approximately 5 minutes. This removed all residual air bubbles from the molten wax and ensured that the TM sample was completely infiltrated. When all of the air had been evacuated from the molten wax and sample, the container and sample were removed from the vacuum environment and left at room temperature to solidify. Once hardened, the sample was removed from the wax and any excess was removed. Finally, in order to keep the cuts consistent from trial to trial, the infiltrated TM sample was fixed in a collet with a rectangular body. The collet's rectangular body enabled it to be held in a vise where it acted as a machining fixture.

4.3 Machine setup and cutting methodology

In order to ensure a consistent experimental process, a cutting methodology was developed. During each machining trial, individual cuts were made across the width of the 0.5 inch diameter sample; this configuration is illustrated in Figure 4.2. The rectangular

www.manaraa.com

collet was clamped into a Chick™ vise with its axis positioned along the x-axis of a Haas 3-axis VMC. This allowed for the tool to make a perpendicular cut along the y-axis.

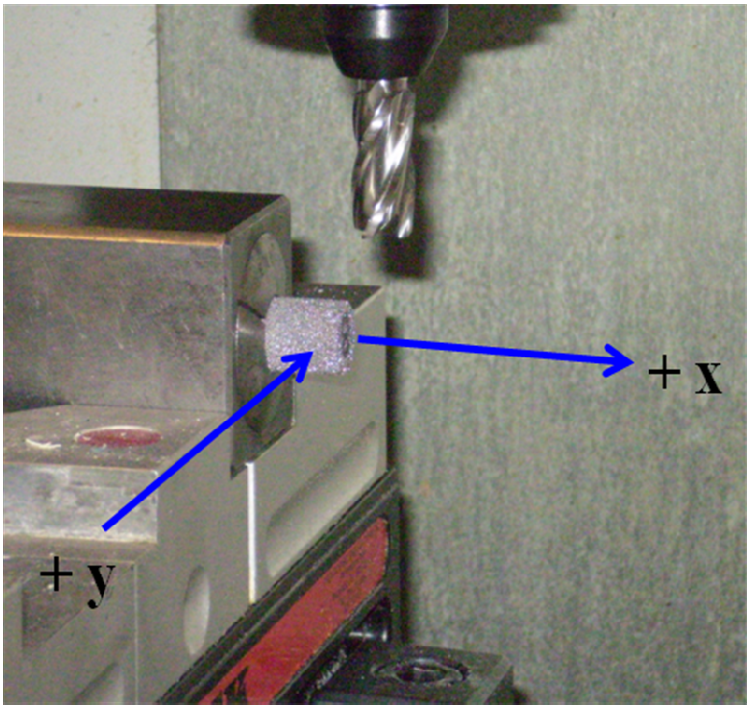

Figure 4.2 – Machining setup showing tool movement along the y-axis

A four flute, 0.5 inch diameter HSS (high speed steel) uncoated end mill was used to make all cuts. A small NC program was inputted to control the movement of the tool as it passed along the subject material at varying feed rates. Prior to running the code, the tool was positioned so that it would cut a 0.25 inch wide (a distance equal to the tool radius) cross section of the material at a cut depth of 0.02 inches. This ensured that a consistent amount of material was removed each time a cut was made. An illustration of this tool positioning is shown for the example cut in Figure 4.3.

www.manaraa.com

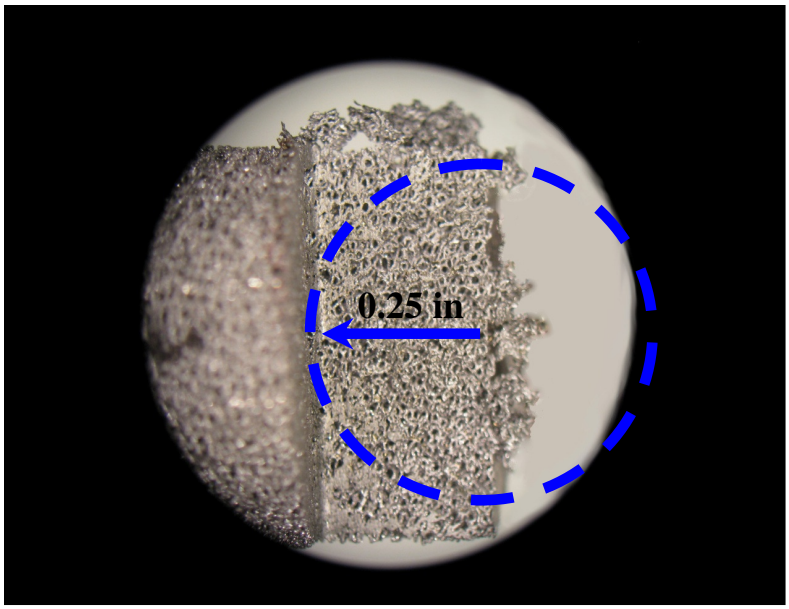

Figure 4.3 – Tool cutting position for an example cut (magnification at 25x), the dashed line represents the tool diameter

At a spindle speed of 1000 RPM, feed values were calculated for the four flute tool when ran at feed rates of 10 IPM and 40 IPM, these resulted in 0.0025 in/tooth and 0.01 in/tooth, respectively. To give an idea of how much foam material this is removing as each flute cuts through, it was found that the strut thickness for TM at an average porosity of 77.5% (average of nominal range) is approximately 0.005 inches (Shimko *et al.*, 2005). This strut thickness is twice the feed value ran at 10 IPM and half that ran at 40 IPM.

When a trial called for some form of cooling, the sample was sprayed with either Cyto-Freeze™ or liquid nitrogen for a 30 second period prior to the start of the NC program. After this time period passed, the machine was started while the sample was continuously sprayed as the tool cut through the material.

www.manaraa.com

4.4 Machined surface data collection and analysis

A surface porosity measurement was recorded for every cut made. After each cut was made, the collet was removed from the Chick™ vise and taken to a station to be examined under a microscope. An Olympus™ SZX12 microscope was used for all microscopic examinations. These magnified views were captured with a Canon™ PowerShot S5IS digital camera attached to the microscope with an Alexis™ Scientific Digital Camera Microscope Adaptor. The camera communicated to a DELL™ Optiplex GX280 (Intel™ Pentium4 processor) with Canon™ EOS Utility software. This software allowed for remote control of camera settings, zoom, image capture, and a limited collection of image processing capabilities. All images used in this research were taken at a magnification of 40x, an example of uncut Trabecular Metal™ at this magnification is shown in Figure 4.4.

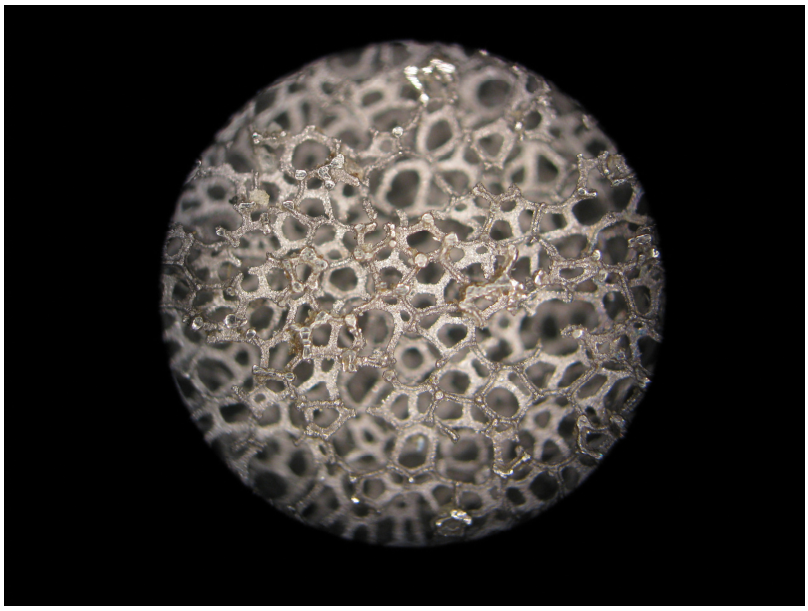

Figure 4.4 – Microscopic image of fresh TM taken at 40x magnification

www.manaraa.com

Three images were taken at different locations about the surface of every cut, these locations were evenly spaced across the surface to ensure a comprehensive capture of data and are illustrated in Figure 4.5.

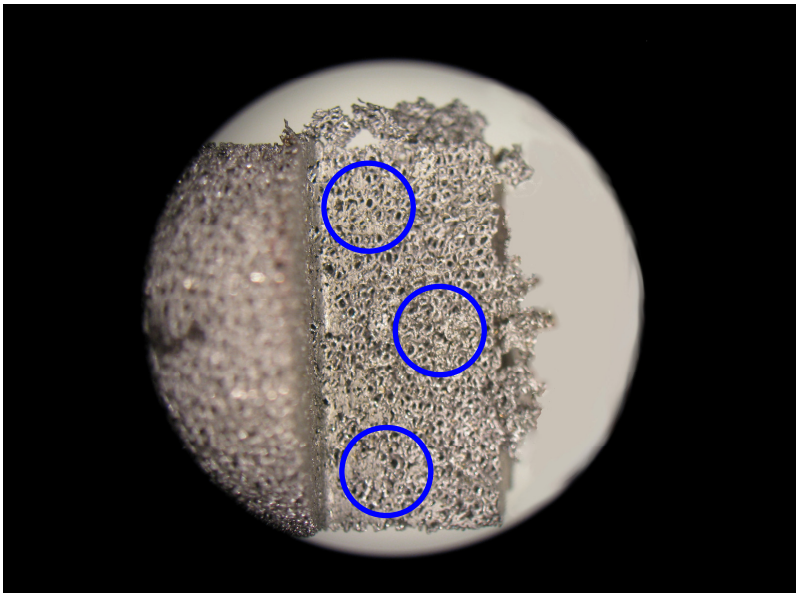

Figure 4.5 – Locations of microscopic images on the cut surface (magnification of 25x)

4.4.1 Reticle analysis methodology

After image capture was complete, the image data were inputted to Adobe™ Photoshop so that a reticle analysis could be performed. Within Photoshop, ten vertical and ten horizontal guide lines were imposed atop the image at equal spacing to create a grid, or reticle, as demonstrated in Figure 4.6.

www.manaraa.com

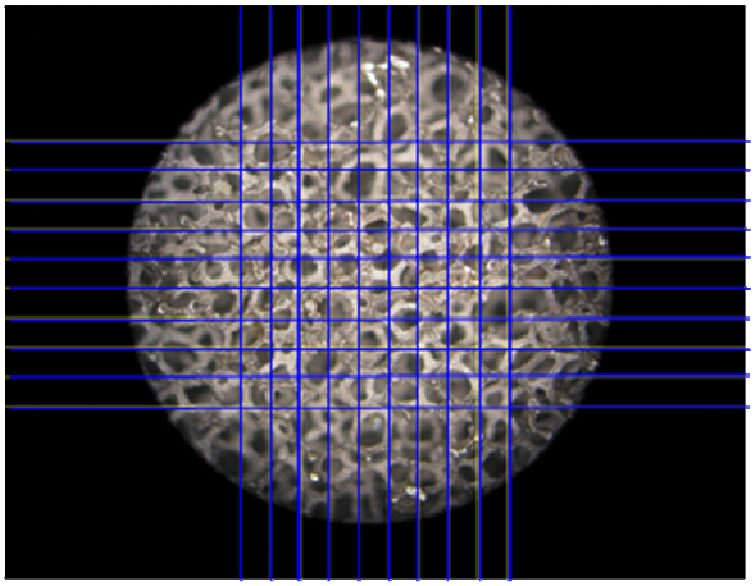

Figure 4.6 – Unprocessed TM with reticle grid imposed atop microscopic image

The intersections of the guide lines made up 100 data points to be analyzed. Intersections above open voids were counted and recorded. After all 100 points had been analyzed, a ratio was calculated to determine surface porosity as a percentage of void space.

$$Surface\ Porosity = \frac{\#\ of\ intersections\ above\ void\ space}{100}$$

For every cut, three images were taken, fit with a reticle, and surface porosity measurement recorded. The average of these three measurements was documented as the final surface porosity score for that specific cut.

The reticle analysis quantifies the amount of surface smearing that has occurred in the form of a measurement of surface porosity. A greater presence of pore occlusion

www.manaraa.com

corresponds to a lower surface porosity measurement, as this is a ratio of pore space to metal. Unprocessed Trabecular Metal™ has a nominal surface porosity of approximately 70 – 85% (Bobyn *et al*., 1999; Callaghan *et al.*, 2006; Levine *et al*., 2006; Levine *et al*., 2008; Medlin *et al*., 2005; Voort *et al*., 2004). If a machining process does not induce surface smearing, the surface porosity of a cut sample should also be between 70 and 85%.

Alternative approaches to measuring surface porosity initially involved the use of ImageJ™ image processing software. One function of ImageJ™ allows the user to calculate the area of user defined selections of an image. An image of a cut could be enhanced to make the contrast between areas comprised of metal and those comprised of void space more discernable before calculating their respective areas. However even after enhancement, the contrast between metal and pore space of cuts filled with wax was not sufficient to distinguish boundaries, thus resulting in inaccurate area calculation. This problem could be avoided by painting over in white the metal locations in the image before calculating the areas, resulting in more distinct boundaries. However, this process was very tedious and deemed infeasible considering the hundreds of measurements taken in this study. After considering all measurement alternatives, it was found that the previously described reticle analysis would be a sufficient method of measuring surface porosity.

4.5 Comprehensive tool wear analysis methodology

In addition to the three factors investigated in the 2^3 full factorial analysis, tool wear was also a variable evaluated in this research; previous research endeavors have found that tool wear and cutting edge geometry variation can influence surface smearing during machining (Bram *et al*., 2003; Chen *et al.*, 2005). An objective of this work was to

www.manaraa.com

determine how tool wear would influence the surface porosity of TM during machining. In order to evaluate this effect on surface smearing, the 2^3 full factorial machining experiment described previously was performed with two different tools. Two previously unused tools were subject to a number of cuts in order to create different amounts of tool wear for each end mill. Over the course of 211 cuts, one tool sustained approximately 1.83 minutes (55 cuts) of cutting while the other endured approximately 5.32 minutes (156 cuts). Because these two tools were exactly alike, the collected data provided an indication of how a tool would affect surface porosity throughout its life.

The 2^3 full factorial experiment was first conducted with a "new" tool after approximately 1.39 minutes of cutting experience. Then a second experiment was performed using a "worn" tool that had incurred approximately 4.95 minutes of cutting time. For clarity in this thesis, the new tool will be referred to as Tool A and the worn tool, Tool B. This allowed for a comprehensive comparison of how the three factors would influence surface porosity between using a relatively new tool and one that had experienced significant tool wear. The benefit of this analysis is that it provided an indication of when in a tool's life certain factors would have a significant effect on surface porosity, if any.

4.6 2^3 full factorial machining experiment results

Both machining experiments were conducted using a randomized order of the parameter combinations shown in Table 4.2. Images were taken after each cut and then a reticle analysis was performed to calculate a surface porosity measurement for the cut resulting from each parameter combination. Two replications of the experiment were run with Tool A and Tool B for a total of 32 data points. The results of the experiments run with

www.manaraa.com

a new tool and a worn tool are shown in Table 4.3 and Table 4.4, respectively. The total amount of cutting time each tool has endured at the time of each cut is also recorded for each cut. The amount of cutting time accrued during this 2^3 full factorial experiment was approximately 0.44 minutes for Tool A and 0.37 minutes for Tool B. The difference between these two times is the amount of time it took to make four cuts with Tool A devoid of infiltrant to represent a control group. However, after the cuts were made it was found that the 2^3 full factorial analysis did not consider a control group

www.manaraa.com

Table 4.3 – 2^3 full factorial machining experiment results with Tool A

Trial	Infiltrant Hardness	Temperature (°C)	Feed Rate (IPM)	Cumulative Cutting Time (Min)	Average Surface Porosity (Void)
1	Hard	-51	10	1.39	0.73
5	Hard	-51	40	1.40	0.81
7	Hard	-196	40	1.41	0.76
6	Very Hard	-51	40	1.42	0.82
8	Very Hard	-196	40	1.43	0.81
2	Very Hard	-51	10	1.50	0.74
4	Very Hard	-196	10	1.55	0.74
3	Hard	-196	10	1.59	0.66
1	Hard	-51	10	1.63	0.67
5	Hard	-51	40	1.64	0.87
7	Hard	-196	40	1.65	0.83
6	Very Hard	-51	40	1.66	0.84
8	Very Hard	-196	40	1.67	0.84
2	Very Hard	-51	10	1.75	0.76
4	Very Hard	-196	10	1.79	0.71
3	Hard	-196	10	1.83	0.70

www.manaraa.com

Table 4.4 – 2^3 full factorial machining experiment results with Tool B

Trial	Infiltrant Hardness	Temperature (°C)	Feed Rate (IPM)	Cumulative Cutting Time (Min)	Average Surface Porosity (Void)
5	Hard	-51	40	4.95	0.69
1	Hard	-51	10	4.98	0.38
2	Very Hard	-51	10	5.02	0.36
7	Hard	-196	40	5.03	0.65
5	Hard	-51	40	5.04	0.69
2	Very Hard	-51	10	5.08	0.38
4	Very Hard	-196	10	5.12	0.36
1	Hard	-51	10	5.16	0.32
3	Hard	-196	10	5.20	0.36
4	Very Hard	-196	10	5.24	0.45
6	Very Hard	-51	40	5.24	0.69
8	Very Hard	-196	40	5.25	0.64
8	Very Hard	-196	40	5.26	0.66
3	Hard	-196	10	5.30	0.40
7	Hard	-196	40	5.31	0.61
6	Very Hard	-51	40	5.32	0.58

As shown in Table 4.3, the second replication of Trial 5 resulted in a surface porosity score of 87%, which exceeds the nominal surface porosity range of unprocessed TM by 2%. The reason for this discrepancy is subject to further investigation; however the value still falls within two standard deviations (±2σ) of the mean so it was still within statistical control

www.manaraa.com

and therefore included in the analysis. This was true for all surface porosity values recorded for both Tool A and Tool B.

In order to ensure that the results recorded from Tool A are different than those recorded from Tool B a *t*-test was conducted; this *t*-test assumed that the two data sets came from distributions with unequal variances. A mean surface porosity value was calculated for Tool A and Tool B that resulted in 0.77 and 0.51, respectively. The *t*-test results are shown in Table 4.5.

Table 4.5 – *t*-test results

	Tool A	**Tool B**
Mean	0.768	0.514
Variance	0.004	0.022
Observations	16	16
Hypothesized Mean Difference	0	
df	21	
t Stat	6.3	
P(T<=t) one-tail	0.000002	
t Critical one-tail	1.721	
P(T<=t) two-tail	0.000003	
t Critical two-tail	2.080	

As shown in Table 4.5, the *p*-value (*P(T<=t)*) resulted in 0.000003. This value is significantly lower than 0.05 so there is in fact a statistically significant difference in means between Tool A and Tool B. It is understood that *p*-values less than 0.05 are considered to be significant (Adams, 2003; *Analyzing Two Level Experimental Designs Video*, 2009). The benefit of this analysis is that the results ensure that there is a statistical difference in Tool A and Tool B, and that their resulting surface porosity values do indicate a difference in tool wear.

www.manaraa.com

After all 16 cuts had been made for both machining experiments, it was determined that the resulting tool wear from these cuts was negligible for both tools. Any tool wear created during the 22 seconds (0.37 minutes) of machining for these 16 cuts did not influence the surface porosity of the Trabecular Metal™ during this machining experiment.

4.7 Analysis of Variance (ANOVA) methodology

After completing all of the machining trials with both Tool A and Tool B, further statistical analysis was conducted on the results to determine fitted main effects of the individual factors, two-factor interactions and combinations of pairs of factors, and interactions and combinations of all three factors. This exposed how infiltrant hardness, temperature, and feed rate interacted with each other to influence the resulting surface porosity.

An ANOVA study was conducted to determine the significant effects of different arrangements of parameters, as well as the effect of each parameter alone. This was done with a supplementary software package within Microsoft™ Excel called SPC for Excel™. This statistical process control software package calculated all of the necessary values to determine which factors, or combination of factors, affected surface smearing based on the recorded surface porosity results shown in Table 4.3 and Table 4.4 (Appendix 1).

www.manaraa.com

4.7.1 ANOVA results – Tool A

Within the ANOVA analysis, the three experimental conditions investigated were referred to as Factors; Factor A corresponds to infiltrant hardness, Factor B is temperature, and Factor C refers to feed rate. Upon completion of the ANOVA, effect results were calculated for the following factors and combinations of factors: *A*, *B*, *C*, *AB*, *AC*, *BC*, and *ABC*. Values for overall means (*Overall*), differences in means (*Difference*), effects, and sum of squares (*SS*) were calculated for each factor or combination. A minimum significant effect (*MSE*) was also calculated based on these values, any factor or combination of factors with an effect value greater than the *MSE* was considered a significant effect (*Analyzing Two Level Experimental Designs Video*, 2009). The ranges for all ANOVA results when using both Tool A and Tool B were found to be within statistical control, meaning there were no outliers as a result of the ANOVA that needed to be considered (*Analyzing Two Level Experimental Designs Video*, 2009). The ANOVA results for the experiment ran with Tool A are discussed first and begin with Table 4.6.

Table 4.6 – All factor analysis results for machining experiment when using Tool A

	Mean	A	B	C	AB	AC	BC	ABC
Sum +	6.145	3.130	3.120	3.290	3.055	3.035	3.075	3.050
Sum -	0.000	3.015	3.025	2.855	3.090	3.110	3.070	3.095
Overall	6.145	6.145	6.145	6.145	6.145	6.145	6.145	6.145
Difference	6.145	0.115	0.095	0.435	-0.035	-0.075	0.005	-0.045
Effect	0.768	0.029	0.024	0.109	-0.009	-0.019	0.001	-0.011
SS		0.003	0.002	0.047	0.000	0.001	0.000	0.001
MSE	**0.042**							

Factor A = Infiltrant Hardness
Factor B = Temperature
Factor C = Feed Rate

www.manaraa.com

As shown in Table 4.6, feed rate (Factor C) was found to be a significant effect with an effect value of 0.109 ($Effect_C = 0.109 > MSE = 0.042$). This conclusion is validated when looking at the ANOVA results that calculated *p*-value. As previously stated, it is understood that factors with *p*-values less than 0.05 are considered to be significant effects (Adams, 2003; *Analyzing Two Level Experimental Designs Video*, 2009). Those with *p*-values between 0.05 and 0.20 may or may not be significant and further investigation is recommended (Adams, 2003; *Analyzing Two Level Experimental Designs Video*, 2009). The *p*-value results for the experiment ran with Tool A are displayed in Table 4.7.

Table 4.7 – *p*-values calculated for all factors and combinations using Tool A

Factor	***p*-value**
A	0.1093
B	0.1750
C	0.0001
AB	0.5985
AC	0.2738
BC	0.9395
ABC	0.5009

In reference to the *p*-value analysis, it was also concluded that infiltrant hardness and temperature (Factors A and B, respectively) may or may not have a significant effect on surface smearing. *P*-values for both infiltrant hardness and temperature were within the range of $0.05 < p < 0.20$, at 0.1093 and 0.1750, respectively.

When analyzing the percent contribution to the total sum of squares for all parameters and their combinations, it was found that feed rate had the greatest contribution.

www.manaraa.com

It should be noted that the contributions from infiltrant hardness and temperature are not negligible but they do fall within the 12.89% contribution from error. This means there is a possibility that one or both of these factors may not be significant and that their contribution is a result of inherent error (*Analyzing Two Level Experimental Designs Video*, 2009). The contribution results are shown in Table 4.8.

Table 4.8 – Contribution to sum of squares using Tool A

Factor	Contribution to Sum of Squares (%)
A	5.23
B	3.57
C	74.80
AB	0.48
AC	2.22
BC	0.01
ABC	0.80
Error	12.89
Total	100.00

A second ANOVA was run with this data that only included infiltrant hardness and temperature. This was done to observe the contribution of only these two factors; however their values did not change from analysis results shown in Table 4.8. Their contribution to the sum of squares remained at 5.23% and 3.57%, again within the 12.89% contribution from error value. Further analysis would be necessary to determine if these two factors are

www.manaraa.com

in fact significant, however this was outside the scope of this research. The ANOVA results considering only infiltrant hardness and temperature are displayed in Appendix 9.

Another way of analyzing the results from ANOVA is the use of effects charts. These visually depict the effect of the factor's interactions on the response. Figure 4.7 shows the individual main effects (infiltrant hardness, temperature, and feed rate) and the resulting average surface porosity values at their low and high parameter settings. The greater the change of magnitude in response values (demonstrated by the slope of a line, be it positive or negative) between the low and high parameter setting, the more significant impact the factor interaction has on the response (*Analyzing Two Level Experimental Designs Video*, 2009).

www.manaraa.com

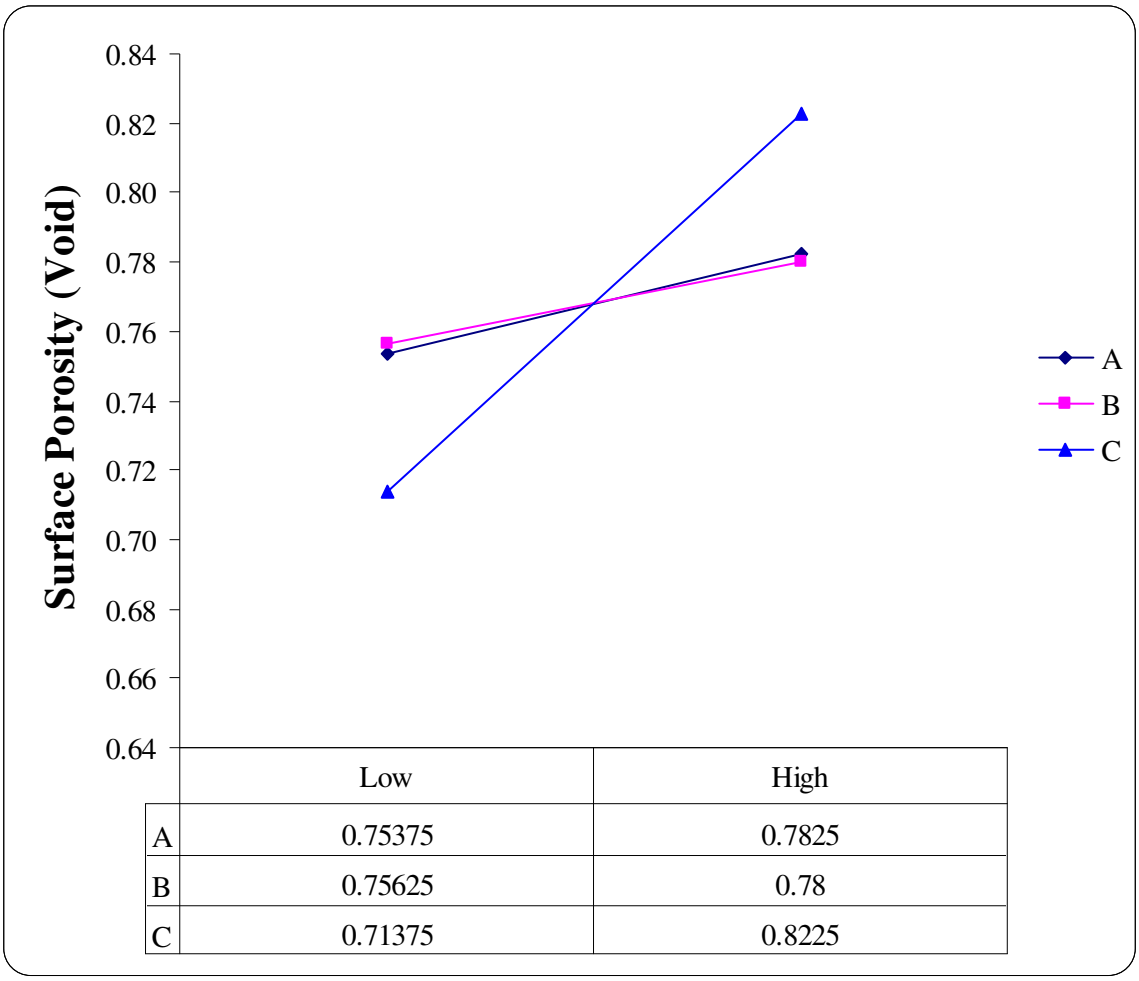

	Low	High
A	0.75375	0.7825
B	0.75625	0.78
C	0.71375	0.8225

Figure 4.7 – Fitted main effects chart for Tool A

The significant effect feed rate (Factor C) has on surface smearing is shown by the great difference in average surface porosity values between trials run at 10 IPM (low setting) and 40 IPM (high setting). A main effect with no significant impact would be represented by a line with a slope of zero (*Analyzing Two Level Experimental Designs Video*, 2009). The slopes of the lines representing infiltrant hardness and temperature do not equal zero, therefore similar to deduction from the *p*-value analysis, they too may have an effect. However, their significance cannot be determined from this data. The effect chart for two-

www.manaraa.com

factor interactions displayed a possible significant interaction between AB and AC. The interaction of ABC may also be significant according to the three-factor effects chart; both the two-factor and three-factor effects charts are shown in Appendix 6.

These effect charts provide the first indication of a trend that was common throughout all of the surface porosity results for the 2^3 full factorial analysis. A positive correlation was found between greater resultant surface porosity measurements and trials with parameters ran at their high settings. This was found true in all cases with the exception of temperature when using Tool B, this anomaly is explained in greater detail with the discussion of the ANOVA results for Tool B.

On average, surface porosity was better maintained when machining parameters were run at their higher settings. For Tool A, the average surface porosity score was higher when the very hard infiltrant was used, Cyto-Freeze™ was the coolant utilized, and cuts were made at a feed rate of 40 IPM. These average results per parameter setting are displayed in Table 4.9.

Table 4.9 – Resulting average surface porosity comparison at low and high parameter settings for Tool A

	Low Setting	High Setting
	Surface Porosity (Void)	
Feed Rate	0.71	0.82
Infiltrant Hardness	0.76	0.78
Temperature	0.76	0.78

www.manaraa.com

Based on the data presented here, this phenomenon indicates that on average when using a tool with less wear, the effect of surface smear caused by milling could be reduced by using harder infiltrants, non-cryogenic machining environments, and faster feed rates. However, this cannot be verified without further analysis.

The two-factor plots from the ANOVA results show that there may be a significant effect with the combination of all factor pairs. However, the combination of machining parameters with the greatest effect was that of infiltrant hardness and temperature. This effect is shown in the two-factor plot for the combination of these two factors, displayed in Figure 4.8. It can be seen that the two lines do not run parallel to each other, nor do they have slopes of zero; this is an indication that the factor combination may affect surface smearing (*Analyzing Two Level Experimental Designs Video*, 2009). This interaction is subject to future research in order to determine its significance. All of the two-factor plots are shown in Appendix 7.

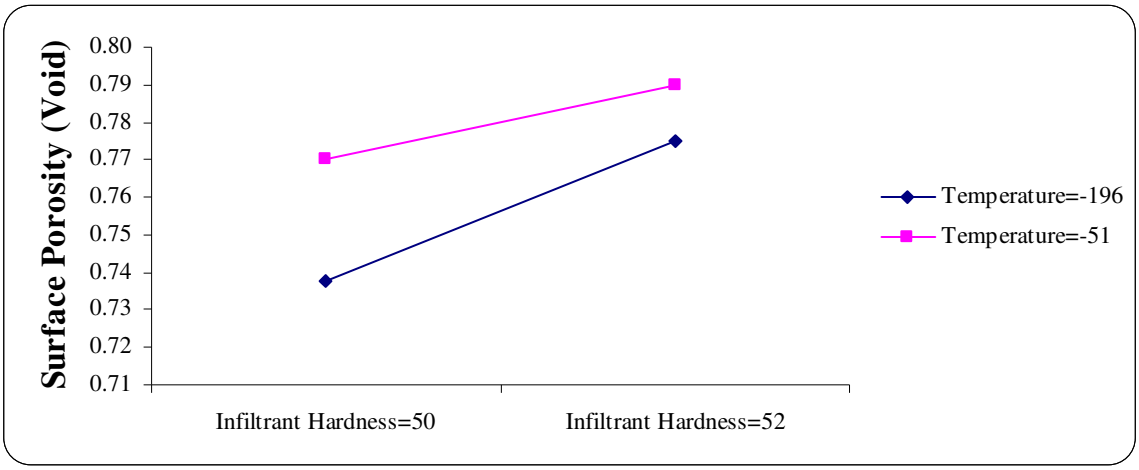

Figure 4.8 – Two-factor plot for factor combination of infiltrant hardness and temperature

www.manaraa.com

4.7.2 ANOVA results – Tool B

As described earlier in this chapter, tool wear was also a factor considered while investigating contributors to surface smearing. The 2^3 full factorial machining experiment was also ran with a worn tool after almost 5 minutes of use (Tool B). The ANOVA results for this experiment are shown in Table 4.10.

Table 4.10 – All factor analysis results for machining experiment when using Tool B

	Mean	A	B	C	AB	AC	BC	ABC
Sum +	4.110	2.060	2.045	2.605	2.015	2.015	2.110	2.020
Sum -	0.000	2.050	2.065	1.505	2.095	2.095	2.000	2.090
Overall	4.110	4.110	4.110	4.110	4.110	4.110	4.110	4.110
Difference	4.110	0.010	-0.020	1.100	-0.080	-0.080	0.110	-0.070
Effect	0.514	0.003	-0.005	0.275	-0.020	-0.020	0.028	-0.018
SS		0.000	0.000	0.303	0.002	0.002	0.003	0.001
MSE	**0.049**							

Factor A = Infiltrant Hardness

Factor B = Temperature

Factor C = Feed Rate

As was the case when machining with Tool A, feed rate was the only factor that was found to be a statistically significant effect from the all factor analysis. The effect value of 0.275 is considerably greater than the minimum significant effect of 0.049. This significance is also proven with a calculated *p*-value of 0.000 for feed rate in Table 4.11.

www.manaraa.com

Table 4.11 – *P*-values calculated for all factors and combinations using Tool B

Factor	*p*-value
A	0.9075
B	0.8164
C	0.0000
AB	0.3653
AC	0.3653
BC	0.2235
ABC	0.4255

The results of the all factor analysis and the resulting *p*-values suggest that there were no significant effects when considering any other individual or combination of factors. This is one difference noticed when using a worn tool rather than a new tool. Further analysis may be warranted to determine the significance of the effects infiltrant hardness or temperature may have on resulting surface porosity when machining with a new tool, however it has been shown here that these two factors do not have a significant effect when using a worn tool.

According to the ANOVA effects charts for Tool B, the only fitted main effect that has a significant influence on surface smearing was feed rate (this corresponds to the results of the *p*-value analysis as well). It can be seen in the chart that infiltrant hardness and temperature have little to no effect by their minute slope values. This is demonstrated in Figure 4.9.

www.manaraa.com

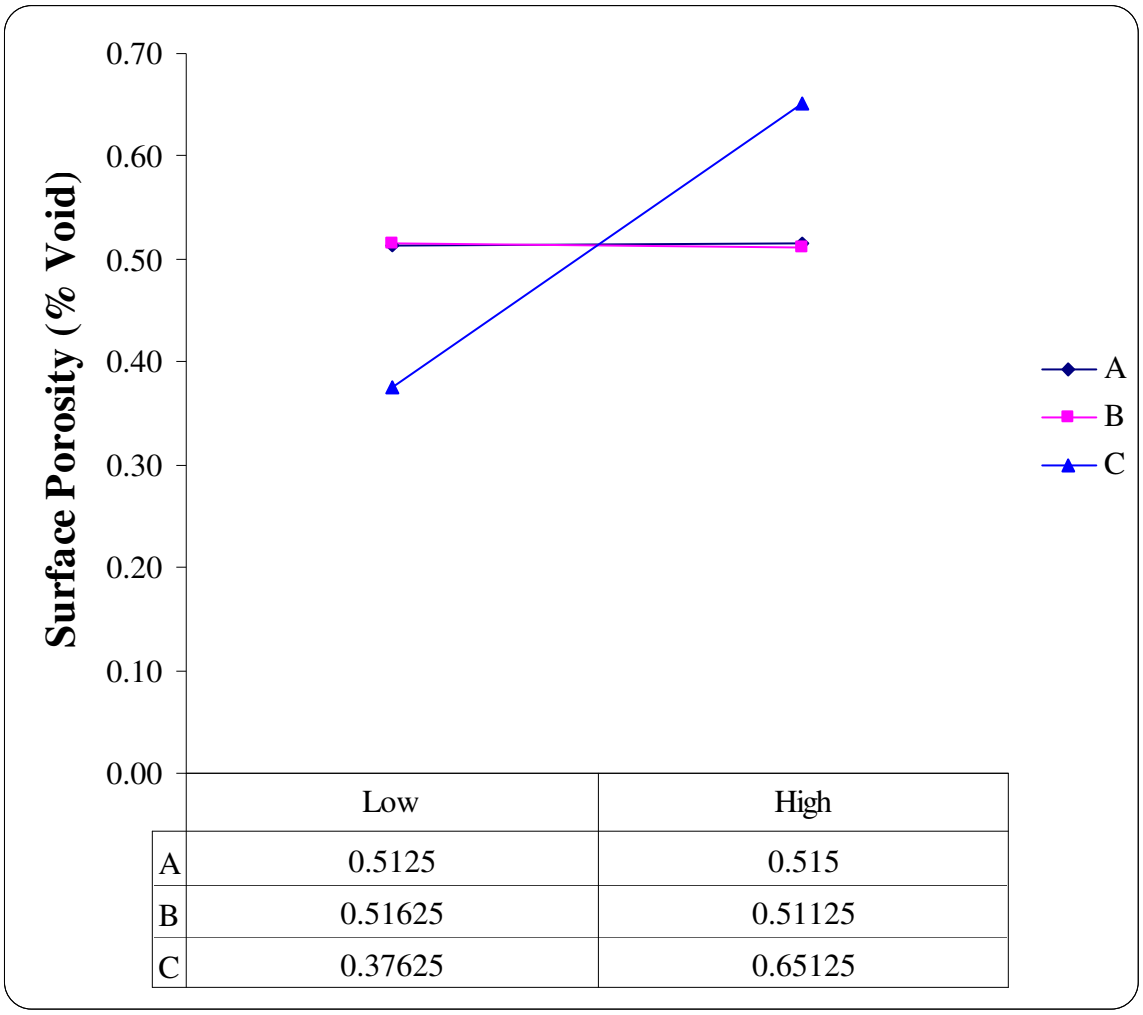

	Low	High
A	0.5125	0.515
B	0.51625	0.51125
C	0.37625	0.65125

Figure 4.9 – Fitted main effects chart for Tool B

Another difference noted between Tool A and Tool B was that when using Tool A, surface porosity was better maintained at all three higher machining parameter settings; however, this was not the case with Tool B when considering temperature. On average, trials ran at the high setting for temperature resulted in a lower surface porosity score than those ran at the low temperature setting. The difference in surface porosity is only 1.0% but

www.manaraa.com

is worthy of further investigation. The average surface porosity measurements are shown in Table 4.12 for each parameter setting.

Table 4.12 - Resulting average surface porosity comparison at low and high parameter settings for Tool B

	Low Setting	High Setting
	Surface Porosity (Void)	
Feed Rate	0.38	0.65
Infiltrant Hardness	0.51	0.52
Temperature	0.52	0.51

As stated before with Tool A, the effect of surface smear caused by milling with a worn tool could be reduced by using harder infiltrants and faster feed rates. However, according to the data presented here it may be beneficial to machine in a cryogenic environment when using a tool with more wear.

The same conclusions derived from the two-factor plots from the ANOVA analysis of Tool A can be said for Tool B. There may be a significant effect with the combination of all factor pairs but again, the combination of infiltrant hardness and temperature was the greatest. The two-factor plots generated from the Tool B ANOVA are shown Appendix 14.

4.8 2^3 full factorial machining experiment results – Comparison of Tool A and Tool B

The results of the ANOVA analysis for both Tool A and Tool B determined the second hypothesis stated in this research to be true. Feed rate does in fact have a significant effect on the amount of surface smearing that occurs during machining. It was also

www.manaraa.com

discovered that this hypothesis holds true regardless of tool wear condition. As shown in Figures 4.10 and 4.11, when machining with Tool A and Tool B, the resulting effect of surface smearing was reduced when utilizing a faster feed rate of 40 IPM, instead of 10 IPM. Both of these graphs display the surface porosity results from the 2^3 full factorial study for both feed rates, however there were also different infiltrant hardness ratings and temperatures used within these data sets.

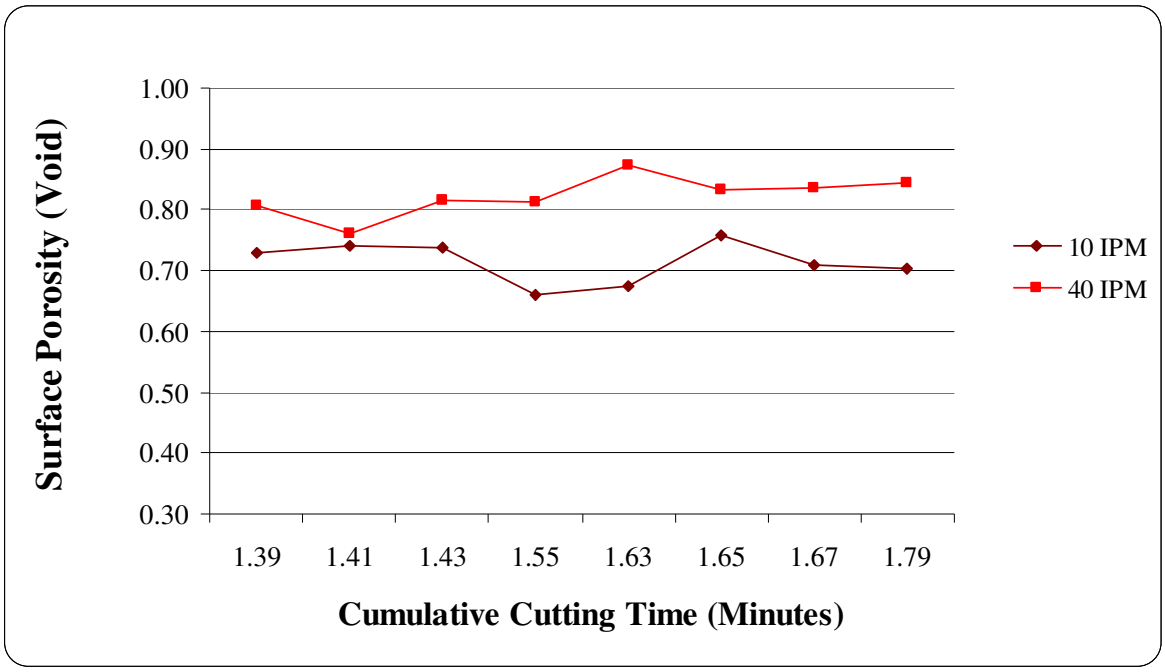

Figure 4.10 – Resulting surface porosity when varying feed rate with Tool A

www.manaraa.com

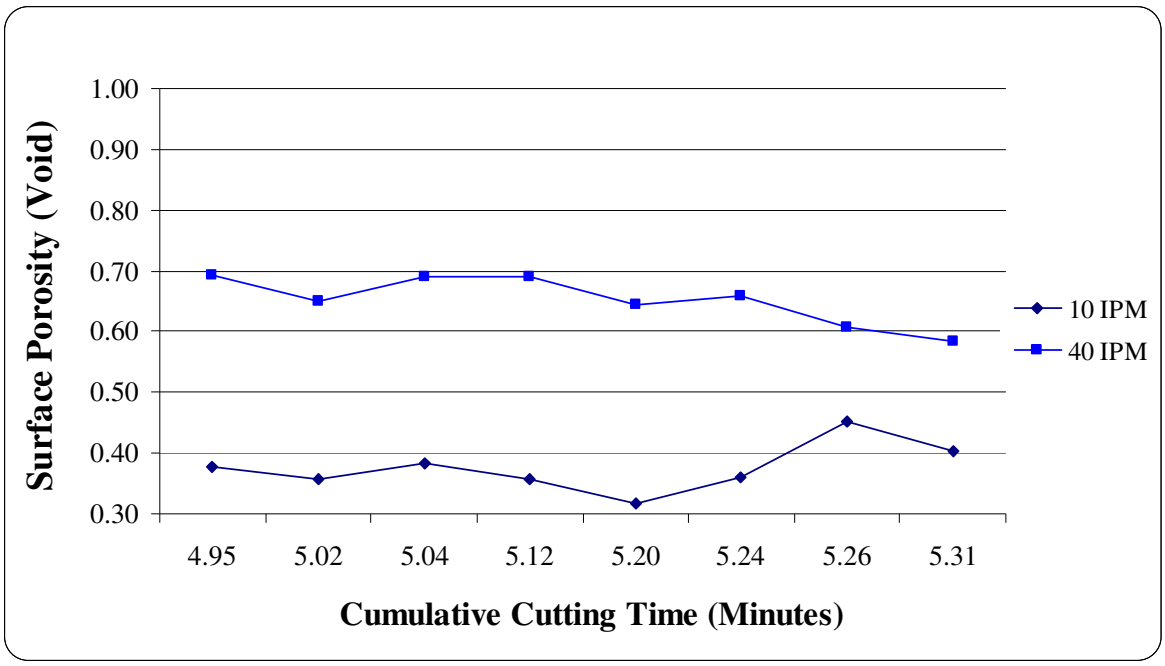

Figure 4.11 – Resulting surface porosity when varying feed rate with Tool B

This conclusion was similar to that of another study investigating the machining of porous titanium by Bram *et al.*, 2003. That study also found that feed rate had a significant effect on surface smearing and also that this smearing was reduced when machining at a higher feed rate setting.

Another result of note from Figures 4.10 and 4.11 is that regardless of feed rate, Tool A maintained a greater surface porosity than Tool B. After a simple analysis of the 2^3 full factorial experimental results, it can be seen that there is a difference in resulting surface porosity when using a new tool, when compared to using a worn tool. This was a common result when looking at all of the collected data; regardless of other machining parameter settings it was found that tool wear does increase the effect of surface smearing.

www.manaraa.com

As shown in Figure 4.12, regardless of any parameter combination, in every trial the worn tool (Tool B) caused greater pore occlusion than the new tool (Tool A). It is noted that with the exception of a few data points, both data series generally follow the same trend.

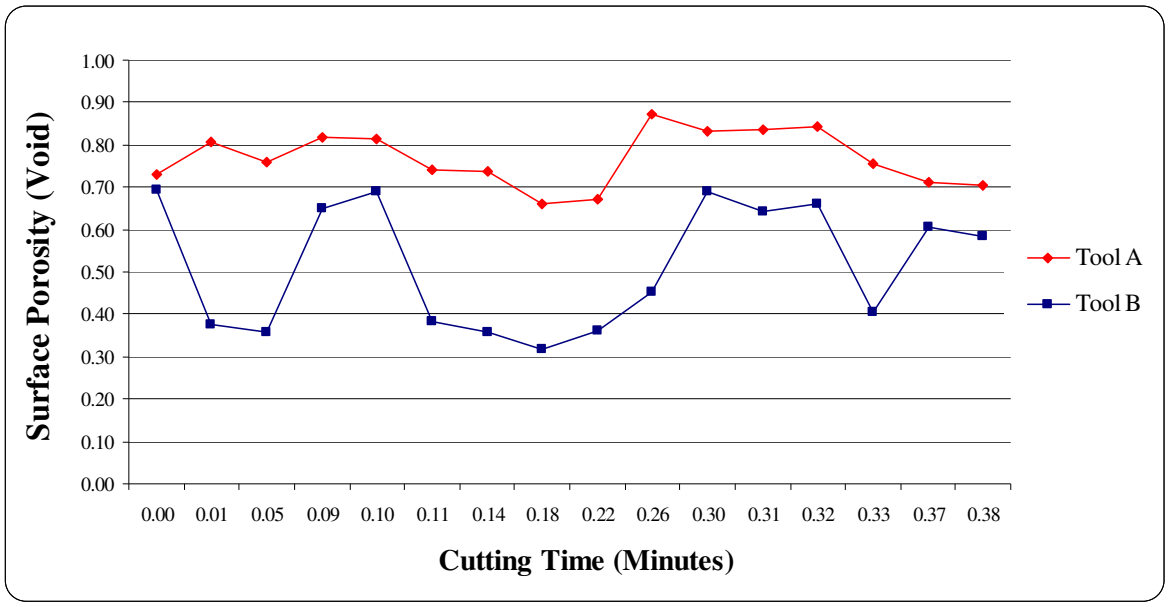

Figure 4.12 – Resulting surface porosity comparison using Tool A and Tool B

When evaluating the surface porosity results when using Tool A and Tool B varying all parameter settings, there seems to be more variability in the resultant surface porosity when the tool is more worn. As demonstrated in Figure 4.13 and Figure 4.14, the surface porosity results generated with Tool A are much more consistent than those generated with Tool B. It seems that tool wear might affect the contribution of each parameter's influence on the resultant surface smearing. The example shown in Figure 4.13 and 4.14 demonstrate this inconsistency when varying infiltrant hardness, however this trend was also present

www.manaraa.com

when varying temperature and feed rate. These examples can be seen in Appendices 16 – 18.

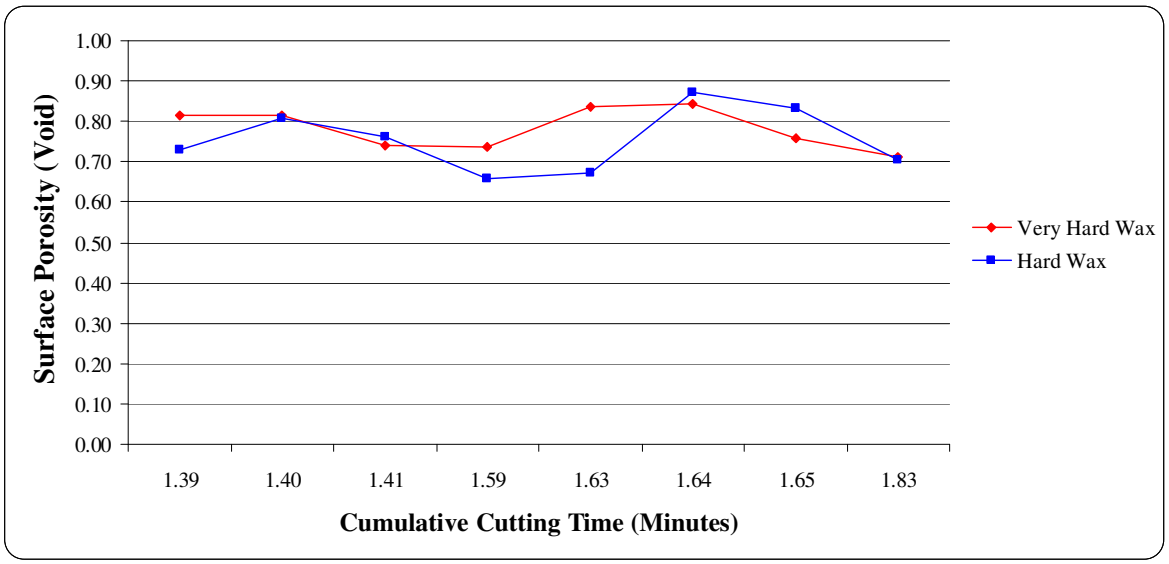

Figure 4.13 – Resulting surface porosity when varying infiltrant hardness with Tool A

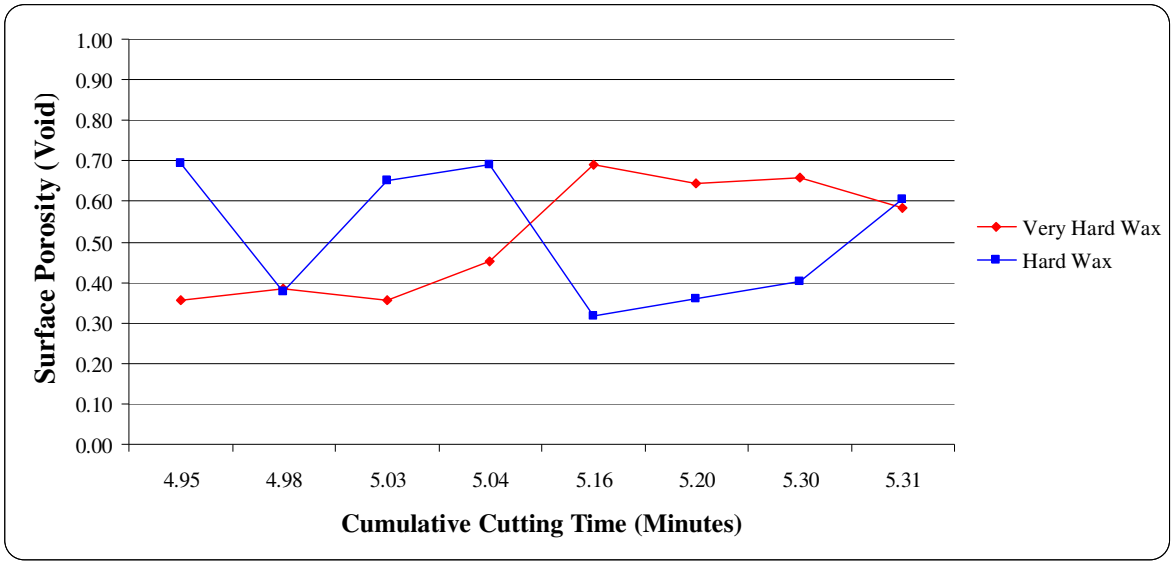

Figure 4.14 – Resulting surface porosity when varying infiltrant hardness with Tool B

www.manaraa.com

It seems that when the tool has experienced more wear, the influence of each factors is exaggerated. This could mean that it may be more difficult to determine the optimal machining parameters when using worn tools than tools with less cutting experience. It should also be noted that the occurrence of greater pore occlusion when using Tool B is demonstrated in these data sets as well, as mentioned previously this is a consistent result of all the surface porosity data collected.

4.9 Comprehensive tool wear analysis results

Over the course of this research, in excess of 200 cuts were made. Reticle surface porosity analysis was performed on the majority of these cuts but only the data collected from two tools are discussed in this thesis; the "new" and "worn" tools as described previously (Tool A and Tool B, respectively). In addition to the 32 cuts evaluated in the 2^3 full factorial machining experiment, 39 more data points were recorded with Tool A and an additional 140 data points were collected from cuts made with Tool B. Figure 4.15 demonstrates where these 16 full factorial cuts occurred for both experiments over the life of a tool, as well as the difference in surface porosity resulting from tool wear.

www.manaraa.com

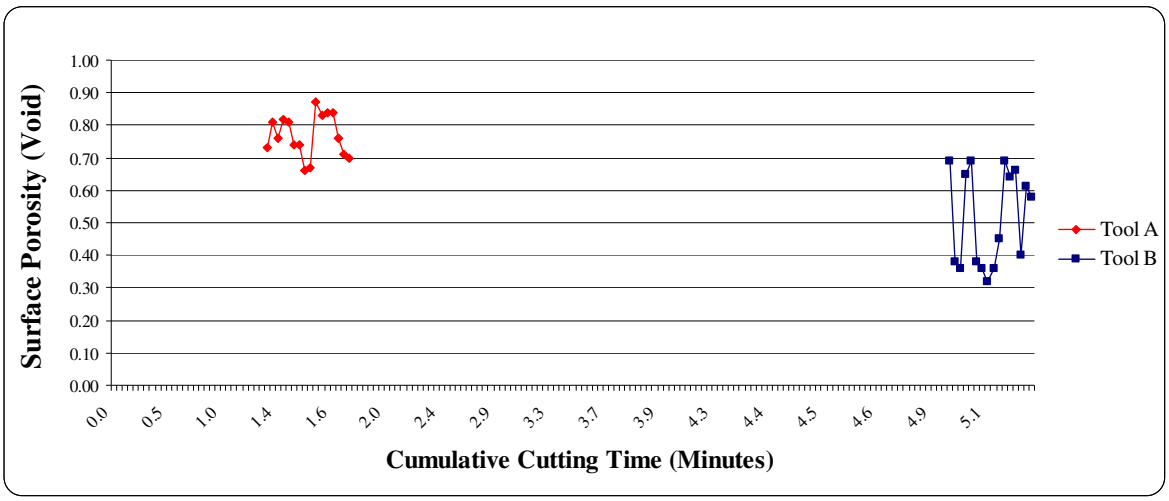

Figure 4.15 – 2^3 full factorial surface porosity results throughout life of tool

It is evident that machining done earlier on in a tool's life maintained a higher surface porosity measurement than when ran after experiencing tool wear. The average surface porosity measurement for the 2^3 full factorial experiment ran with Tool A was 77%, which falls within the nominal range of unprocessed TM porosity. After approximately 5 minutes of cutting, the 2^3 full factorial ran with Tool B maintained an average surface porosity of 51%. This is approximately 24% less porous than the lower limit of the unprocessed TM nominal range. As previously discussed, it should also be noted that the surface porosity results calculated later on in a tool's life were much more volatile than those same cuts made earlier. Again, this could be an indication of tool wear's varying influence on machining parameters and is subject to further research.

A graphical representation is shown in Figure 4.16 of all of the surface porosity measurements recorded from all of the cuts made by Tool A and Tool B, with the exception of some anomalies. Outlier data points exceeding values two standard deviations ($\pm 2\sigma$) away from the mean were not represented.

www.manaraa.com

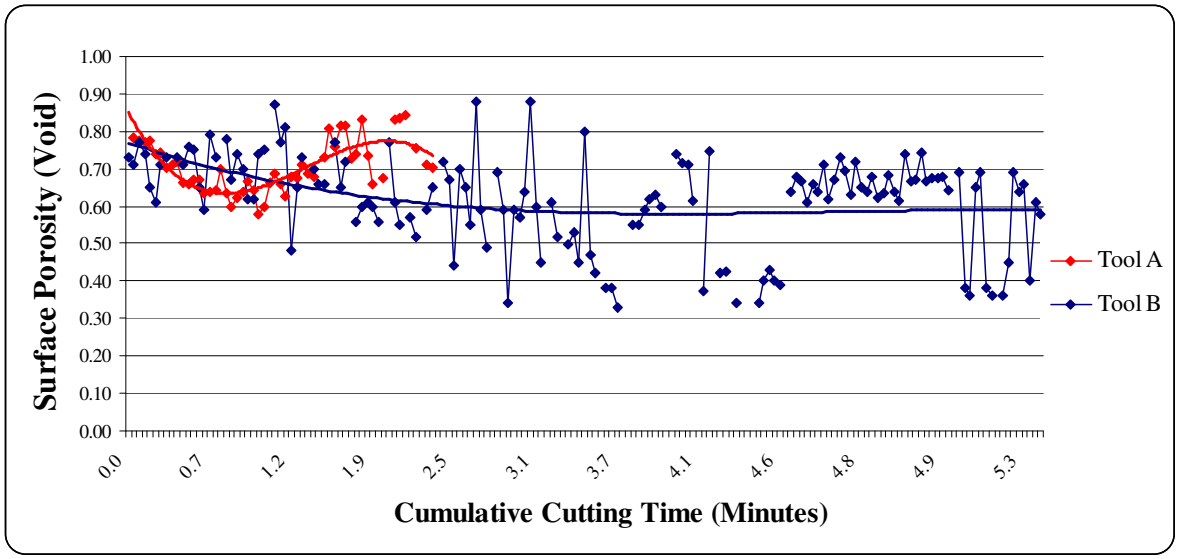

Figure 4.16 – Resulting surface porosity across tool life of Tool A and Tool B

As demonstrated in Figure 4.16, the 3rd order polynomial trend line for Tool A seems to begin a downward progression in the last few trials. As cutting time accumulated for Tool B, the surface porosity decreased as well except for those cuts made between approximately 4.66 and 4.94 minutes. This series of data points represents an experiment ran to investigate the influence of cryogenic machining on worn tools, this is discussed in more detail later on.

The downward succession for both tool's trend lines corresponds to the decrease in surface porosity resulting from tool wear. Also, similar to Figure 4.15, the results become more volatile as tool wear increases over time.

www.manaraa.com

4.9.1 Comprehensive tool wear analysis – tool wear condition results

Much like when using traditional machining methods, increasing tool wear can affect the surface of the material being cut. The surface condition of a metal can change vastly over the lifespan of a cutting tool. The difference in tool wear is evident when looking at a microscopic view of a tool's cutting edge after 1.83 and 5.32 minutes of cutting. The presence of tool wear is characterized by a rounded cutting edge; the greater the tool wear, the more rounded the edge. Images taken of each tool after all machining had been completed are compared to the cutting edge of an unused tool shown in Figure 4.17a. Tool A is shown in Figure 4.17b and Tool B is represented in Figure 4.17c.

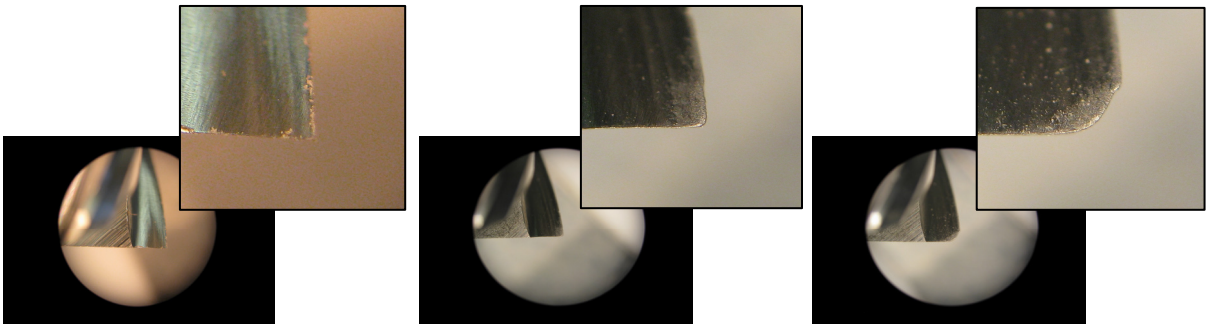

(a) (b) (c)

Figure 4.17 – Tool wear after machining for (a) zero minutes, (b) 1.83 minutes, and (c) 5.32 minutes (magnification of 25x)

After seeing this large amount of tool wear after 5.32 minutes of machining, it was hypothesized that surface smear could be reduced by machining at cryogenic temperatures when using a worn tool. If the reduced surface porosity is a result of the excessive heat generated by a worn tool, perhaps applying a cryogenic cooling agent during machining would counter this heat and resulting infiltrant softening. An additional machining

www.manaraa.com

investigation was developed that looked at 10 cuts (30 measurements) of TM infiltrated with hard wax and very hard wax. As mentioned before, these 10 cuts are represented by the horizontal grouping of data points in Figure 4.16 between time 4.66 and 4.94 minutes. All cuts were done at a feed rate of 40 IPM while being cooled with liquid nitrogen (-196℃). It was thought that liquid nitrogen might maintain the material hardness of each wax differently. The results of this analysis are shown in Figure 4.18.

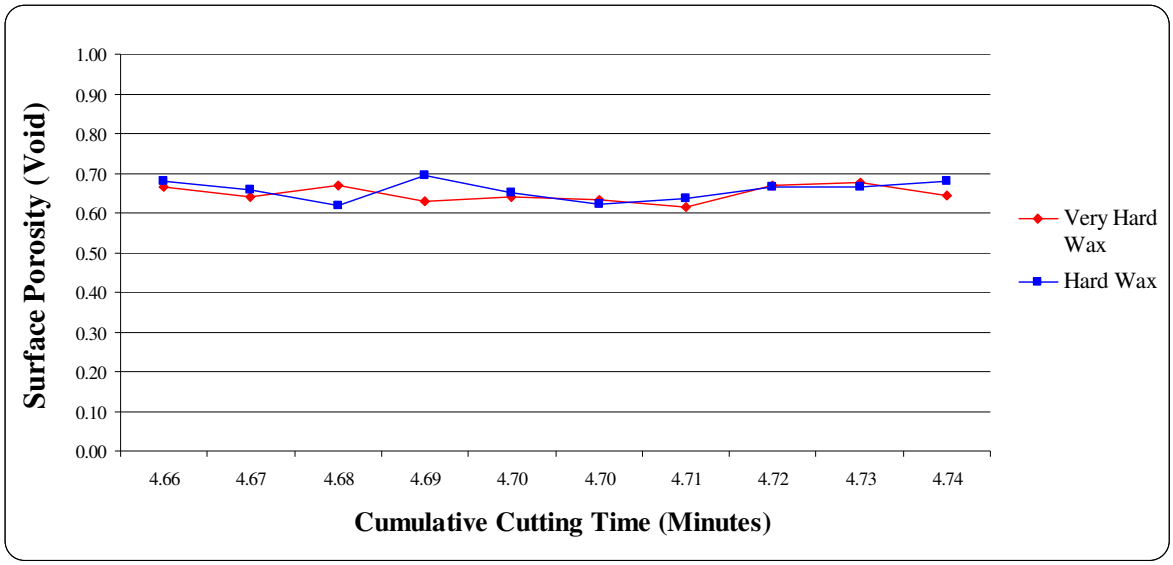

Figure 4.18 – Worn tool surface porosity analysis cooling with liquid nitrogen

As demonstrated in Figure 4.18 using liquid nitrogen to machine in a cryogenic environment while using a worn tool was of little benefit. Using liquid nitrogen to maintain the hardness of the hard wax and very hard wax had no effect on the resulting surface porosity. This could mean that when machining Trabecular Metal™ with a worn tool, it may make no difference which infiltrant is used when cooling with liquid nitrogen.

www.manaraa.com

4.9.2 Comprehensive tool wear analysis – machining environment temperature results

Throughout the course of these machining experiments, it was seen that the resulting surface porosity varied depending upon the temperature of the machining environment. Figure 4.19 illustrates all of the machining trials ran while cooling with liquid nitrogen (-196℃) and Cyto-Freeze™ (-51℃), as well as those ran at room temperature (21℃). It should be noted that those trials ran at room temperature did not utilize an infiltrant and were intended to represent a control group. As illustrated in Figure 4.19, there was a greater presence of pore occlusion when machining in warmer environments. It seems that utilizing liquid nitrogen as a cooling agent maintained the original surface porosity more often than when cooling with Cyto-Freeze™. Machining at room temperature resulted in more surface smearing than when machining with a cooling agent. This increase in pore occlusion may not be a result of the temperature, but rather a result of machining without an infiltrant. Further investigation is required to determine what is actually contributing to this increase in surface smearing.

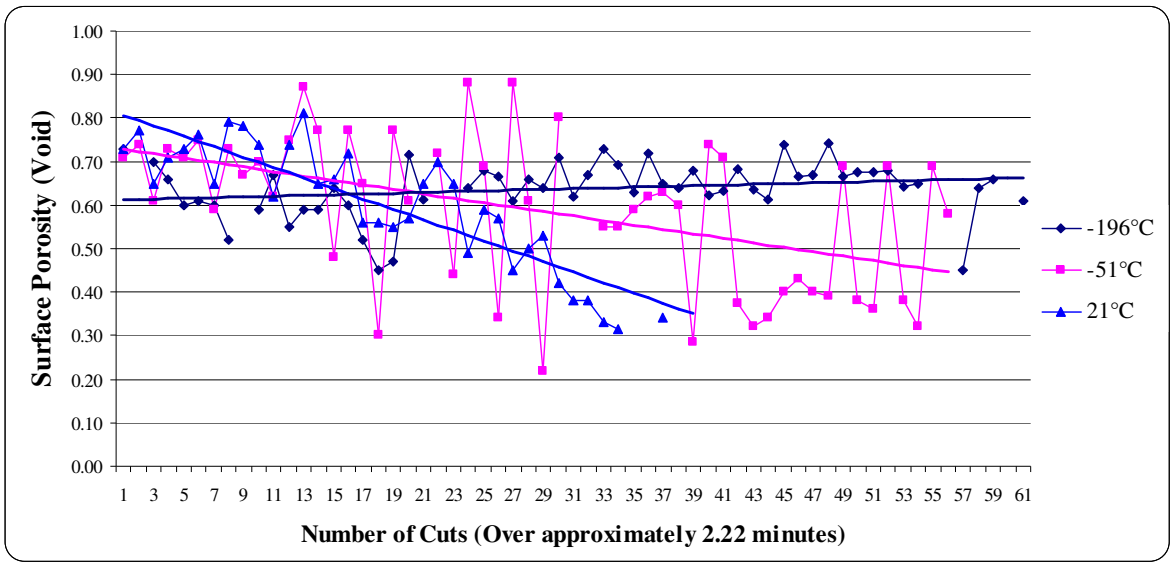

Figure 4.19 – Surface porosity results at different machining temperatures using Tool B

www.manaraa.com

The third hypothesis of this work predicted that using a cooling agent to maintain infiltrant hardness during machining will result in reduced smearing effect. Upon analysis of the results it was found that this hypothesis is true when using a worn tool. As expected, the graph indicates that there is a greater downward slope to the surface porosity results when machining without an infiltrant than with an infiltrant. Although surface porosity still decreased over time, it was maintained longer when using liquid nitrogen or Cyto-Freeze™. The effect of surface smearing was reduced more often when machining with either cooling agent as opposed to machining at room temperature. There was not sufficient data to conclude whether this is true when using a new tool but it is predicted that using a cooling agent would have the same effect. This is another investigation that fell outside the scope of this research but will be discussed later with other future work opportunities.

The results explained here were a great contribution to the knowledge and understanding of what actually influences the surface porosity of Trabecular Metal™ during machining. There is now statistical evidence to support how surface porosity will be affected when machining with various settings of infiltrant hardness, temperature, and feed rate. Further explanation and suggested future scientific experimentation is discussed in the sixth and final chapter of this thesis. Chapter 5 describes how the knowledge gained from this experimentation was used to machine a bone fragment prototype utilizing the infiltration process.

www.manaraa.com

CHAPTER 5. IMPLEMENTATION

This chapter describes the process steps taken to machine a custom shaped high-impact bone fracture fragment from Trabecular Metal™ and natural bone. As a result of the research explained in this thesis, utilizing the infiltration method presented reduces the effect of surface smearing while machining metal foam. In order to demonstrate this process is applicable for functional part geometries, the process was used to machine a bone fracture fragment from TM and a range of other clinically relevant materials. The CAD model of the bone fragment was created from CT data taken from a human patient who sustained a high-impact leg fracture. Specifically, the fracture was diagnosed as a comminuted tibial plafond fracture, meaning the distal portion of the tibia shattered upon impact, resulting in multiple segmental defects. The CT data of the patient's leg was used to excise geometric data for a large bone fragment to be machined.

The bone fragment geometric data was extracted using Geomagic Studio® software to reverse engineer the segmental bone defects into individual sets of data points. The data points were then inputted to Mastercam® where a 3-dimensional CAD file was created. From the CAD model, CNC-RP software automatically analyzed the bone fracture fragment geometry and determined part orientation, sacrificial fixture support structures, cutting orientations, and cutting toolpaths before outputting the NC code (Frank *et al*., 2008). The results of the CNC-RP analysis centered the fragment within the respective material bar stock along the x-axis. Each fragment was then fitted with three sacrificial supports. It was determined that all geometric features could be machined from two cutting orientations. After the NC code was generated, fresh bar stock material was set within the opposing

www.manaraa.com

chucks of a 4th axis indexer and fixed by clamping at both ends. The indexer was used in order to enable cutting from two orientations. The processing sequence carried out to convert geometric data from the patient's CT scan to the machining of the bone fracture fragment is illustrated in Figure 5.1.

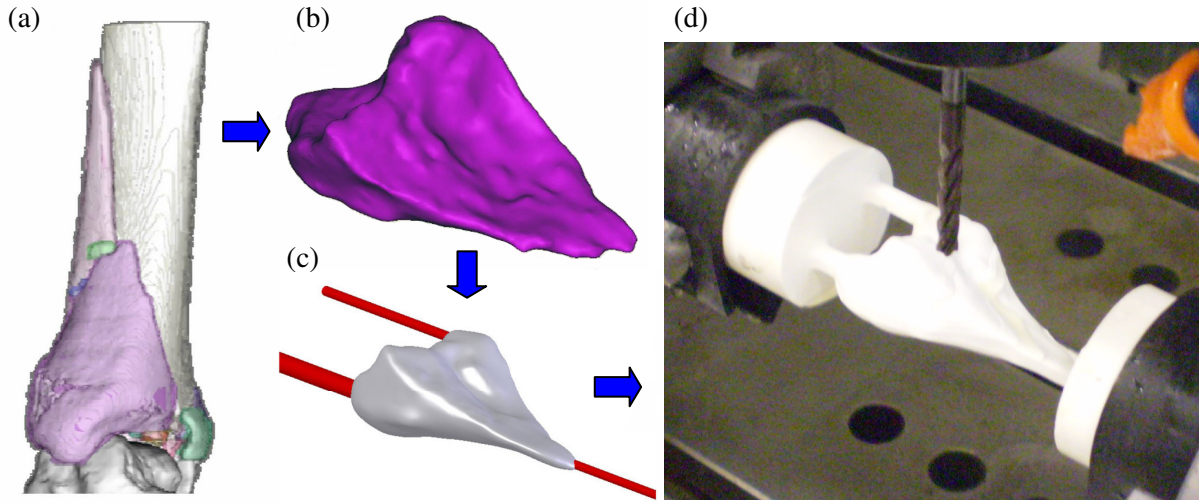

Figure 5.1 – Bone fracture fragment data processing sequence: (a) CT data, (b) CAD file, (c) CAD file with support structures, and (d) machining of bone fragment geometry

To demonstrate the versatility of this process, the bone fragment was first made from three material types, aluminum, ceramic, and Delrin™ plastic. All bone fragment prototypes were fabricated utilizing CNC-RP methodology and the same CNC vertical machining center used in the 2^3 full factorial study. Due to the different diameter stock sizes of material, the geometric CAD data for the bone fragment had to be scaled to fit within the specific bar of material; this manipulation was done in Mastercam®. Each fracture fragment was scaled about the central axis of the material stock along the x-axis, this ensured that the

www.manaraa.com

fragment would fit in the center of the material and it allowed for equivalent amounts of material removal from both machining orientations. When the bone fragment was correctly positioned at the appropriate size, the CAD file was analyzed with CNC-RP software as previously described and the resulting NC code was generated.

The first bone fracture fragment prototype was machined from a 2 inch diameter bar stock of aluminum with a 3/16 inch flat end mill. The second and third prototypes were fabricated from ceramic and Delrin™ plastic, respectively. These two materials were selected for prototyping due to their biocompatibility. Ceramic has a far greater presence of use in orthopaedic implants than Delrin™ but providing evidence that this method can be used to fabricate bone implants from a range of synthetic biomaterials is still of benefit. The ceramic fragment was cut from a 1.5 inch diameter ceramic bar stock while the Delrin™ fragment was machined within a plastic bar stock of 2.0 inches in diameter. All three prototypes are shown in Figure 5.2.

(a) (b) (c)

Figure 5.2 – Bone fracture fragment prototypes: (a) aluminum, (b) ceramic, and (c) Delrin™ plastic

www.manaraa.com

The fracture fragment machined from Trabecular Metal™ was created from a 0.5 inch diameter bar stock. Due to the small diameter of the stock material, the same indexer used on the other prototypes could not be used. Instead, the bar was held within a collet that was secured to the machine table within a Chick™ vise (just like the setup used in the 2^3 full factorial surface porosity analysis). Due to the small diameter of the stock material, the geometric data of the fragment had to be scaled down in order to fit within a 0.5 inch diameter. This scaling operation was done within Mastercam® and then saved to be analyzed with CNC-RP software. Again, the CNC-RP software was run to determine all necessary cutting parameters. The parameters calculated for the TM sample were identical to those used before; however the inability to use an indexer required the support structures to be modified. The three sacrificial supports created by CNC-RP were replaced with a single support centrally placed along the x-axis. It was determined that all geometry could be machined from two orientations so instead of rotating the stock material in an indexer the collet was simply removed from the vise, rotated 180 degrees, and then replaced. The final CAD representation with the sacrificial support and finished part are shown in Figure 5.4.

www.manaraa.com

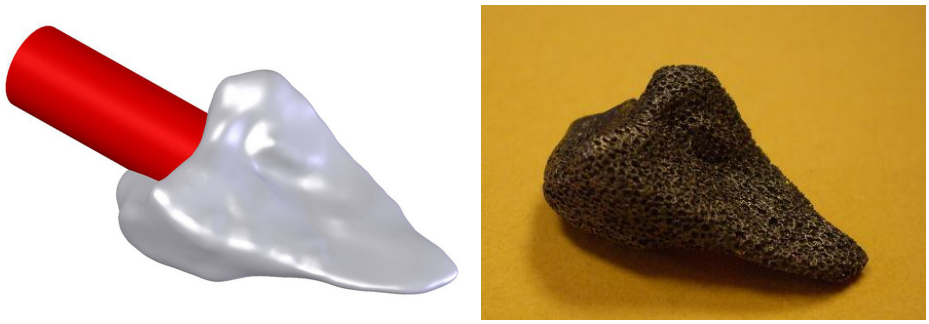

(a) (b)

Figure 5.4 – (a) CAD file with sacrificial support and (b) finished TM bone fracture fragment

Before machining, the Trabecular Metal™ bar stock was infiltrated with very hard wax. During machining, the sample was incessantly sprayed with Cyto-Freeze™ to keep the TM, wax, and tool cool. The fragment was cut with a 0.25 inch flat four flute HSS end mill. Upon machining completion the bone fragment was cut from the remaining bar stock, the support was manually eliminated, and all residual infiltrant was removed. A reticle analysis was performed in the same manner as done in the 2^3 full factorial analysis and a surface porosity of 69% was calculated from the measurements displayed in Table 5.1.

Table 5.1 – Surface porosity analysis of TM bone fracture fragment

Measurement	Surface Porosity (Void)	Average Surface Porosity (Void)
1	0.71	**0.69**
2	0.66	
3	0.70	

www.manaraa.com

A surface porosity measurement of 69% after being machined is exceptional considering unprocessed Trabecular Metal™ has a nominal surface porosity of approximately 70 – 85% (Bobyn *et al*., 1999; Callaghan *et al.*, 2006; Levine *et al*., 2006; Levine *et al*., 2008; Medlin *et al*., 2005; Voort *et al*., 2004). This is an excellent example of the use of this new machining method; a custom bone fracture fragment was machined from patient-specific CT data, that post processing maintained a surface porosity value acceptable for osseointegration in orthopaedic surgery.

www.manaraa.com

CHAPTER 6. CONCLUSION AND FUTURE WORK

The concept of custom orthopaedic implants begins with the ability to machine freeform geometries based on a patient's unique bone structure. In order for these implants to successfully attach to host bone, their surface must maintain a sufficient porosity measure to enable osseointegration. This thesis presents a novel machining method for metal foams that enables the creation of organic shapes without significant surface smearing.

The machining method presented in this work was subject to thorough experimentation in order to investigate the effects of certain machining parameters on the resulting surface porosity. Machining experiments were conducted that analyzed the influence of infiltrant hardness, machining temperature, and machining feed rate on surface porosity during milling. Statistical analysis showed that feed rate does have a significant effect on surface porosity. Additional analysis indicated that tool wear and machining temperature also may influence surface porosity; however these are subject to further investigation and are discussed later in this chapter.

Through the use of this infiltration method and RP technologies, it is now possible to machine the freeform geometries characteristic of custom, patient-specific, bone implants. This application was demonstrated through the manufacture of bone fragments from a variety of clinically relevant materials, including Trabecular Metal™.

At the beginning of this research there were some preconceived ideas of how each factor would affect surface porosity but there was little insight as to how these factors would interact with each other and affect surface porosity. Through observations of the experimental design and results generated from an analysis of variance, much knowledge

www.manaraa.com

was gained to better understand how infiltrant type, machining environment temperature, and feed rate influence surface porosity during the milling of Trabecular Metal™.

It was found that regardless of tool wear condition feed rate has a significant effect on resulting surface porosity during the milling of Trabecular Metal™. Experimental data has shown that machining at higher feed rates will reduce the effect of resultant surface smearing. It is thought that feed rate softens the infiltrant material due to the high amount of heat generated and introduced into the material at lower feed rates; however this should be further investigated. A machining trial should be designed such that an optimal feed rate is determined for machining metal foam with hard and very hard waxes. Once this is determined, an optimal cooling agent could be evaluated per infiltrant hardness.

A common trend from the 2^3 full factorial surface porosity analysis results was that those trials ran at higher parameter settings resulted in greater resulting surface porosity. This was true for all parameters when using Tool A but was not the case for temperature when using Tool B. In this case, machining at the higher temperature setting caused more pore occlusion than when machining at the lower temperature. The cause for this is not known and is subject to further analysis.

As a result of the ANOVA study, there was data that suggested temperature and infiltrant hardness may also be significant when machining with a newer tool. The ANOVA produced *p*-values for these two factors within a range where significance cannot be determined with present data. Further analysis is recommended to determine if infiltrant hardness and temperature contribute to surface smearing individually.

Effects charts and two-factor plots generated from the ANOVA results indicated that all combinations and interactions of the three machining parameters may influence surface

www.manaraa.com

smearing, with the exception of a two conditions. The two-factor effects chart, for Tool A, representing the interaction of temperature and feed rate illustrated no indication of a significant impact. Also, the main effects chart for Tool B showed no indication that infiltrant hardness or temperature had any effect on surface porosity. No definitive conclusions can be determined based on these charts or plots alone so additional ANOVA studies should be performed that focus only on these individual factors to determine if they truly have no effect on surface porosity.

The influence of tool wear on surface smearing is obvious when analyzing the results of this study. In each machining trial executed the resulting surface porosity was greater when using a tool with less wear (Tool A). Present data does not suggest any statistical reason for this but it is thought a tool with more wear is more likely to induce surface smearing. There was also an indication that as tool wear increased, the influence of each parameter becomes more variable. Both of these observations should be investigated, it would be beneficial to know how a tool will influence the effect of certain machining parameters on the resulting surface porosity. A tool's influence may be a function of its tool wear condition.

Experimental results presented in this thesis suggest that the use of cooling agents does reduce the effect of surface smearing. Additional experimentation is recommended in order to discover which cooling agent works best in preserving the surface porosity value during machining. There seems to be a greater maintenance of surface porosity while milling when using liquid nitrogen when compared to Cyto-Freeze™, as well as when using Cyto-Freeze™ compared to no coolant at all.

www.manaraa.com

All of the machining trials in this research were run at a spindle speed on 1000 rotations per minute. This value was chosen based on observations made in preliminary experiments. A future research endeavor should involve further exploration into what spindle speed should be used to minimize pore occlusion in different machining scenarios.

There is still much to be learned of how infiltrant hardness, temperature, and feed rate influence the surface porosity of Trabecular Metal™ during milling. There would be great benefit in developing a metric to determine the optimal infiltrant material, machining temperature, and feed rates to use that would minimize surface smearing while machining with tools of varying degrees of wear.

By combining this infiltration method with rapid prototyping technologies, the manufacture of custom orthopaedic implants may be feasible in the near future. As demonstrated in the implementation section, custom bone fracture fragments were machined based on a patient's CT data. This is advantageous in cases of high impact trauma where bone is shattered beyond repair or fragments cannot be recovered. Theoretically, if an integral fragment of bone was obliterated, using CT data, an exact geometric replica could be machined from Trabecular Metal™ and used to help repair a fracture. This implant could be machined before surgery to eliminate any geometric modifications that currently are performed during. The research presented in this thesis describes an initial step toward the design and manufacture of custom orthopaedic implants that could some day provide patients with more functionality and less discomfort due to a better fitting, stronger host bone attachment.

www.manaraa.com

REFERENCES

Adams, Dany Spencer. Lab Math A Handbook of Measurements, Calculations, and Other Quantitative Skills for Use at the Bench. New York: Cold Spring Harbor Laboratory P, 2003

Analyzing Two Level Experimental Designs Video. Dir. BPI Consulting, LLC. SPC Software Videos - BPI Consulting. 2009. 2 Mar. 2009 <http://www.spcforexcel.com/analyzing-two-level-experimental-designs-video>

Aponte, Javier, Carlos Cedeno, Carlos Ortiz, Francisco Samalot, and Gian Tiragallo. Biomechanics of Bone and Artery Replacement. Rep. 2003

Ashby, Michael F., Anthony Evans, Norman A. Fleck, Lorna J. Gibson, John W. Hutchinson, and Haydn N. Wadley. Metal Foams : A Design Guide. Chicago: Butterworth-Heinemann Limited, 2000. 194-99

Banhart, John. "Manufacture, characterisation and application of cellular metals and metal foams." Progress in Materials Science 46 (2001): 559-632

Bram, Martin, Christoph Kempmann, Alexander Laptev, Detlef Stover, and Klaus Weinert. "Investigations on the Machining of Sintered Titanium Foams Utilizing Face Milling and Peripheral Grinding." Advanced Engineering Materials 5 (2003): 441-447. 27 Aug. 2007

Black J. Biological performance of tantalum. Clin Materials. 1994;16:167-173

JD Bobyn, SA Hacking, JJ Krygier, SP Chan, KK Toh, M Tanzer, "Characterization of a New Porous Tantalum Biomaterial for Reconstructive Surgery", 66th Annual AAOS Anaheim, CA, Feb 4-8, 1999. Scientific exhibit

Bobyn, J. D., G. J. Stackpool, S. A. Hacking, M. Tanzer, and J. J. Krygier. "Characteristics of bone ingrowth and interface mechanics of a new porous tantalum biomaterial." The Journal of Bone and Joint Surgery 81 (1999): 907-914

Callaghan, John J., Aaron G. Rosenberg, and Harry E. Rubash. The Adult Hip. Philadelphia: Lippincott Williams & Wilkins, 2006

Callister, William D. Materials science and engineering an introduction. New York: Wiley, 1994

Chen, Shi, Dustin Head, Michael Effgen, and I. S. Jawahir. "An Investigation of Sustained Machining Performance for Controlled Surface Quality Requirements in Porous Tungsten." IEEE Transactions on Electron Devices 52 (2005): 903-908. 5 June 2008

www.manaraa.com

Claar, D., V. Irick, J. Adkins, and K. Kremer. "Multifunctional Properties and Processing." Multifunctionality of Closed-cell Aluminum Foams. Proc. of The Minerals, Metals & Materials Society (TMS) Annual Meeting, Seattle, WA. Warrendal, PA: TMS, 2002. 3-13

Shimko, Daniel A., Valerie F. Shimko, Edward A. Sander, Kyle F. Dickson, and Eric A. Nauman. "Effect of Porosity on the Fluid Flow Characteristics and Mechanical Properties of Tantalum Scaffolds." Journal of Biomedical Materials Research 73B (2005): 315-24

Deglurkar, Mukund, Dwight T. Davy, Matthew Stewart, Victor M. Goldberg, and Jean F. Welter. "Evaluation of Machining Methods for Trabecular Metal Implants in a Rabbit Intramedullary Osseointegration Model." Journal of Biomedical Materials Research Part B: Applied Biomaterials 80B (2006): 528-540. Compendex. Iowa State University Library, Ames, Iowa. 27 Mar. 2008

Evans, Anthony G., John W. Hutchinson, and Michael F. Ashby. "Cellular metals." Solid State & Materials Science 3 (1998): 288-303

Frank, M.C., Joshi, S., and Wysk, R.A., "CNC-RP: A Technique for Using CNC Machining as a Rapid Prototyping Tool in Product/Process Development" Proceedings of the Industrial Engineering Research Conference, Orlando, FL, 2002

Frank, Matthew C., Richard A. Wysk, and Sanjay B. Joshi. "Rapid Planning for CNC Milling - A New Approach for Rapid Prototyping." Journal of Manufacturing Systems 23 (2004): 242-55

Frank, M.C. "Implementing Rapid Prototyping Using CNC Machining (CNC-RP) Through a CAD/CAM Interface", Proceedings of the Solid Freeform Fabrication Symposium, 2007

Frank, Matthew C., Christopher V. Hunt, Donald D. Anderson, Todd O. McKinley, and Thomas D. Brown. "Rapid Manufacturing in Biomedical Materials: Using Subtractive Rapid Prototyping for Bone Replacement", Proceedings of the Solid Freeform Fabrication Symposium 2008, August 4–6, 2008, Austin, Texas

Frank, M.C., "A method for machining metallic foam", Provisional Patent Application # 61/024,945, United States Patent and Trade Office, January 31st 2008

Gagliardi, F., L. Filice, D. Umbrello, and R. Shivpuri. "Forging of metallic foams to reproduce biomechanical components." Materials Science & Engineering A (2008): 510-16

www.manaraa.com

Gibson, L.J., The mechanical behaviour of cancellous bone, J. Biomechanics, 18, 317-328, 1985

Gibson, Lorna J., and Michael F. Ashby. Cellular Solids : Structure and Properties. New York: Pergamon, 1988

Groover, Mikell P. Fundamentals of Modern Manufacturing: Materials, Processes, and Systems. 2nd ed. Hoboken, NJ: John Wiley & Sons, Inc., 2002. 772-785

Harrysson, Ola L., Omer Cansizoglu, Denis J. Marcellin-Little, Denis R. Cormier, and Harvey A. West II. "Direct Metal Fabrication of Titanium Implants with Tailored Materials and Mechanical Properties Using Electron Beam Melting Technology." Materials Science & Engineering C (2008): 366-373

Hieu, L C., Zlatov, N., Sloten, J.V., Bohez, E., Khanh, L., Binh, P.H., Oris, P., and Toshev, Y., "Medical Rapid Prototyping Applications and Methods." Assembly Automation 25 (2005): 284-292

Huston, Ronald. Principles of Biomechanics. Boca Raton, FL: CRC, 2008

Laptev, A., M. Bram, H. P. Buchkremer, and D. Stover. "Study of Production Route for Titanium Parts Combining Very High Porosity and Complex Shape." Powder Metallurgy 47 (2004): 85-92. 6 June 2008

Levine, Brett. "A New Era in Porous Metals: Applications in Orthopaedics." Advanced Engineering Materials 10 (2008): 788-92

Levine, Brett R., Scott Sporer, Robert A. Poggie, Craig J. Della Valle, and Joshua J. Jacobs. "Experimental and clinical performance of porous tantalum in orthopedic surgery." Biomaterials 27 (2006): 4671-681

"Machinable Wax." Advertisement. McMaster-Carr Online Catalog - Page 3570. 31 Mar. 2009 <http://www.mcmaster.com/#machinable-wax/=18qptt>

Maji, Palash K., P. S. Banerjee, and A Sinha. "Application of Rapid Prototyping and Rapid Tooling for Development of Patient-Specific Craniofacial Implant: an Investigative Study." International Journal of Advanced Manufacturing Technology 36 (2007): 510-515. 3 June 2008

Medlin, D. J., J. Scrafton, and R. Shetty. "Metallurgical Attachment of a Porous Tantalum Foam to a Titanium Substrate for Orthopedic Applications." Titanium, Niobium, Zirconium, and Tantalum for Medical and Surgical Applications. Proc. of ASTM Symposium on Titanium, Niobium, Zirconium, and Tantalum for Medical and Surgical Applications, Washington, DC. West Conshohocken, PA: ASTM International, 2005. 30-39

www.manaraa.com

Patnaik, Surya. Strength of materials a unified theory. Amsterdam: Butterworth-Heinemann, 2004

Porous Metal Design Guidebook. Princeton, NJ: Metal Powder Industries Federation, 2007. Metal Powder Industries Federation PM Design Center. 31 May 2007. Metal Powder Industries Federation. 7 Jun. 2007

Ratliff, Thomas A. The Laboratory Quality Assurance System A Manual of Quality Procedures and Forms. New York: Wiley-Interscience, 2003

Sarment, D.P., Sukovic, P., and Clinthorne, N., "Accuracy of Implant Placement with a Stereolithographic Surgical Guide." The International Journal of Oral & Maxillofacial Implants 18 (2003): 571-577

Schwartz, M. Brazing - For the engineering technologist (Manufacturing Processes and Materials). New York: Springer, 1995

Shimko, Daniel A., Valerie F. Shimko, Edward A. Sander, Kyle F. Dickson, and Eric A. Nauman. "Effect of Porosity on the Fluid Flow Characteristics and Mechanical Properties of Tantalum Scaffolds." Journal of Biomedical Materials Research Part B: Applied Biomaterials 73B (2005): 315-24

Singare, S., L. Dichen, L. Binheng, G. Zhenyu, and L. Yaxiong. "Customized Design and Manufacturing of Chin Implant Based on Rapid Prototyping." Rapid Prototyping Journal 11 (2005): 113-1118. 28 May 2008

Singare, Sekou, Liu Yaxiong, Li Dichen, Lu Bingheng, He Sanhu, and Li Gang. "Fabrication of Customised Maxillo-Facial Prosthesis Using Computer-Aided Design and Rapid Prototyping Techniques." Rapid Prototyping Journal 12 (2006): 206-213. 28 May 2008

Soboyejo, Winston O., and T. S. Srivatsan, eds. Advanced structural materials properties, design optimization, and applications. Boca Raton, FL: CRC P, 2007

"Trabecular Metal™ Technology." Trabecular Metal™ Technology. 3 Mar. 2009. Zimmer, Inc. 31 Mar. 2009 <http://www.zimmer.com/z/ctl/op/global/action/1/id/33/template/MP/navid/294>

Truscott, Michele, Deon De Beer, George Vicatos, Keith Hosking, Ludrick Barnard, Gerrie Booysen, and R. I. Campbell. "Using RP to Promote Collaborative Design of Customised Medical Implants." Rapid Prototyping Journal 13 (2007): 107-114. 29 May 2008

Vardeman, Stephen B., and J. M. Jobe. Statistical Quality Assurance Methods for Engineers. New York, NY: John Wiley & Sons, Inc, 1999

www.manaraa.com

Voort, George F. Vander. ASM Handbook Metallography and Microstructures (ASM Handbook). New York: ASM International, 2004

Warner, Rebecca M. Applied Statistics From Bivariate Through Multivariate Techniques. Minneapolis: Sage Publications, Inc, 2007

Werner, A., Z. Lechniak, K. Skalski, and K. Kedzior. "Design and Manufacture of Anatomical Hip Joint Endoprostheses Using CAD/CAM Systems." Journal of Materials Processing Technology 107 (2000): 181-186. 29 May 2008

www.manaraa.com

APPENDIX 1. 2^3 Full Factorial Experimental Results

Run	A	B	C
1	Hard	-51	10
2	Very Hard	-51	10
3	Hard	-196	10
4	Very Hard	-196	10
5	Hard	-51	40
6	Very Hard	-51	40
7	Hard	-196	40
8	Very Hard	-196	40
9	None	21	10
10	None	21	40

Tool A

Replicate	Run	Measurement 1	2	3	Average Surface Porosity (Void)	Control Analysis (±2σ)	Cumulative Time (Minutes)
1	**1**	0.73	0.69	0.77	**0.73**	Not Outlier	1.39
	5	0.78	0.85	0.79	**0.81**	Not Outlier	1.40
	7	0.72	0.79	0.77	**0.76**	Not Outlier	1.41
	6	0.8	0.81	0.84	**0.82**	Not Outlier	1.42
	8	0.84	0.79	0.81	**0.81**	Not Outlier	1.43
	2	0.71	0.77	0.74	**0.74**	Not Outlier	1.50
	4	0.79	0.71	0.71	**0.74**	Not Outlier	1.55
	3	0.66	0.64	0.68	**0.66**	Not Outlier	1.59
2	**1**	0.66	0.68	0.68	**0.67**	Not Outlier	1.63
	5	0.87	0.89	0.86	**0.87**	Not Outlier	1.64
	7	0.85	0.84	0.81	**0.83**	Not Outlier	1.65
	6	0.84	0.83	0.84	**0.84**	Not Outlier	1.66
	8	0.83	0.85	0.85	**0.84**	Not Outlier	1.67
	2	0.74	0.74	0.79	**0.76**	Not Outlier	1.75
	4	0.7	0.69	0.74	**0.71**	Not Outlier	1.79
	3	0.72	0.7	0.69	**0.70**	Not Outlier	1.83

Avg **0.77**
Std Dev **0.06**

www.manaraa.com

Tool B

Replicate	Run	Measurement 1	2	3	Average Surface Porosity (Void)	Control Analysis (±2σ)	Cumulative Time (Minutes)
1 and 2 (DOE created in SPC)	**5**	0.67	0.67	0.74	**0.69**	Not Outlier	4.95
	1	0.3	0.39	0.44	**0.38**	Not Outlier	4.98
	2	0.35	0.26	0.46	**0.36**	Not Outlier	5.02
	7	0.65	0.67	0.63	**0.65**	Not Outlier	5.03
	5	0.62	0.71	0.74	**0.69**	Not Outlier	5.04
	2	0.39	0.3	0.46	**0.38**	Not Outlier	5.08
	4	0.44	0.24	0.39	**0.36**	Not Outlier	5.12
	1	0.17	0.39	0.39	**0.32**	Not Outlier	5.16
	3	0.31	0.39	0.38	**0.36**	Not Outlier	5.20
	4	0.52	0.42	0.42	**0.45**	Not Outlier	5.24
	6	0.72	0.62	0.73	**0.69**	Not Outlier	5.24
	8	0.65	0.6	0.68	**0.64**	Not Outlier	5.25
	8	0.77	0.59	0.62	**0.66**	Not Outlier	5.26
	3	0.42	0.37	0.42	**0.40**	Not Outlier	5.30
	7	0.54	0.67	0.61	**0.61**	Not Outlier	5.31
	6	0.57	0.61	0.57	**0.58**	Not Outlier	5.32
				Avg	**0.51**		
				Std Dev	**0.15**		

www.manaraa.com

APPENDIX 2. Average 2^3 Full Factorial Surface Porosity Results Per Factor

Tool A

	Low Setting	High Setting
	Avg. Surface Porosity (Void)	
Feed Rate	0.71	0.82
Infiltrant Hardness	0.76	0.78
Temperature	0.76	0.78

Tool B

	Low Setting	High Setting
	Avg. Surface Porosity (Void)	
Feed Rate	0.38	0.65
Infiltrant Hardness	0.51	0.52
Temperature	0.52	0.51

www.manaraa.com

APPENDIX 3. 2^3 Full Factorial ANOVA All Factor Analysis - Tool A

Design Table											
Standard Run Order	Mean	A	B	*C*	AB	AC	BC	ABC	Avg	Range	
1	+	-	-	-	+	+	+	-	0.68	0.04	
2	+	+	-	-	-	-	+	+	0.725	0.03	
3	+	-	+	-	-	+	-	+	0.7	0.06	
4	+	+	+	-	+	-	-	-	0.75	0.02	
5	+	-	-	+	+	-	-	+	0.795	0.07	
6	+	+	-	+	-	+	-	-	0.825	0.03	
7	+	-	+	+	-	-	+	-	0.84	0.06	
8	+	+	+	+	+	+	+	+	0.83	0.02	
Sum +	6.145	3.13	3.12	3.29	3.055	3.035	3.075	3.05		***The significant effects are in bold in the effects row. These are larger than MSE.***	
Sum -	0	3.015	3.025	2.855	3.09	3.11	3.07	3.095			
Overall	6.145	6.145	6.145	6.145	6.145	6.145	6.145	6.145			
Difference	6.145	0.115	0.095	0.435	-0.035	-0.075	0.005	-0.045			
Effect	0.768	0.0288	0.0237	**0.109**	-0.00875	-0.0187	0.00125	-0.0113			
SS		0.00331	0.00226	0.0473	0.000306	0.00141	0.00000625	0.000506			
MSE	0.0422										

Range Chart Results		
Rbar	0.0413	***The ranges are in statistical control.***
UCLr	0.1348	
LCLr	None	

www.manaraa.com

ANOVA Table Based on All Factors and Interactions							
Source	SS	df	MS	F	p value	% Cont	
A	0.00331	1	0.00331	3.245	0.1093	5.23%	
B	0.00226	1	0.00226	2.215	0.1750	3.57%	
C	0.0473	1	0.0473	46.436	0.0001	74.80%	
AB	0.000306	1	0.000306	0.301	0.5985	0.48%	
AC	0.00141	1	0.00141	1.380	0.2738	2.22%	
BC	0.00000625	1	0.00000625	0.006	0.9395	0.01%	
ABC	0.000506	1	0.000506	0.497	0.5009	0.80%	
Error	0.00815	8	0.00102			12.89%	
Total	0.0632	15				100.00%	

The significant factors are in dark shade (p <= 0.05). Factors in light shade (0.05 < p <=0.20) may or may not be significant.

ANOVA for Model					
Source	SS	df	MS	F	p value
Model	0.0551	7	0.00787	7.726	0.0049

Average	0.768125
Standard Deviation	0.0319
Coefficient of Variation	4.155
R Square	87.11%
Adjusted R Square	75.84%
PRESS	0.0326
R Square Prediction	48.45%

Factor Information					
Factor	Coeff	Degrees of Freedom	Standard Error	95% Lower	95% Upper
Intercept	0.768	1	0.008	0.750	0.787
A	0.0144	1	0.0080	-0.0040	0.0328
B	0.0119	1	0.0080	-0.0065	0.0303
C	0.0544	1	0.0080	0.0360	0.0728
AB	-0.0044	1	0.0080	-0.0228	0.0140
AC	-0.0094	1	0.0080	-0.0278	0.0090
BC	0.0006	1	0.0080	-0.0178	0.0190
ABC	-0.0056	1	0.0080	-0.0240	0.0128

المنارة للاستشارات
www.manaraa.com

APPENDIX 4. 2^3 Full Factorial ANOVA Normal Plot of Effects - Tool A

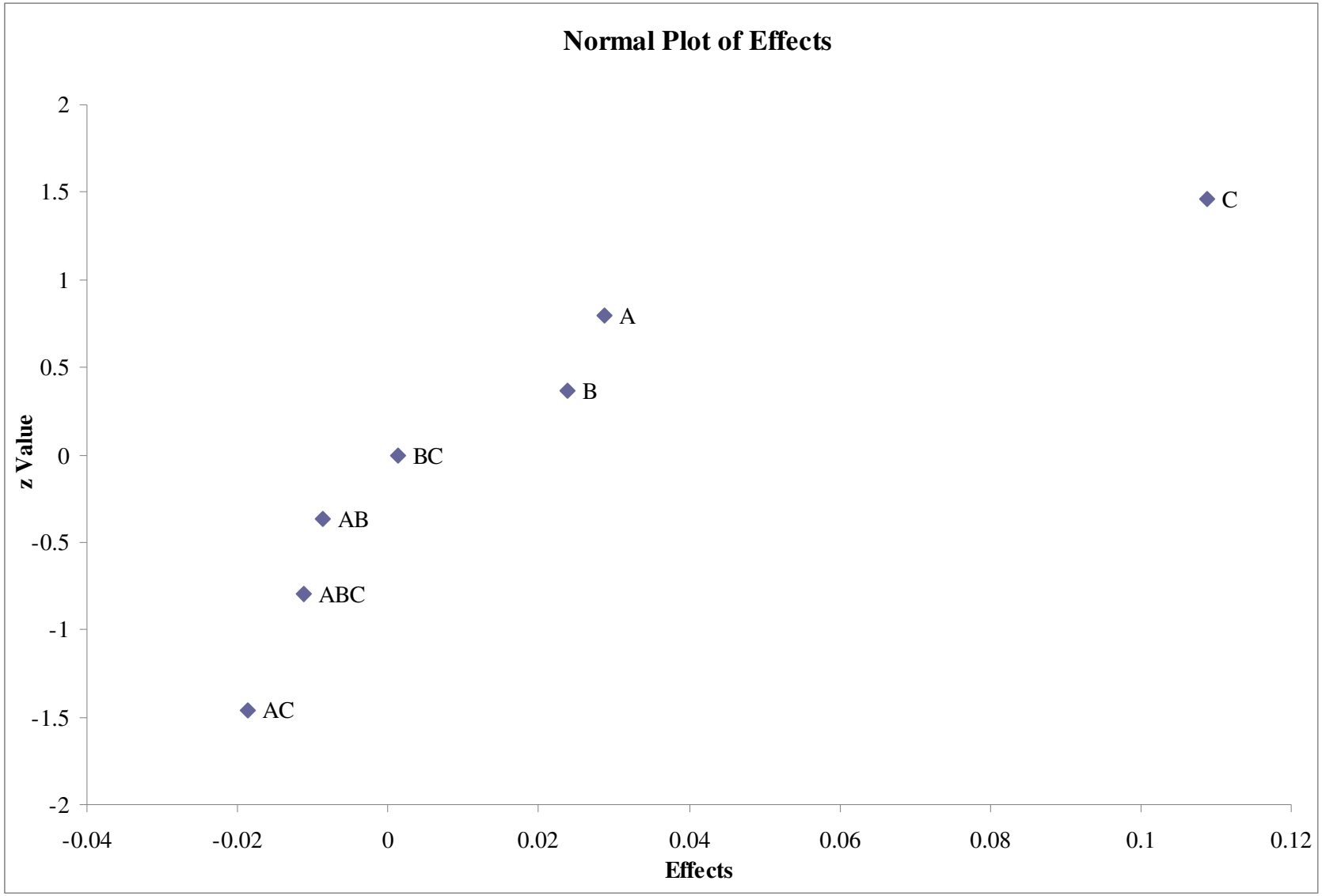

www.manaraa.com

APPENDIX 5. 2^3 Full Factorial ANOVA Half-Normal Plot of Effects - Tool A

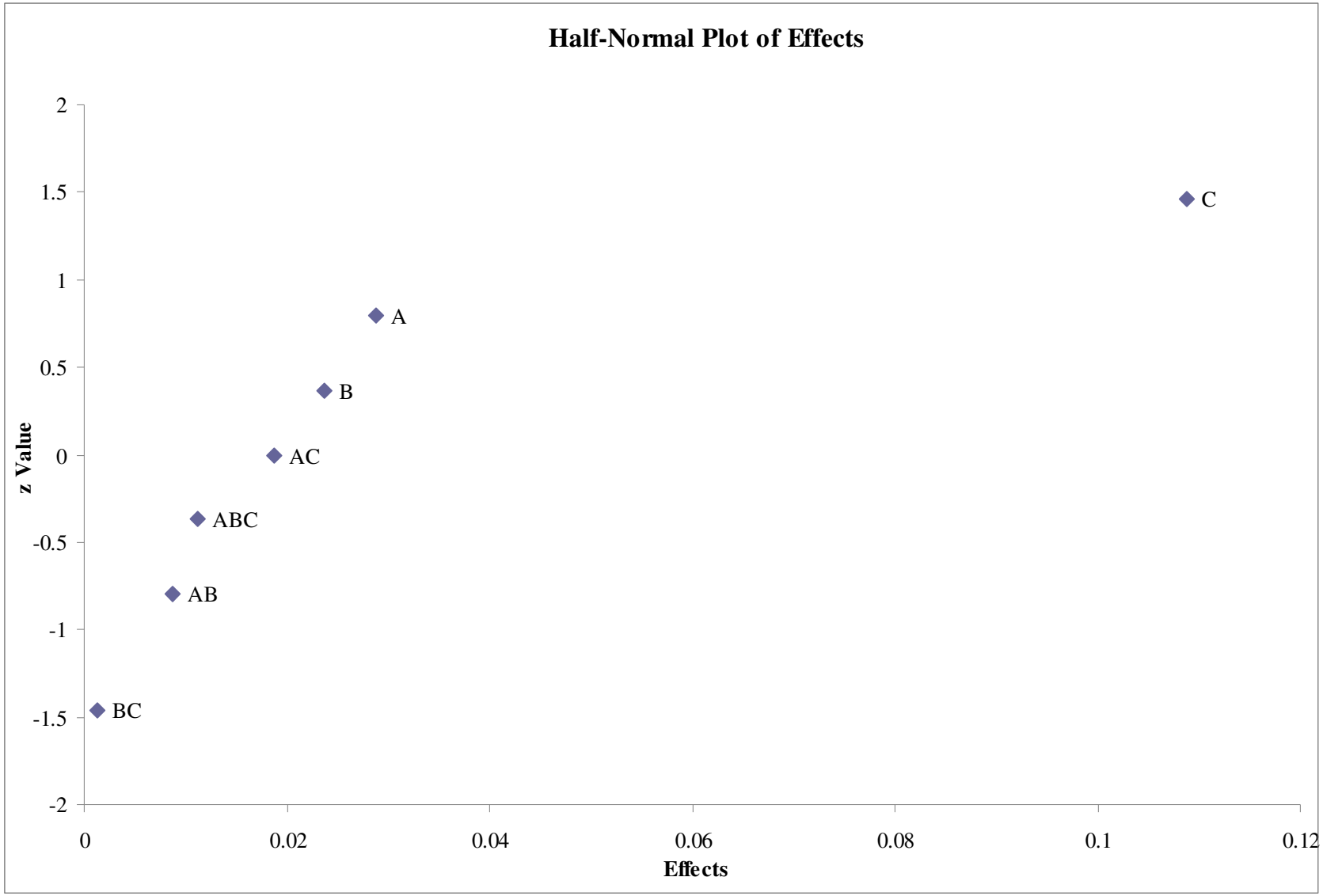

www.manaraa.com

APPENDIX 6. 2^3 Full Factorial ANOVA Effects Charts - Tool A

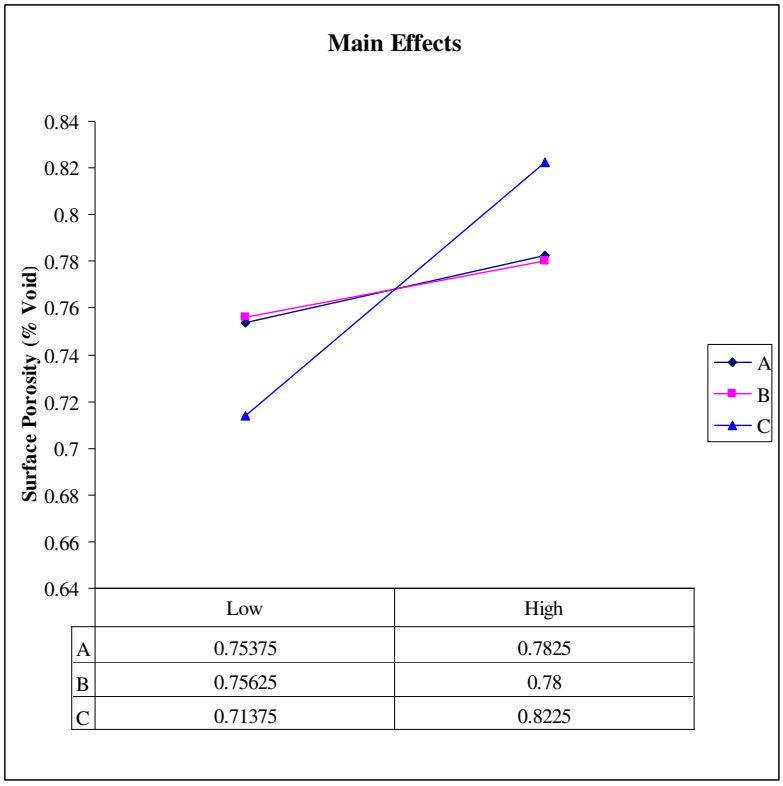

	Low	High
A	0.75375	0.7825
B	0.75625	0.78
C	0.71375	0.8225

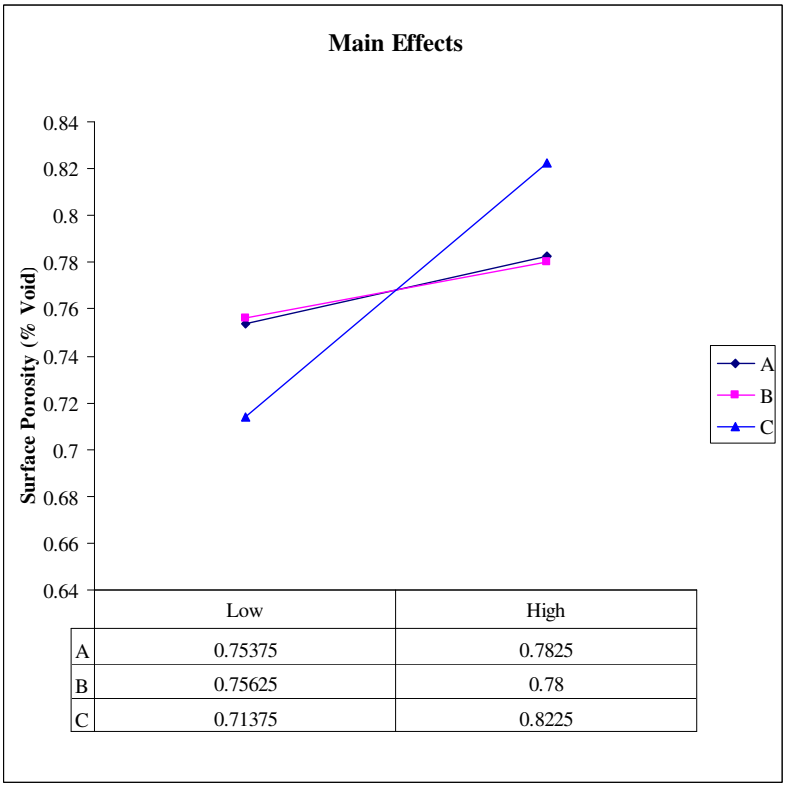

	Low	High
A	0.75375	0.7825
B	0.75625	0.78
C	0.71375	0.8225

www.manaraa.com

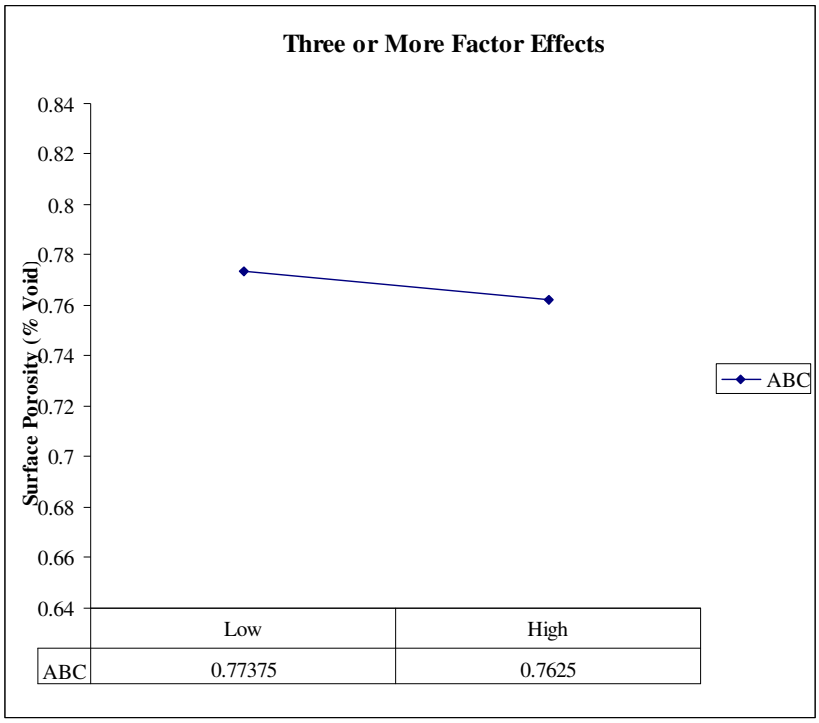

www.manaraa.com

APPENDIX 7. 2^3 Full Factorial ANOVA Two-Factor Plots - Tool A

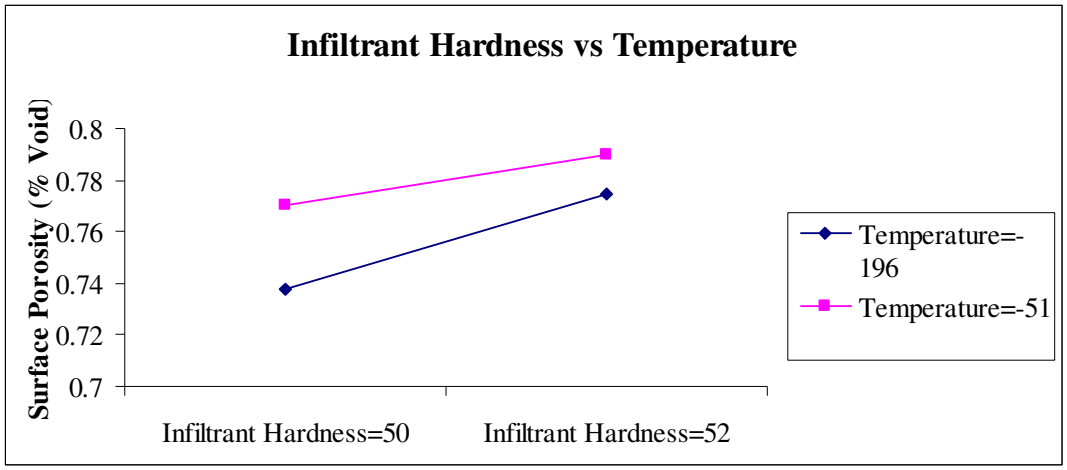

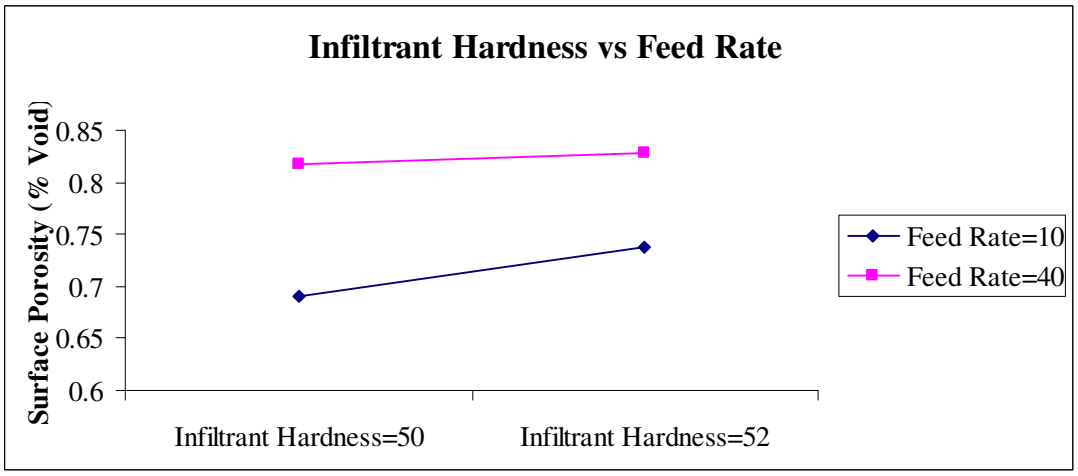

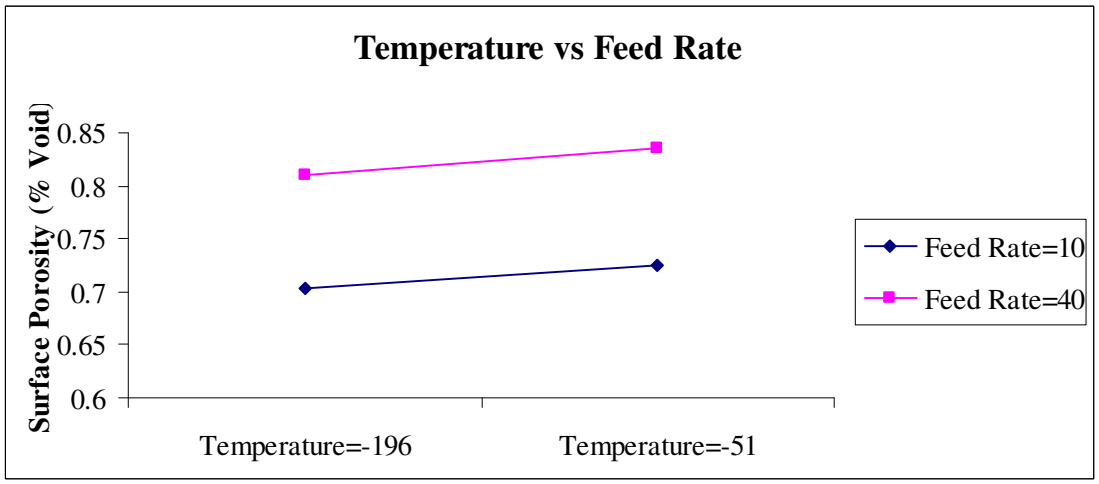

www.manaraa.com

APPENDIX 8. 2^3 Full Factorial ANOVA All Factors Residuals Information - Tool A

Standard Run Order	Actual Run Order	Observed Value	Predicted Value	Residuals	Leverage	Standardized Residuals	Internally Studentized Residuals	Externally Studentized Residuals	DFFITS	Cook's Distance
1	9	0.66	0.680	-0.0200	0.500	-0.627	-0.886	-0.873	-0.873	0.0982
1	14	0.7	0.680	0.0200	0.500	0.627	0.886	0.873	0.873	0.0982
2	7	0.74	0.725	0.0150	0.500	0.470	0.665	0.640	0.640	0.0552
2	10	0.71	0.725	-0.0150	0.500	-0.470	-0.665	-0.640	-0.640	0.0552
3	2	0.73	0.700	0.0300	0.500	0.940	1.329	1.409	1.409	0.2209
3	8	0.67	0.700	-0.0300	0.500	-0.940	-1.329	-1.409	-1.409	0.2209
4	3	0.74	0.750	-0.0100	0.500	-0.313	-0.443	-0.420	-0.420	0.0245
4	6	0.76	0.750	0.0100	0.500	0.313	0.443	0.420	0.420	0.0245
5	4	0.76	0.795	-0.0350	0.500	-1.097	-1.551	-1.735	-1.735	0.3006
5	15	0.83	0.795	0.0350	0.500	1.097	1.551	1.735	1.735	0.3006
6	12	0.81	0.825	-0.0150	0.500	-0.470	-0.665	-0.640	-0.640	0.0552
6	13	0.84	0.825	0.0150	0.500	0.470	0.665	0.640	0.640	0.0552
7	1	0.81	0.840	-0.0300	0.500	-0.940	-1.329	-1.409	-1.409	0.2209
7	5	0.87	0.840	0.0300	0.500	0.940	1.329	1.409	1.409	0.2209
8	11	0.82	0.830	-0.0100	0.500	-0.313	-0.443	-0.420	-0.420	0.0245
8	16	0.84	0.830	0.0100	0.500	0.313	0.443	0.420	0.420	0.0245

Notes:

Any values that fail the following are colored in red and could be outliers.
Leverage > 2p/n
Standardized, internally standardized, externally standardize residuals outside the range of -3 to 3
Absolute value DFFITS > 2Sqrt(p/n)
Cook's Distance > 1
where p is the number of regressor variables (including b0) and n is the number of observations

www.manaraa.com

APPENDIX 9. 2^3 Full Factorial ANOVA All Factor Analysis (Infiltrant Hardness and Temperature Only) - Tool A

ANOVA Table Based on Selected Factors and Interactions						
Source	SS	df	MS	F	p value	% Cont
A	0.00331	1	0.00331	0.745	0.4037	5.23%
B	0.00226	1	0.00226	0.509	0.4884	3.57%
Error	0.0577	13	0.00444			12.89%
Lack of Fit	0.04953	5	0.00991	9.724	0.0030	78.32%
Pure Error	0.00815	8	0.00102			12.89%
Total	0.0632	15				100.00%

ANOVA for Model					
Source	SS	df	MS	F	p value
Model	0.00556	2	0.00278	0.627	0.5497

Average	0.76813
Standard Deviation	0.0666
Coefficient of Variation	8.672
R Square	8.80%
Adjusted R Square	-5.24%
PRESS	0.08738
R Square Prediction	-38.16%

Factor Information					
Factor	Coeff	Degrees of Freedom	Standard Error	95% Lower	95% Upper
Intercept	0.768	1	0.017	0.732	0.804
A	0.0144	1	0.0167	-0.0216	0.0504
B	0.0119	1	0.0167	-0.0241	0.0479

www.manaraa.com

APPENDIX 10. 2^3 Full Factorial ANOVA All Factor Analysis - Tool B

Design Table												
Standard Run Order	Mean	A	B	*C*	AB	AC	BC	ABC	Average	Range		
1	+	-	-	-	+	+	+	-	0.38	0.04		
2	+	+	-	-	-	-	+	+	0.405	0.09		
3	+	-	+	-	-	+	-	+	0.35	0.06		
4	+	+	+	-	+	-	-	-	0.37	0.02		
5	+	-	-	+	+	-	-	+	0.63	0.04		
6	+	+	-	+	-	+	-	-	0.65	0.02		
7	+	-	+	+	-	-	+	-	0.69	0		
8	+	+	+	+	+	+	+	+	0.635	0.11		
Sum +	4.11	2.06	2.045	2.605	2.015	2.015	2.11	2.02		***The significant effects are in bold in the effects row. These are larger than MSE.***		
Sum -	0	2.05	2.065	1.505	2.095	2.095	2	2.09				
Overall	4.11	4.11	4.11	4.11	4.11	4.11	4.11	4.11				
Difference	4.11	0.01	-0.02	1.1	-0.08	-0.08	0.11	-0.07				
Effect	0.514	0.00250	-0.00500	**0.275**	-0.0200	-0.0200	0.0275	-0.0175				
SS		0.0000250	0.000100	0.303	0.00160	0.00160	0.00303	0.00122				
MSE	0.0486											

Range Chart Results		
Rbar	0.0475	***The ranges are in statistical control.***
UCLr	0.1552	
LCLr	None	

www.manaraa.com

ANOVA Table Based on All Factors and Interactions							
Source	SS	df	MS	F	p value	% Cont	
A	0.0000250	1	0.0000250	0.014	0.9075	0.01%	
B	0.000100	1	0.000100	0.058	0.8164	0.03%	
C	0.303	1	0.303	174.101	0.0000	93.37%	
AB	0.00160	1	0.00160	0.921	0.3653	0.49%	
AC	0.00160	1	0.00160	0.921	0.3653	0.49%	
BC	0.00303	1	0.00303	1.741	0.2235	0.93%	
ABC	0.00122	1	0.00122	0.705	0.4255	0.38%	
Error	0.0139	8	0.00174			4.29%	
Total	0.324	15				100.00%	

The significant factors are in dark shade (p <= 0.05). Factors in light shade (0.05 < p <=0.20) may or may not be significant.

ANOVA for Model					
Source	SS	df	MS	F	p value
Model	0.310	7	0.0443	25.494	0.0001

Average	0.51375
Standard Deviation	0.0417
Coefficient of Variation	8.114
R Square	95.71%
Adjusted R Square	91.96%
PRESS	0.0556
R Square Prediction	82.84%

Factor Information					
Factor	Coeff	Degrees of Freedom	Standard Error	95% Lower	95% Upper
Intercept	0.514	1	0.010	0.490	0.538
A	0.00125	1	0.01042	-0.02278	0.02528
B	-0.00250	1	0.01042	-0.02653	0.02153
C	0.13750	1	0.01042	0.11347	0.16153
AB	-0.01000	1	0.01042	-0.03403	0.01403
AC	-0.01000	1	0.01042	-0.03403	0.01403
BC	0.01375	1	0.01042	-0.01028	0.03778
ABC	-0.00875	1	0.01042	-0.03278	0.01528

المنارة للاستشارات
www.manaraa.com

APPENDIX 11. 2^3 Full Factorial ANOVA Normal Plot of Effects - Tool B

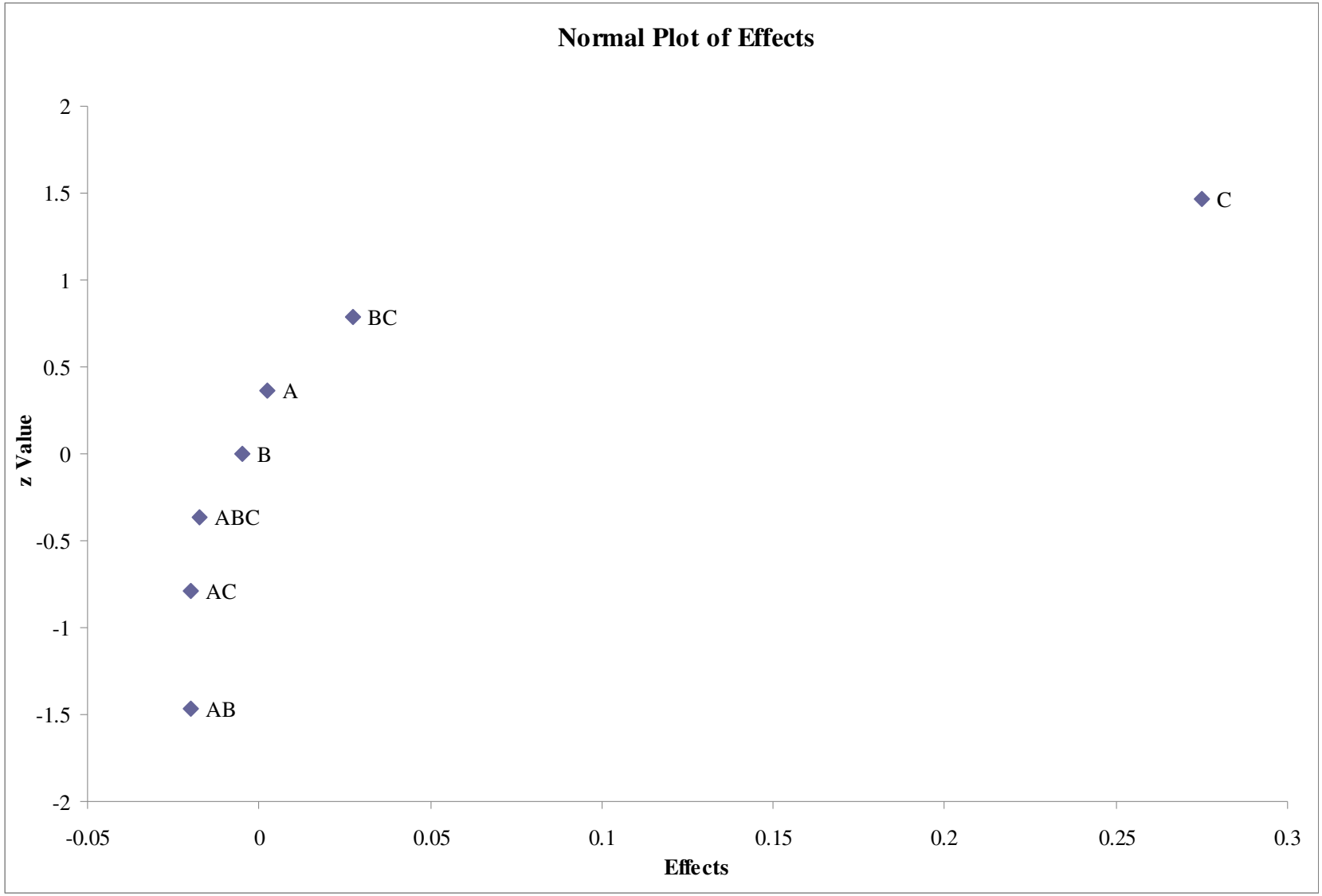

www.manaraa.com

APPENDIX 12. 2^3 Full Factorial ANOVA Half-Normal Plot of Effects - Tool B

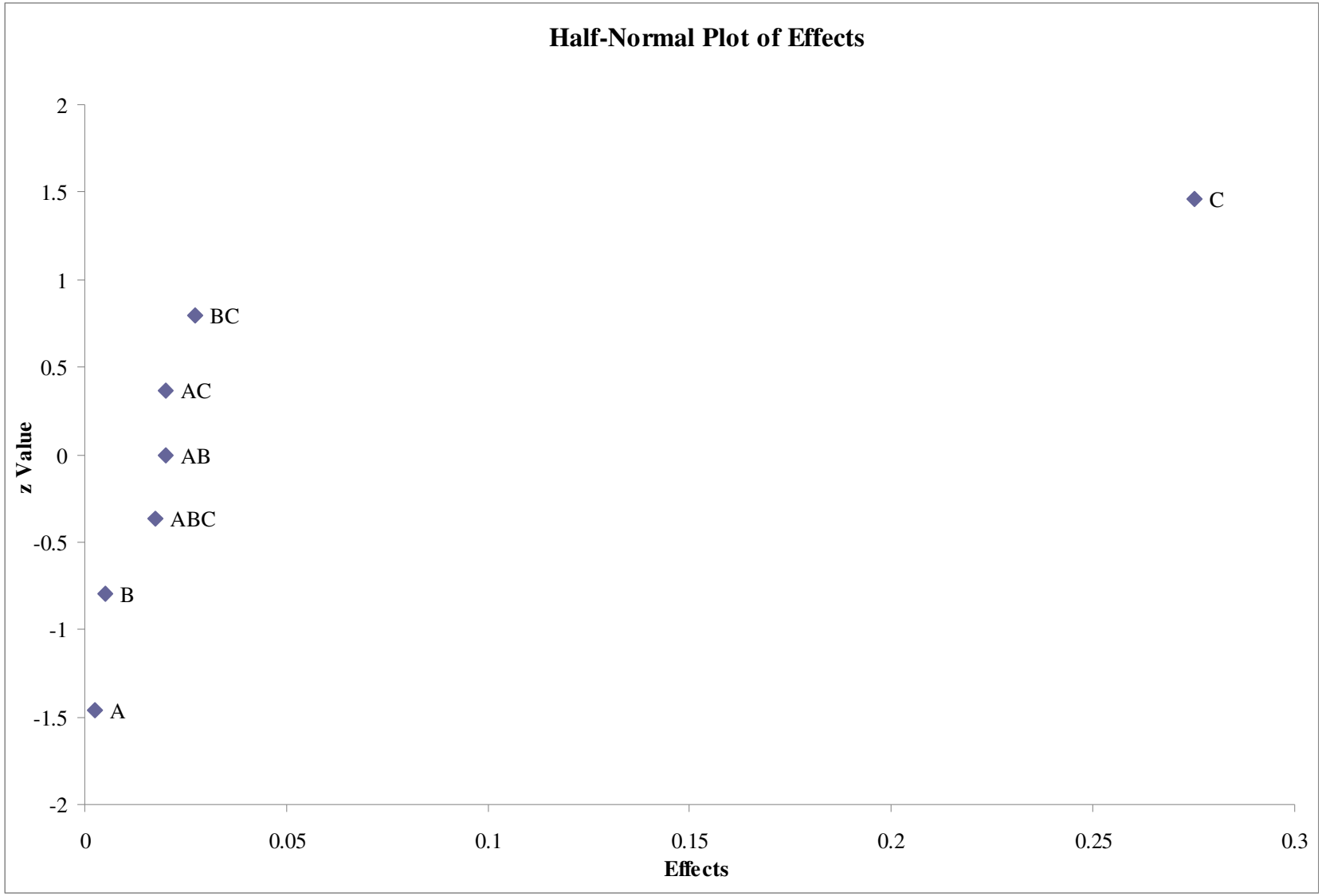

www.manaraa.com

APPENDIX 13. 2^3 Full Factorial ANOVA Effects Charts - Tool B

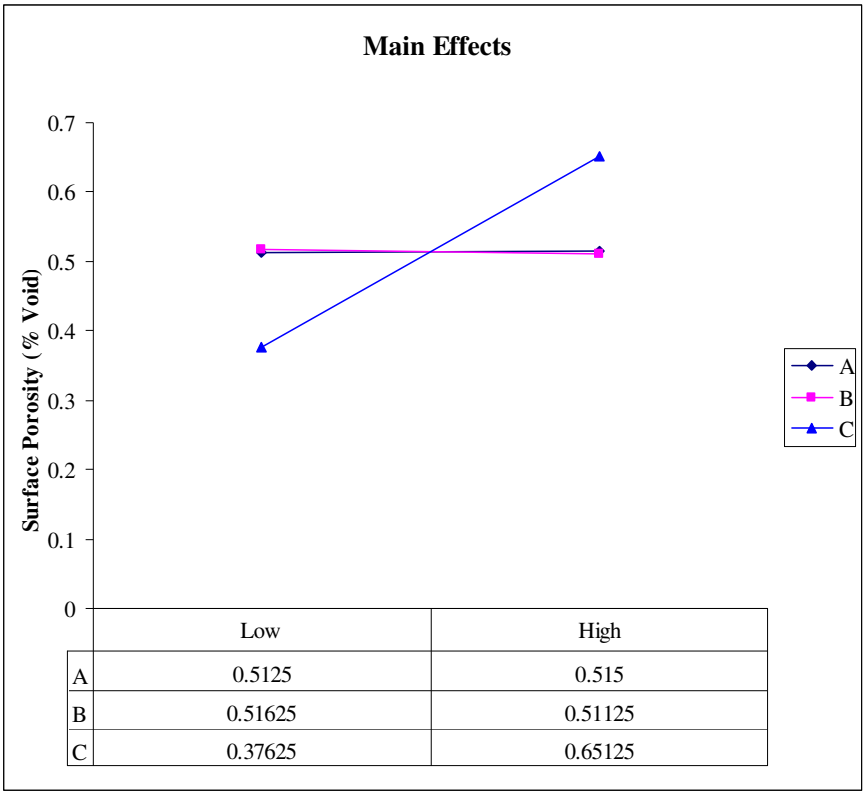

	Low	High
A	0.5125	0.515
B	0.51625	0.51125
C	0.37625	0.65125

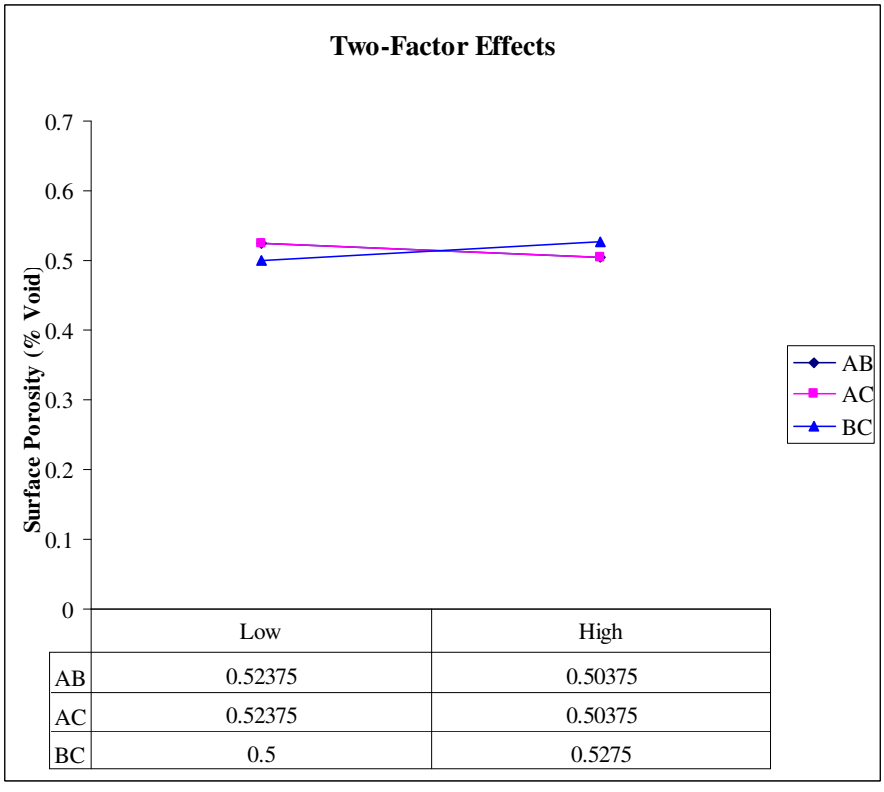

	Low	High
AB	0.52375	0.50375
AC	0.52375	0.50375
BC	0.5	0.5275

www.manaraa.com

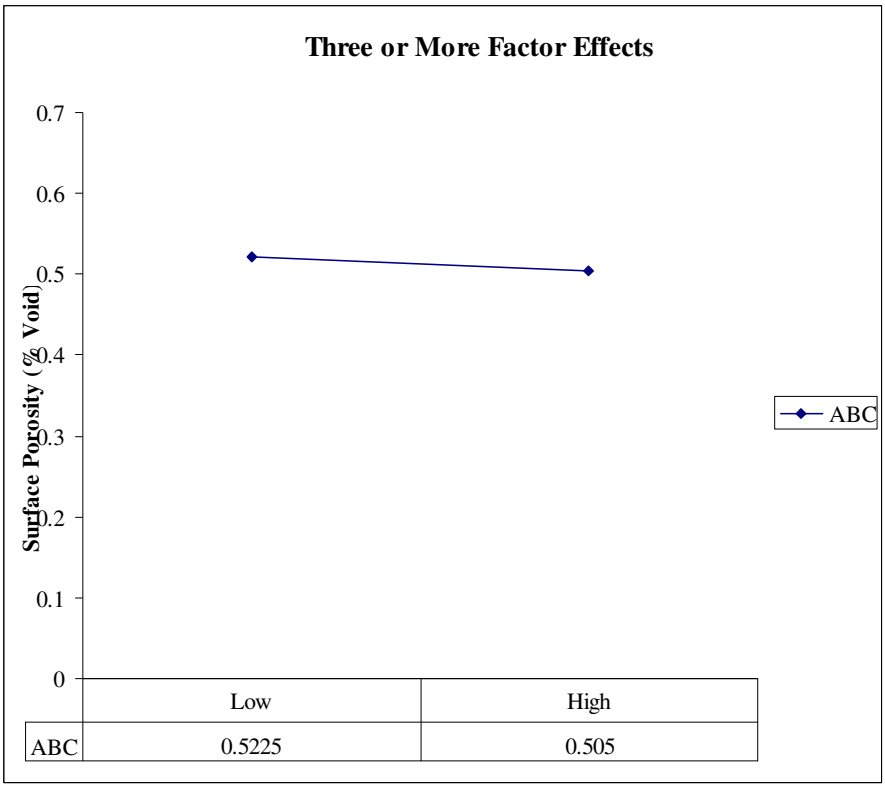

www.manaraa.com

APPENDIX 14. 2^3 Full Factorial ANOVA Two-Factor Plots - Tool B

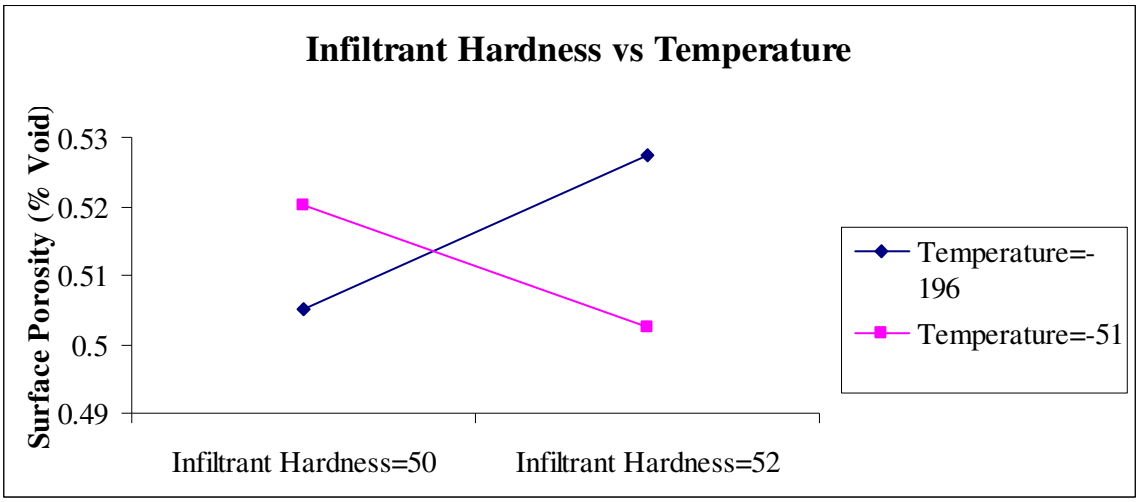

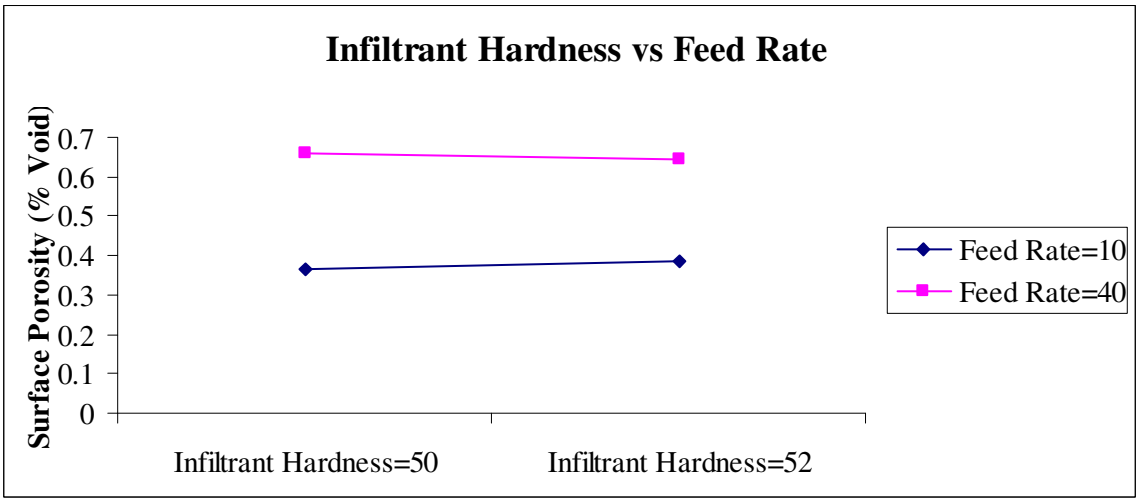

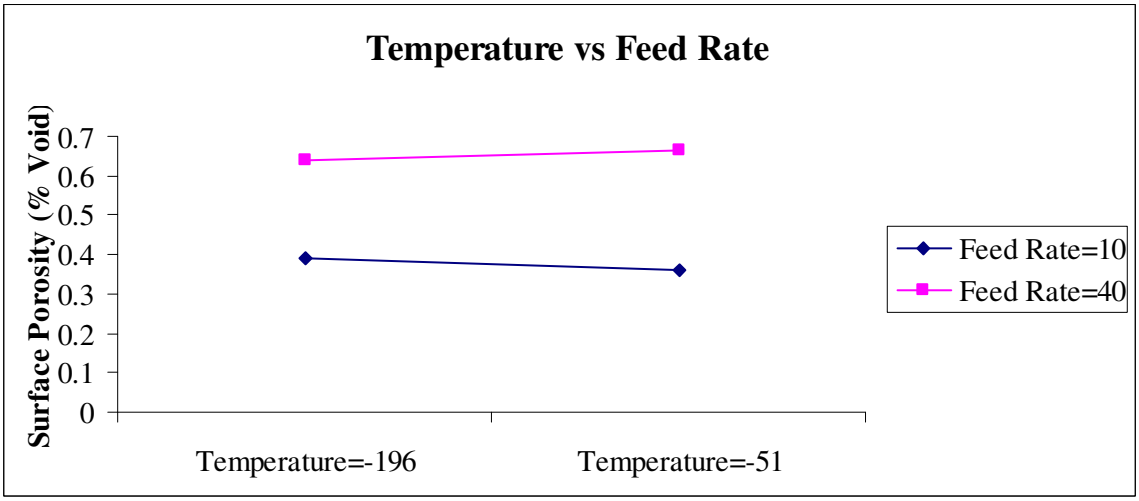

www.manaraa.com

APPENDIX 15. 2^3 Full Factorial ANOVA All Factors Residuals Information - Tool B

Standard Run Order	Actual Run Order	Observed Value	Predicted Value	Residuals	Leverage	Standardized Residuals	Internally Studentized Residuals	Externally Studentized Residuals	DFFITS	Cook's Distance
1	7	0.36	0.380	-0.0200	0.500	-0.480	-0.679	-0.654	-0.654	0.0576
1	15	0.4	0.380	0.0200	0.500	0.480	0.679	0.654	0.654	0.0576
2	2	0.36	0.405	-0.0450	0.500	-1.080	-1.527	-1.697	-1.697	0.2914
2	5	0.45	0.405	0.0450	0.500	1.080	1.527	1.697	1.697	0.2914
3	10	0.38	0.350	0.0300	0.500	0.720	1.018	1.020	1.020	0.1295
3	16	0.32	0.350	-0.0300	0.500	-0.720	-1.018	-1.020	-1.020	0.1295
4	6	0.36	0.370	-0.0100	0.500	-0.240	-0.339	-0.320	-0.320	0.0144
4	11	0.38	0.370	0.0100	0.500	0.240	0.339	0.320	0.320	0.0144
5	3	0.65	0.630	0.0200	0.500	0.480	0.679	0.654	0.654	0.0576
5	8	0.61	0.630	-0.0200	0.500	-0.480	-0.679	-0.654	-0.654	0.0576
6	4	0.64	0.650	-0.0100	0.500	-0.240	-0.339	-0.320	-0.320	0.0144
6	12	0.66	0.650	0.0100	0.500	0.240	0.339	0.320	0.320	0.0144
7	1	0.69	0.690	0.000	0.500	0.000	0.000	0.000	0.000	0.0000
7	14	0.69	0.690	0.000	0.500	0.000	0.000	0.000	0.000	0.0000
8	9	0.69	0.635	0.0550	0.500	1.319	1.866	2.323	2.323	0.4353
8	13	0.58	0.635	-0.0550	0.500	-1.319	-1.866	-2.323	-2.323	0.4353

Notes:

Any values that fail the following are colored in red and could be outliers.
Leverage > 2p/n
Standardized, internally standardized, externally standardize residuals outside the range of -3 to 3
Absolute value DFFITS > 2Sqrt(p/n)
Cook's Distance > 1
where p is the number of regressor variables (including b0) and n is the number of observations

www.manaraa.com

APPENDIX 16. Surface Porosity Analysis - Varying Feed Rate

Tool A

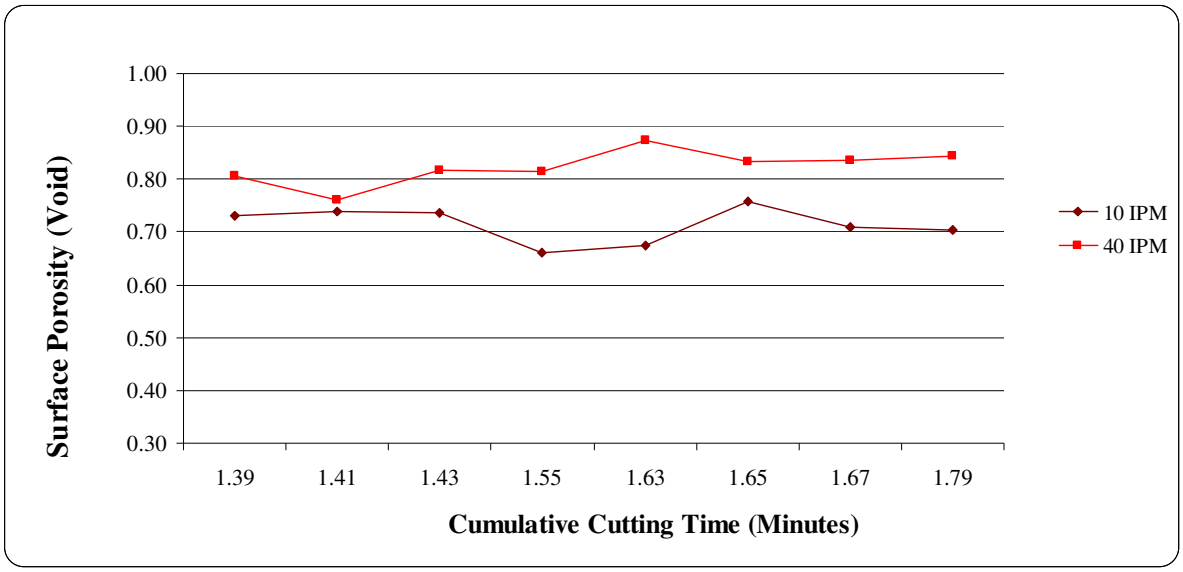

Tool B

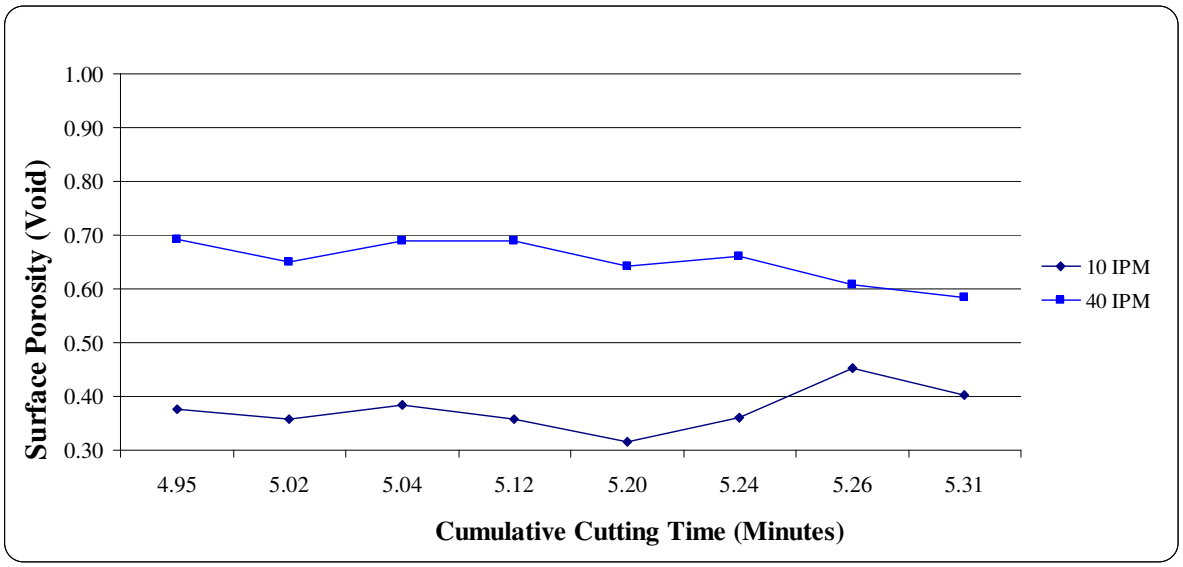

www.manaraa.com

APPENDIX 17. Surface Porosity Analysis - Varying Infiltrant Hardness

Tool A

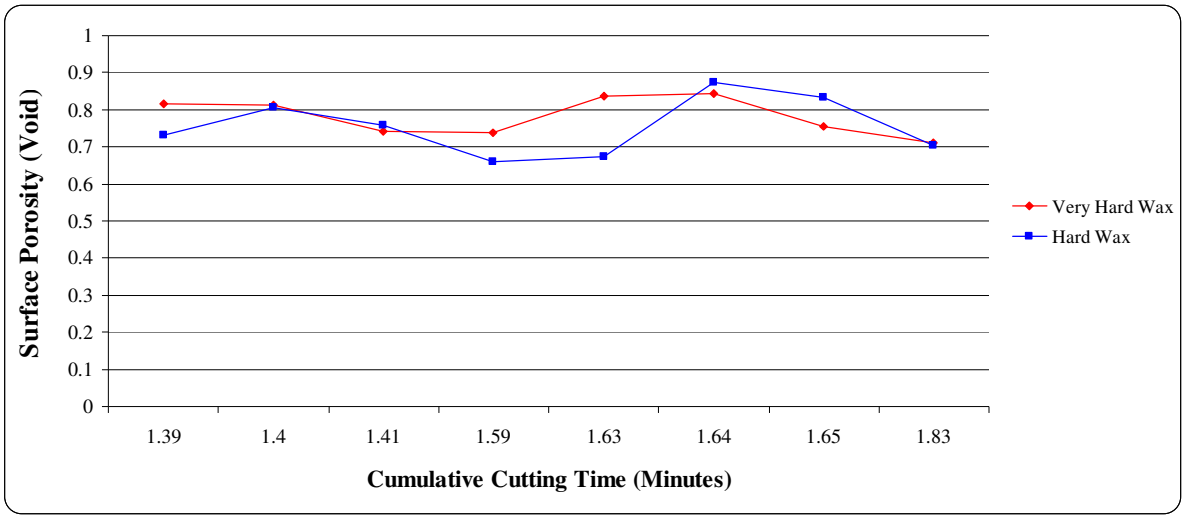

Tool B

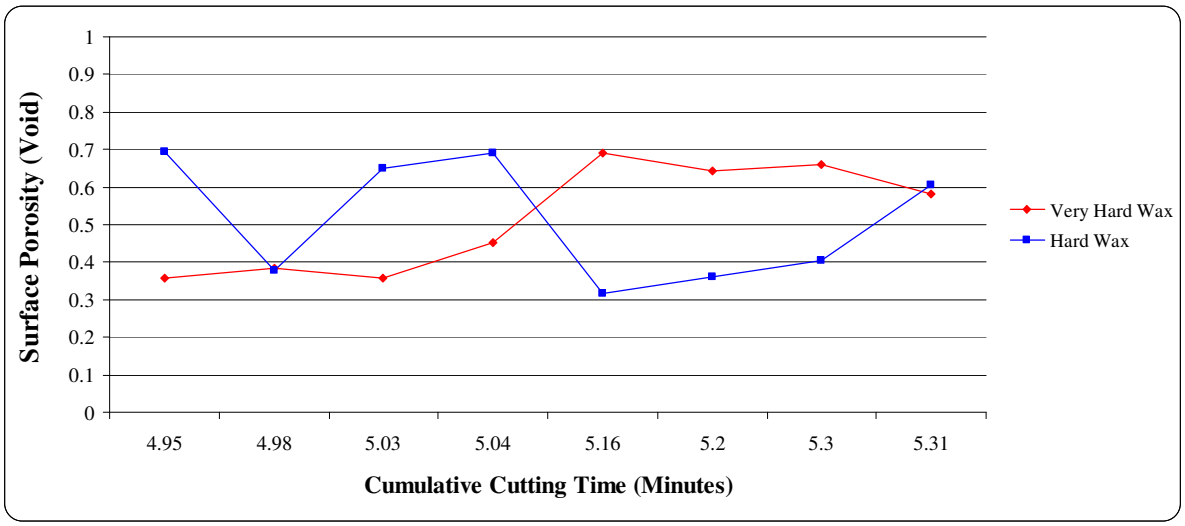

www.manaraa.com

APPENDIX 18. Surface Porosity Analysis - Varying Temperature

Tool A

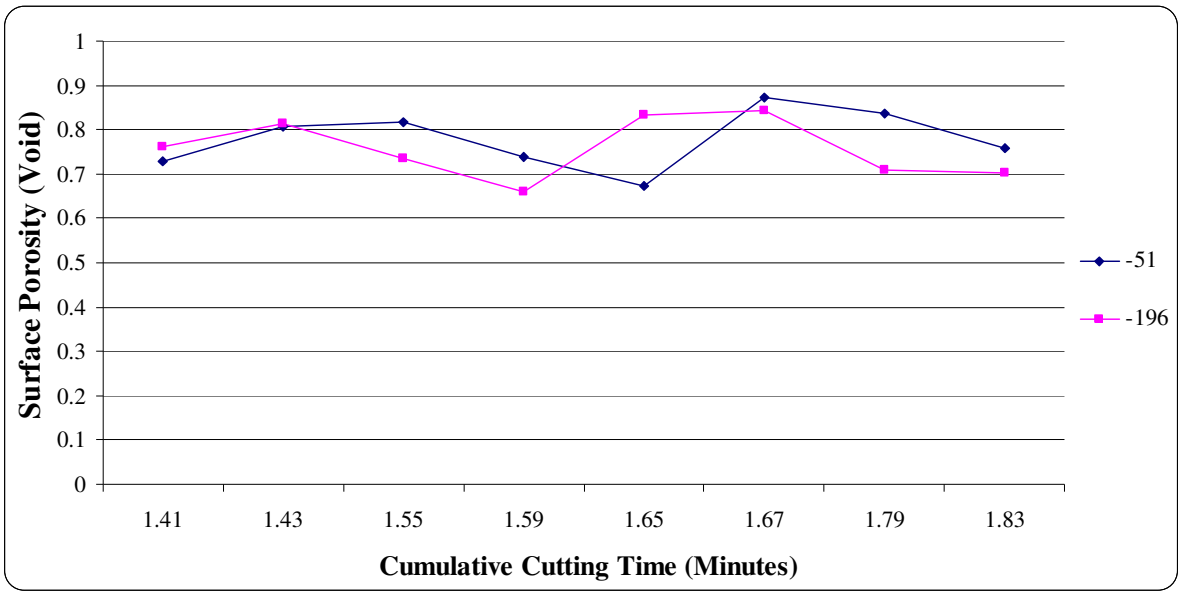

Tool B

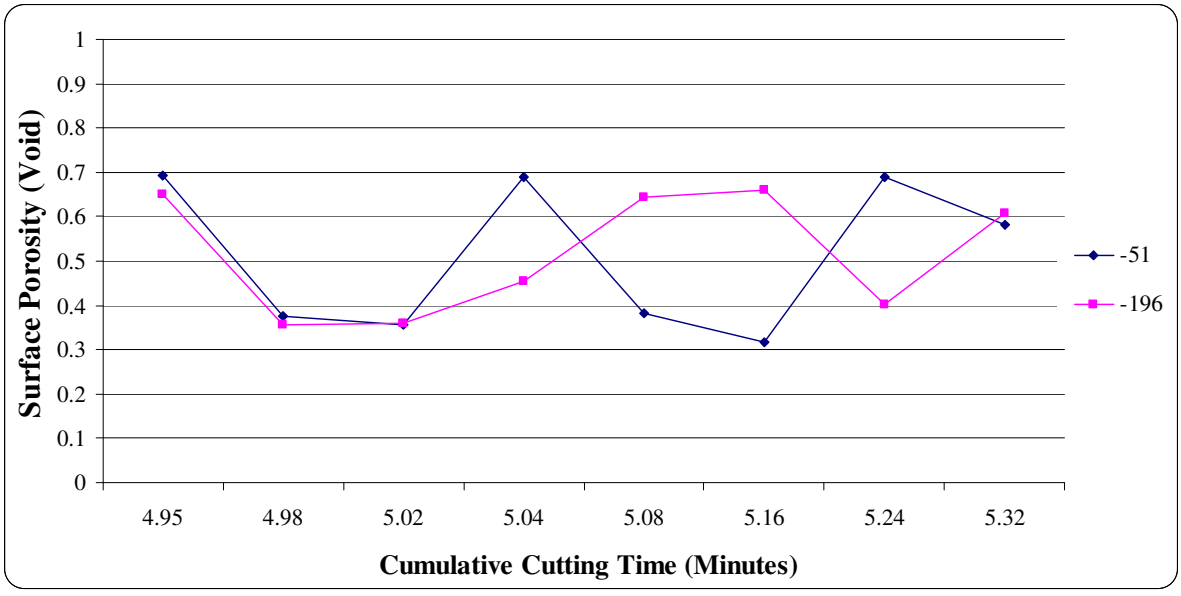

www.manaraa.com

ACKNOWLEDGEMENTS

I would like to thank Dr. Matthew C. Frank for all of his support and guidance throughout my time at Iowa State University. His encouragements lead me to continue my education in graduate school and for that I will be forever grateful. This research would not be possible without him and I am very thankful to have had the opportunity to work with Dr. Frank and his research team.

Secondly, I would like to extend my gratitude to Dr. Frank E. Peters for all that he has done for me during my study. I have learned a great deal from Dr. Peters over the years through mutual research work, onsite facility audits with the Industrial Assessment Center, and of course in the classroom. His lessons and insight have made me a better engineer and that I will never forget.

I would also like to thank Dr. L Scott Chumbley for his expert advice and contribution to this research. His guidance and outside perspective were invaluable to this work.

Finally, I would like to thank all of my family and friends for their love and support throughout my entire period of study. Without their patience, understanding, and guidance I would not be where I am at today and I am very fortunate to have been inspired by so many great individuals.

www.manaraa.com